

# Current Trends in Deep Learning for Earth Observation: An Open-source Benchmark Arena for Image Classification

Ivica Dimitrovski<sup>a,b</sup>, Ivan Kitanovski<sup>a,b</sup>, Dragi Kocev<sup>a,c</sup>, Nikola Simidjievski<sup>a,c,d</sup>

<sup>a</sup>*Bias Variance Labs, d.o.o., Ljubljana, Slovenia*

<sup>b</sup>*Faculty of Computer Science and Engineering, University Ss Cyril and Methodius, Skopje, N. Macedonia*

<sup>c</sup>*Department of Knowledge Technologies, Jožef Stefan Institute, Ljubljana, Slovenia*

<sup>d</sup>*Department of Computer Science and Technology, University of Cambridge, Cambridge, United Kingdom*

Correspondence to: [ivica,ivan,dragi,nikola]@bvlabs.ai

---

## Abstract

We present *AiTLAS: Benchmark Arena* – an open-source benchmark suite for evaluating state-of-the-art deep learning approaches for image classification in Earth Observation (EO). To this end, we present a comprehensive comparative analysis of more than 500 models derived from ten different state-of-the-art architectures and compare them to a variety of multi-class and multi-label classification tasks from 22 datasets with different sizes and properties. In addition to models trained entirely on these datasets, we benchmark models trained in the context of transfer learning, leveraging pre-trained model variants, as it is typically performed in practice. All presented approaches are general and can be easily extended to many other remote sensing image classification tasks not considered in this study. To ensure reproducibility and facilitate better usability and further developments, *all of the experimental resources* including the trained models, model configurations, and processing details of the datasets (with their corresponding splits used for training and evaluating the models) are *publicly available on the repository*: <https://github.com/biasvariancelabs/aitlas-arena>.

**Keywords:** Deep learning (DL), Earth observation (EO), Image Classification, Benchmark study

---

## 1 Introduction

Recent trends in machine learning (ML) have ushered in a new era of image-data analyses, repeatedly achieving great performance across a variety of computer-vision tasks in different domains [1, 2]. Deep learning (DL) approaches have been at the forefront of these efforts – leveraging novel, modular and scalable deep neural network (DNN) architectures able to process large amounts of data. The inherent capabilities of these approaches also extend to various areas of remote sensing, in particular Earth Observation (EO), employed for analyzing different types of large-scale satellite data [3]. Many of these contributions are instances of image-scene classification, such as land-use and/or land-cover (LULC) identification tasks, focusing on image-scene analyses, characterizations, and classifications of changes in the landscape caused either by human activities or by the elements.

Historically, from the perspective of ML, many of these tasks have been addressed mostly through the paradigms of either pixel-level [4, 5] or object-level classification tasks [6]. The former refers to classification tasks focusing on each pixel in the image, associating it with the appropriate semantic label. Such approaches typically do not scale well on high-resolution images, but more importantly, many times struggle to capture more high-level patterns in the image that can span over many pixels [7]. The latter, object-level classification methods, focus on analyzing distinguishable and meaningful objects in the image (as a collection of pixels) rather than independent pixels. This generally allows for better scalability and performance; however, such approaches may struggle with images containing more diverse and hard-to-distinguishable objects, which prevail in most high-resolution remote-sensing data. Methods based on pixel-level and object-level paradigms have shown decent performance and are still actively researched, mostly as instances of image segmentation and object detection tasks. More recently, however, methods based on a new paradigm of scene-level classification [8, 9] have shown significant performance improvements, focusing on learning semantically meaningful representations of more sophisticated patterns in an image by leveraging the capabilities of deep learning.

Deep learning approaches have been successfully applied in various remote-sensing scenarios, be it learning models from scratch or via transfer learning [10, 11], in a fully supervised or self-supervised setting [12, 13], exploiting the heterogeneity [14] and temporal properties [15] of the available data. As a result, this synergy of accurate DL approaches, on the one hand, and accessible high-resolution aerial/satellite imagery, on the other, has led to important contributions in various domains ranging from agriculture [16, 17, 18], ecology [19, 20], geology [21] and meteorology [22, 23, 11] to urban mapping/planning [24, 25, 26] and archaeology [27].

Nevertheless, most of these efforts typically focus on very narrow tasks stemming from domain-specific and/or spatially constrained datasets. As a result, models have been evaluated in different settings and under different conditions [28] – hardly reproducible and comparable. These persistent challenges, akin to a lack of standardized and consistent validation and evaluation of novel approaches, have also been identified by the community [29]. Citing the lack of available documentation on the design and evaluation of the employed machine learning approaches, the community highlights the urgent need for standardized benchmarks that will not only enable proper and fair model comparison across datasets and similar tasks but will also facilitate faster progress in designing better and more accurate modeling approaches.

Motivated by this, in this work, we introduce *AiTLAS: Benchmark Arena* – an *open-source EO benchmark suite* for evaluating state-of-the-art DL approaches for EO image classification. To this end, we present extensive comparative analyses of models derived from ten different state-of-the-art architectures, comparing them on a variety of multi-class and multi-label classification tasks from 22 datasets with different sizes and properties. We benchmark models trained from scratch and in the context of transfer learning, leveraging pre-trained model variants as it is typically performed in practice. While in this work, we mainly focus on EO-image classification tasks, such as LULC, all presented approaches are general and easily extendable to other remote-sensing image classification tasks. More importantly, to ensure reproducibility, facilitate better usability, and further exploitation of the results from our work, we provide *all*

*of the experimental resources* - freely available on our repository<sup>1</sup>. The repository includes the complete study details, such as the trained models, model parameters, train/evaluation configurations, and measured performance scores, as well as the details on all of the datasets and their preprocessed versions (with the appropriate train/validation/test splits) used for training and evaluating the models.

To our knowledge, we present a unique systematic review and evaluation of different state-of-the-art DL methods in the context of EO image classification across many classification problems – benchmarked in the same conditions and using the same hardware. Related efforts, while relevant, have mainly focused on evaluating approaches on particular datasets [8, 28, 30, 31]; evaluating different aspects of method-design [32, 14] relevant to remote-sensing classification tasks; or providing a more general overview of the common tasks at hand [33, 34]. In particular, Cheng et al. [8] introduce a dataset and surveys several ML representation-learning approaches commonly used for remote-sensing classification tasks, comparing their performance when combined with traditional convolutional neural network (CNN) architectures. Xia et al. [31] also introduce a benchmark dataset for aerial-image classification, providing a comparison similar to Cheng et al. [8] of representation-learning approaches combined with three deep networks. Another, more recent study [28], discusses and compares more recent DL approaches and surveys several applications on three different datasets. In particular, the authors showcase the performance of the different methods for each dataset, as reported in the respective papers. The underlying, persistent conclusions from these studies show that model performances are associated with a particular dataset and study design, presenting difficulties for fair and general model comparisons. This is expected, but in our work, we seek to remedy this issue by training and evaluating all models under the same conditions.

In this context, our work is related to one of Zhai et al. [32], which presents a large-scale study on more recent representation-learning approaches, benchmarking different aspects of method design and model parameters. However, Zhai et al. [32] considers a relatively broad scope of different datasets with only a few relevant to remote-sensing and LULC classification. Neumann et al. [14] present a large-scale study on five different benchmark datasets; however, they investigate the effect of transfer learning on these tasks. More specifically, they evaluate different variants of the same model architecture, trained under different circumstances, rather than comparing different model architectures. Another related study by Stewart et al. [35] reports on the comparison of different variants of ResNets on EO-image classification tasks from four datasets. More recently, and arguably most related to our work in terms of the number of evaluated models, Papoutsis et al. [30] present an extensive empirical evaluation of different state-of-the-art DL architectures suitable for EO-image classification tasks, specifically LULC tasks, focusing exclusively on the BigEarthNet [36] dataset. Namely, the authors benchmark different classes of model architectures across different criteria and introduce an efficient and well-performing model tailored specifically for BigEarthNet.

In this work, we go beyond all the aforementioned studies, significantly extending the scope of research in two directions: the number of model architectures (and model variants) being evaluated and the datasets being considered.

---

<sup>1</sup><https://github.com/biasvariancelabs/aitlas-arena>

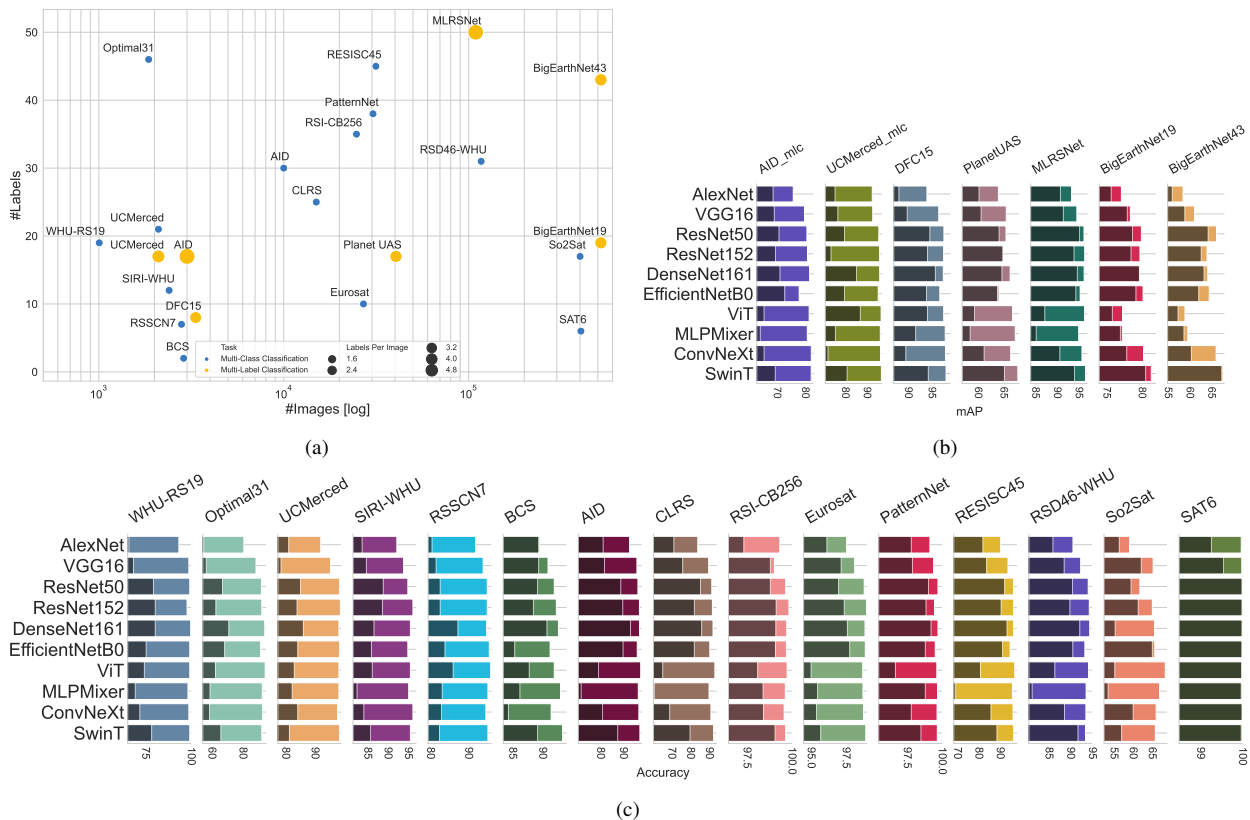


Figure 1: **Overview of the study:** We benchmarked more than 500 models from 10 different model architectures on tasks from (a) 22 datasets with different sizes and properties; comparing them on (b) multi-label and (c) multi-class classification tasks. We evaluate two versions of each model architecture: (i) trained from scratch (denoted with *darker shading*) and (ii) pre-trained on ImageNet-1K (denoted with *lighter shading*). Note the varying scales in (b) and (c), made purposely for better visibility. Detailed results are presented in Section 4 and Appendices B, C and D.

This results in assessing more than 500 different models with different architectures, varying designs, and learning paradigms across 22 datasets. We provide essential study-design principles and model training details that will aid in more systematic and rigorous experiments in future work. The proposed *AiTLAS: Benchmark Arena* builds on the *AiTLAS* toolbox [37]<sup>2</sup> – a recent open-source library for exploratory and predictive analysis of satellite imagery pertaining to different remote-sensing tasks. *AiTLAS* implements various methods and libraries for data handling, processing, and analysis, with PyTorch [38] as a backbone for constructing and learning DL models. By having all of the methods and datasets under the same umbrella, we provide the means for a fair, unbiased, and reproducible comparison of approaches across different criteria that include: overall model performance, data- and task-dependent model performance, model size, and learning efficiency as well as the effect of transfer learning via model pre-training.

The results, summarized in Figure 1, show that many of the current state-of-the-art architectures for vision tasks can lead to decent predictive performance when applied to EO image classification tasks. While, in some cases,

<sup>2</sup><https://aitlas.bvlabs.ai>

training models from scratch can lead to satisfactory performance, using pre-trained models and fine-tuning them on each dataset leads to the best performance overall. We observed this in all cases, regardless of the dataset properties, the type of classification tasks, or the model architecture. We found more considerable performance gains on tasks from smaller datasets, which, as expected, benefited more from the pre-training process than models trained on larger datasets. In terms of model architectures, our experiments showed that pre-trained Transformer models, i.e. both Vision Transformer [39] and Swin Transformer [40] models, were, in general, able to achieve the best performance. Specifically, Vision Transformer models showed the best performance on various multi-classification tasks, while Swin Transformer models led to much better performance on multi-label tasks, albeit at the cost of much longer training time. Throughout the paper, we further evidence and discuss these findings.

In summary, in this paper, we make several contributions. Specifically, we:

- Introduce *AiTLAS: Benchmark Arena* – an open-source benchmark suite that enables standardized evaluation of machine learning models for Earth Observation (EO) applications;
- Provide study-design principles for training and evaluating state-of-the-art deep learning models on various supervised EO image classification tasks from 22 datasets with different sizes and properties;
- Implement and benchmark more than 500 models stemming from 10 state-of-the-art architectures, including models trained from scratch and their pre-trained variants;
- Investigate models’ generalization abilities to unseen in-domain datasets;
- Evaluate different pre-training strategies that relate to pre-training models from in-domain EO datasets and investigate their effect on the downstream predictive performance;
- Discuss common issues that typically affect the models’ performance, specifically in the context of EO tasks.
- Provide open-source access to all experimental details, including trained models, dataset details, train/evaluation configurations, and detailed performance scores.

## 2 Data & models

### 2.1 Data description

With the ever-growing availability of remote sensing data, there has been a significant effort by many research groups to prepare, label, and provide proper datasets that will support the development and evaluation of sophisticated machine learning methods. While there are many such datasets, both proprietary and publicly available, in this work, we focus on the latter – open-access publicly available dataset. Given this criterion, we select 22 open-access datasets usually considered in different EO studies for benchmarking DL approaches. The selected datasets have varying sizes (number of images), varying image types, image sizes, and formats, and, more importantly, related to different classification tasks.

Namely, we consider datasets related to multi-class and multi-label classification tasks, mainly addressing LULC applications. The objective of *multi-class classification* tasks is to predict one (and only one) class (label) from a set of predefined classes for each image in a dataset. *Multi-label classification*, on the other hand, refers to predicting multiple labels from a predefined set of labels for each image in the dataset [41] (e.g., an image can belong to more than one class simultaneously). In our experimental study, we consider 15 multi-class and seven multi-label datasets.

Table 1: Summary of the multi-class classification (MCC) datasets.

Name	Image type	#Images	Image size	Spatial resolution	#Labels	Predefined splits	Image format
UC Merced [9]	Aerial RGB	2100	256×256	0.3m	21	No	tif
WHU-RS19 [42]	Aerial RGB	1005	600×600	0.5m	19	No	jpg
AID [31]	Aerial RGB	10000	600×600	0.5m - 8m	30	No	jpg
Eurosat [43]	Sat. Multispectral	27000	64×64	10m	10	No	jpg/tif
PatternNet [44]	Aerial RGB	30400	256×256	0.06m - 4.69m	38	No	jpg
Resisc45 [8]	Aerial RGB	31500	256×256	0.2m - 30m	45	No	jpg
RSI-CB256 [45]	Aerial RGB	24747	256×256	0.3 - 3m	35	No	tif
RSSCN7 [46]	Aerial RGB	2800	400×400	n/a	7	No	jpg
SAT6 [47]	RGB + NIR	405000	28×28	1m	6	Yes	mat
Siri-Whu [48]	Aerial RGB	2400	200×200	2m	12	No	tif
CLRS [49]	Aerial RGB	15000	256×256	0.26m - 8.85m	25	No	tif
RSD46-WHU [50]	Aerial RGB	116893	256×256	0.5m - 2m	46	Yes	jpg
Optimal 31 [51]	Aerial RGB	1860	256×256	n/a	31	No	jpg
Brazilian Coffee Scenes (BSC) [52]	Aerial RGB	2876	64×64	10m	2	No	jpg
So2Sat [53]	Sat. Multispectral	400673	32×32	10m	17	Yes	h5

Table 2: Summary of the multi-label classification (MLC) datasets.

Name	Image type	#Images	Image size	Spatial resolution	#Labels	#Labels per image	Predefined splits	Image format
UC Merced (mlc) [54]	Aerial RGB	2100	256×256	0.3m	17	3.3	No	tif
MLRSNet [55]	Aerial RGB	109161	256×256	0.1m - 10m	60	5.0	No	jpg
DFC15 [56]	Aerial RGB	3342	600×600	0.05m	8	2.8	Yes	png
AID (mlc)[57]	Aerial RGB	3000	600×600	0.5m - 8m	17	5.2	Yes	jpg
PlanetUAS [58]	Aerial RGB	40479	256×256	3m	17	2.9	No	jpg/tiff
BigEarthNet 19 [36]	Sat. Multispectral	519284	20×20	60m	19	2.9	Yes	tif, json
			60×60	20m				
BigEarthNet 43 [59]	Sat. Multispectral	519284	20×20	60m	43	3.0	Yes	tif, json
			60×60	20m				
			120×120	10m				

Tables 1 and 2 summarizes the properties of the considered multi-class (MCC) and multi-label (MLC) classification datasets, respectively. The number of images across datasets is quite diverse, ranging from datasets with  $\sim 2K$

images to datasets with  $\sim 500K$  images. This also extends toward the number of labels per image, ranging from 2 to 60. Figure 1a visualizes the datasets with respect to their sizes, with the x-axis denoting the number of images (on a log scale) and the y-axis indicating the number of labels (with marker size denoting the number of labels per image) for each of the different datasets. Most of the datasets consist of Aerial RGB images (with only a few comprised of satellite multi-spectral data) that are different in spatial resolution, size, and format. Finally, we note the datasets that include predefined splits (for training, validation, and testing) given by the original authors and provide the splits for the ones that are missing, as further discussed in Section 3.1. An extended description of each dataset is given in Appendix D.

## 2.2 Model architectures

Current trends in EO image classification leverage the capabilities of DL architectures for computer vision, learning data representations that often lead to superior predictive performance. We recognize that there are many different approaches stemming from different model architectures and model variants. These can differ in various 'finer' details (e.g., number and width of layers, hyper-parameter values, and learning regimes), often developed for a particular task. Rather than seeking a state-of-the-art performance for each EO problem/dataset, in this study, we are interested in providing a more general evaluation framework and benchmarking models by analyzing their characteristics and unique properties through the lens of their predictive performance and learning efficiency across all datasets.

Therefore, our model-architecture (and parameter) choices are motivated by different architecture 'classes', such as the traditional convolutional architectures and the more recent attentional and multilayer-perceptron (MLP) architectures. This renders models with different sizes, training/inference time, different abilities in a transfer-learning setting, etc. More specifically, we investigate several architectures which have been traditionally used for EO image classification tasks, such as: AlexNet [60], VGG16 [61], ResNet [62] and DenseNet [63]. Moreover, we investigate more recent architectures, which include EfficientNet [64], ConvNeXt [65], Vision Transformer [39], Swin Transformer [40] and MLP Mixer [66], that have shown state-of-the-art performance in various vision tasks. In the following, we provide a brief overview of these architectures, highlighting their properties in Table 3.

Table 3: Summary of the representative model architectures considered in this study.

<b>Model</b>	<b>Year</b>	<b>#Layers</b>	<b>#Parameters</b>	<b>FLOPS</b>	<b>Based on</b>
AlexNet [60]	2012	8	$\sim 57 \cdot 10^6$	0.72 G	[67]
VGG16 [61]	2014	16	$\sim 134.2 \cdot 10^6$	15.47 G	[67]
ResNet50 [62]	2015	50	$\sim 23.5 \cdot 10^6$	4.09 G	[67]
ResNet152 [62]	2015	152	$\sim 58.1 \cdot 10^6$	11.52 G	[67]
DenseNet161 [63]	2017	161	$\sim 26.4 \cdot 10^6$	7.73 G	[67]
EfficientNet B0 [64]	2019	237	$\sim 5.2 \cdot 10^6$	0.39 G	[67] version: B0
Vision Transformer (ViT) [39]	2020	12	$\sim 86.5 \cdot 10^6$	17.57 G	[68] version: b_16_224
MLPMixer [66]	2021	12	$\sim 59.8 \cdot 10^6$	12.61 G	[68] version: b_16_224
ConvNeXt [65]	2022	174	$\sim 28 \cdot 10^6$	4.46 G	[67] version: tiny
Swin Transformer [40]	2022	24	$\sim 49.7 \cdot 10^6$	11.55 G	[67] version: v2 small

The first class of models we consider relies on convolutional architectures, which, in recent years, have driven many of the advances in computer vision. The architecture of convolutional neural networks (CNN) consists of many (hidden) layers stacked together, designed to process (image) data in the form of multiple arrays. Most typically, CNNs consist of a series of convolutional layers, which apply convolution operation (passing the data through a kernel/filter), forwarding the output to the next layer. This serves as a mechanism for constructing feature maps, with former layers typically learning low-level features (such as edges and contours), subsequently increasing the complexity of the learned features with deeper layers in the network. Convolutional layers are typically followed by pooling operations, which serve as a downsampling mechanism by aggregating the feature maps through local non-linear operations. In turn, these feature maps are fed to fully-connected layers, which perform the ML task at hand – in this case, classification. All the layers in a network employ an activation function. In practice, the intermediate, hidden layers employ a non-linear function such as rectified linear unit (ReLU) or Gaussian Error Linear Unit (GELU) as common choices. The choice of activation function in the final layer relates to the tasks at hand, typically a sigmoid function in the case of classification. CNN architectures can also include different normalization and/or dropout operators embedded among the different layers, which can further improve the network’s performance.

CNN architectures have been widely researched, with models applied in many contexts of remote sensing, and in particular EO image classification [11, 69, 70, 30]. This includes *AlexNet* [60], a pioneering architecture that introduced and successfully demonstrated the utility of the CNN blueprint, mentioned earlier, for computer vision tasks. Namely, even though the architecture of AlexNet has a modest depth (relative to more recent architectures) consisting of eight layers, it remains an efficient baseline approach for a variety of EO tasks [8, 10], leading to decent performance, especially when pre-trained with large image datasets [71]. We also consider the more sophisticated *VGG* [61], which employs a deeper architecture inspired by AlexNet. VGG has shown great performance in a variety of vision tasks, including EO-image classification problems [72, 73, 44]. There are two variants of VGG in practice, VGG16 and VGG19; both extend AlexNet mainly by increasing the depth of the network with 13 and 16 convolutional layers, respectively. In this study, we evaluate the performance of the former *VGG16*. VGGs employ kernels with smaller sizes than the ones typically used in AlexNet, demonstrating that stacking multiple smaller kernels are better able to extract more complex representations than one larger filter. While, in general, increasing the network depth by adding convolutional layers helps for learning more complex and more informative representations thereof, in practice, this can lead to several issues, such as the vanishing gradient problem [74], which impairs the network training.

The Residual neural networks (*ResNets*) [62, 75] tackle this issue explicitly by employing skip connections between blocks, therefore enabling better backprop gradient flow, better training, and, in general, better predictive performance. ResNet architecture follows a typical CNN blueprint: Stacking residual blocks (typically same-size CNN layers) and convolutional blocks (typically introducing a bottleneck via different-size CNN layers) together, followed by fully-connected layers. By employing skip connections, the ResNet architecture allows stacking multiple layers in a block, therefore training models with much deeper architectures. Here we investigate two variants with varying depths, *ResNet50* and *ResNet152*, with 50 and 152 layers, respectively. Since their inception, ResNets have

been a prevalent choice in practice. This also extends towards their utility for EO tasks, applied in the context of image classification and semantic segmentation [8, 76, 35, 30]. Dense Convolutional Networks (*DenseNets*) [63] are another well-performing architecture variant of ResNets that has demonstrated state-of-the-art results on many classification tasks, including applications in the domain of remote sensing [77, 78, 79]. As the name suggests, DenseNets consist of dense blocks, where each layer is connected to every preceding layer, taking an additional (channel-wise) concatenated input of the feature maps learned in the former layers. This differs from the ResNets, which propagate (element-wise) aggregated feature maps through the network layers. The architecture of DenseNets encourages feature reuse throughout the network, leading to well-performing and more compact models (with fewer trainable parameters than a ResNet of equivalent size), albeit at the cost of increased memory during training.

*EfficientNets* [64] are a recent class of lightweight architecture that alleviate such common computational difficulties, typical when scaling deep architectures on larger and/or harder problems. Namely, rather than scaling the architecture in one aspect of increasing the depth (number of layers) [62], width (number of channels) [75] or (input image) resolution [80]; EfficientNets implement compound scaling, that uniformly scales the architecture along the three dimensions simultaneously. Compound scaling seeks an optimal balance between these three dimensions, given the available resources and the task at hand. In turn, such an approach leads to substantially smaller models (than CNN variants of equivalent performance) while retaining state-of-the-art predictive performance. In the context of EO tasks, (variants of) EfficientNets have been successfully applied in different settings [81, 82, 83, 79], and have also been thoroughly investigated in the context of multi-label image classification tasks from BigEarthNet [30]. While there are eight variants of EfficientNets, differing in the size and complexity of the architectures, here we investigate the performance of the baseline *EfficientB0* architecture with 5.2M parameters, substantially lower than any of the other competing model architectures. Most recently, [65] introduce *ConvNeXt*, a novel class of convolutional architectures that leverage various successful design decisions of preceding convolutional and attentional architectures typically applied for vision tasks. Namely, ConvNeXt models implement various techniques at different levels: from reconfiguring details like activation functions and normalization layers, to redesigning more general architecture details related to residual/convolutional blocks, to modifications in the training strategies. This, in turn, leads to models that achieve good predictive performance, not only better than popular models from the class of convolutional architectures but also better than the more recent attentional architectures, such as transformers, discussed next. While there are several variants of the ConvNeXt architecture that mainly differ in their size, in this study, we evaluate the performance of the smallest variant, *ConvNeXt.tiny*. Note that, to our knowledge, this is the first application of ConvNeXt on EO-image classification tasks.

We next take the notion of the recent success of the class of attentional network architectures and study the performance of *Vision Transformers* (ViT) [39] in the context of EO-image classification tasks. Namely, ViTs inspire by the popular NLP (natural language processing) Transformer architecture [84], leveraging an attention mechanism for vision tasks. Much like the original Transformer that seeks to learn implicit relationships in sequences of word-tokens via multi-head self-attention, ViTs focus on learning such relationships between image patches. Typically they

employ a standard transformer encoder that takes a lower-dimensional (linear) representation of these image patches together with additional positional embedding from each, in turn, feeding the encoder-output to a standard MLP head. ViTs have shown excellent performance on various vision tasks, particularly when combined with pre-training from large datasets. This also includes several applications in remote sensing [85, 30, 86].

More recent and sophisticated, attentional network architectures such as the *Swin Transformers* (SwinT) [87, 40] rely on additional visual inductive biases by introducing hierarchy, translation invariance, and locality in the attention mechanism. Like ViTs, SwinT architectures also attempt to learn relationships between image patches but operate on image windows (a group of neighboring image patches). SwinTs focus on computing attention between patches within a window (locality), in turn shifting these windows to allow learning of cross-window attention (translation invariance). Starting with windows with smaller patches and increasing their size at each subsequent stage, SwinTs also allow for learning representations at different granularity (hierarchy). All this leads to SwinTs performing well in practice on a variety of vision tasks, including in the domain of remote sensing [88, 89, 90], often outperforming ViTs and other convolutional architectures. In this study, we evaluate the 'small' architecture variant of the latest version of Swin Transformers V2 [40].

In the context of vision tasks, an attention mechanism can be achieved differently (e.g., attending over channels and/or spatial information, etc.) and even employed with typically convolutional architectures [81, 91, 83]. One alternative that builds only on the classical MLP architecture is the *MLPMixer* [66]. Namely, similar to a transformer architecture, an MLP Mixer operates on image patches; and contains two main components: A block of MLP layers for 'mixing' the spatial, patch-level information on every channel; and a block of MLP layers for 'mixing' the channel-information of an image. This renders lightweight models, with performance on par with many much more sophisticated architectures, on a variety of vision problems, both more general as well as specific EO tasks [92, 30, 86]. We employ an MLP Mixer with an input size of 224x224 and a patch resolution of 16x16 pixels.

From each of the ten highlighted architectures, we evaluate two model versions: trained entirely on a given dataset and fine-tuned models that have been pre-trained on a different image dataset. This results in comparing 20 models on each predictive task, which are available on our repository.

### 3 Experimental design

#### 3.1 Training and evaluation protocol

To establish a unified evaluation framework and support the results' reproducibility, we generated train, validation, and test splits using 60%, 20%, and 20% fractions, respectively. All of the data splits were obtained using stratified sampling. This technique ensures that the distribution of the target variable(s) among the different splits remains the same [93]. We performed such stratification for all datasets except the ones which include predefined splits provided by the original authors. More specifically, for the *BigEarthNet* and *So2Sat* datasets, we use the train, validation, and test splits as provided in [59, 36, 53]. Since *SAT6*, *RSD46-WHU*, *DFC15* and *AID* datasets consist only of predefined

train and test splits, we further take 20% from the train part for validation. Finally, note that the PlanetUAS dataset was part of a competition, and as such, the test data is not publicly available. Therefore, we generated train, validation, and test splits from the original train data using the 60%, 20%, and 20% fractions, respectively.

All the models were trained using the same train splits, with parameters selection/search performed using the same validation splits. Additionally, to overcome over-fitting, we perform early stopping on the validation split for each dataset; the best checkpoint/model found (with the lowest validation loss) is saved and then applied to the original test split to obtain the final assessment of the predictive performance. All the train/validation/test splits for each dataset are available on our repository.

To better assess the generalization capabilities of the trained models, we evaluate their performance on different (in-domain) datasets not used for training. Specifically, we present two schemes of this evaluation: (1) performance measured on a holdout set compiled of test images with the same labels but from different datasets; (2) an exhaustive cross-dataset evaluation between pairs of datasets that contain the same labels. The former variant refers to a new test set consisting of 3216 images from the test splits of seven datasets (*RESISC45*, *UC Merced*, *CLRS*, *PatternNet*, *AID*, *RSI-CB256* and *WHU-RS19*) with labels present in all datasets (in our experiments, this results in five common labels: 'Forest', 'Parking', 'River', 'Harbor' and 'Beach'). We employ this evaluation setting only for multi-class classification tasks. In the latter variant, in a pairwise fashion, we evaluate every model on test splits from other datasets not used for training it. We measure the performance only on images with labels shared between the pairs of source (used for training the model) and target (used for evaluating the model) datasets. We employ this setting in both multi-class and multi-label classification scenarios. Note that in all cases, the models are only evaluated on the unseen datasets without additional fine-tuning. These configurations are also available on our repository.

During training, we perform *data augmentation* for each dataset by first resizing all the images to 256x256, followed by selecting a random crop of size 224x224. We then perform random horizontal and/or vertical flips. During evaluation/testing, we first resize the images to 256x256, followed by a central crop of size 224x224. We believe that this, in general, helps our models to generalize better on a given dataset. Also note that in the study, we are using only RGB images. In the case of the multispectral datasets (*Eurosat*, *So2Sat* and *BigEarthNet*), we computed the images in the RGB color space by combining the red (B04), green (B03), and blue (B02) bands. For the *Brazilian Coffee Scenes* dataset, we use images in green, red, and near-infrared spectral bands since these are most useful and representative for distinguishing vegetation areas, as suggested by the authors.

Since we train models on 22 datasets with a different number of classes, different training samples, and class distributions (as shown in Tables 1 and 2), we perform a hyperparameters search for each model and each dataset, to account for these variations. Namely, we search over different learning-rate values: 0.01, 0.001, and 0.0001. We use *ReduceLRonPlateau* as a learning scheduler which reduces the learning rate when the loss has stopped improving. Models often benefit from reducing the learning rate by a factor once learning stagnates. This scheduler tracks the values of the loss measure, reducing the learning rate by a given factor when there is no improvement for a certain number of epochs (denoted as 'patience'). In our experiments, we track the value of the validation loss with patience

set to 5 and a reduction factor set to 0.1 (the new learning rate will be  $lr * factor$ ). The maximum number of epochs is set to 100. Additionally, we also apply early stop criteria if no improvements in the validation loss are observed over 10 epochs. We use fixed values for some of the hyperparameters, such as batch size, which we set to 128. For optimization, we use *RAdam optimizer* [94] without weight decay. RAdam is a variant of the standard Adam [95], with a mechanism that rectifies the variance from the adaptive learning rate. This, in turn, allows for an automated warm-up tailored to the particular dataset at hand.

For each model architecture, we train two variants: (i) models trained entirely on a given dataset and (2) fine-tuned models previously trained on a different (and larger) image dataset. The former, which we refer to as models 'trained from scratch', refer to models trained only on the dataset at hand and initialized with random weights in the training procedure. The latter leverages transfer learning via model pre-training. The next section provides further details on how we use and fine-tune these pre-trained models. All models were trained on NVIDIA A100-PCIe GPUs with 40 GB of memory running CUDA version 11.5. We used the AiTLAS toolbox <sup>3</sup> to configure and run the experiments. All configuration files for each experiment are also available in our repository, along with the trained models. We believe this provides a standardized evaluation framework for EO image classification tasks.

### 3.2 Transfer learning strategy

In this study, we take the notion of *transfer learning* as a strategy that can lead to performance improvements of vision models on image classification tasks [32], in particular in EO domains [96]. In our problem setting, transfer learning allows downstream, task-specific models to leverage learned representations from model architectures pre-trained on much larger image datasets. This, in turn, often leads to (fine-tuned) models with much better generalization power using fewer training data (and training iterations), which is especially useful for tasks that stem from smaller datasets. In the case of DL models for image classification, two strategies are often used for performing transfer learning: (1) fine-tuning the model weights only for the last classifier layer or (2) fine-tuning the model weights of all layers in the network. The former approach retains the values of all but the last layer's weights of the model from the pre-training, keeping them 'frozen' during fine-tuning. The latter, on the other hand, allows the weights to change throughout the entire network during fine-tuning. In practice, this can lead to better generalization [97, 98] and higher accuracy.

In our experiments, we implement the latter approach. Starting with a pre-train model, we fine-tune each network entirely (the entire parameter set) for each specific dataset. Note that the choice of the pre-training dataset, and its relation to the domain of the downstream task, may also influence the predictive performance of the fine-tuned model [14]. Since here we are interested in a more general evaluation that considers 22 different datasets, we evaluate a standard approach for transfer learning using pre-trained model architectures on the ImageNet-1K [60] dataset (version V1). More specifically, we use implementations from the PyTorch vision catalog [67] for most models, except ViT and MLP Mixer, for which we base the implementations on [68].

---

<sup>3</sup><https://github.com/biasvariancelabs/aitlas>

Furthermore, to evaluate the effect of the pre-training dataset on the performance of the downstream model, in a set of smaller-scale experiments, we benchmark architectures that have been pre-trained using different 'in-domain' EO datasets. In particular, we evaluate two strategies: (i) models pre-trained entirely on an EO dataset and (ii) models pre-trained on both ImageNet-1K and an EO dataset. The latter relates to a two-stage pre-training strategy, where models are first pre-trained on ImageNet-1K, followed by intermediate tuning on an in-domain EO dataset, and finally, fine-tuning them on the target EO dataset. We evaluate these pre-training strategies by comparing models from two architectures (ViT and DenseNet) using four in-domain EO datasets for pre-training.

### 3.3 Evaluation measures

Evaluating the performance of machine learning models is a non-trivial task that is specific to the learning task at hand and dependent on the general objectives of the model being learned. Different evaluation metrics capture different aspects of the models' behavior and their predictive capabilities measured on image samples not used for training. Since the goal of this study analyzing the predictive performance of different DL models across different datasets on multi-class and multi-label classification tasks – we examine the experimental work through the lens of evaluation measures most suitable for these two tasks.

More specifically, for multi-class classification tasks, we report the following measures: Accuracy, Macro Precision, Weighted Precision, Macro Recall, Weighted Recall, Macro F1 score, and Weighted F1 score. Note that, since for these tasks, the micro-averaged measures such as F1 score, Micro Precision, and Micro Recall have values equal to accuracy, we do not report them. Note that, for image classification tasks, it is customary to report *top-n accuracy* (typically  $n$  is set to 1 or 5) [60], where the score is computed based on the correct label being among the  $n$  most probable labels outputted by the model. In this paper, we report *top-1 accuracy*, denoted as 'Accuracy' unless stated otherwise. For multi-label classification tasks, we report Micro Precision, Macro Precision, Weighted Precision, Micro Recall, Macro Recall, Weighted Recall, Micro F1 score, Macro F1 score, Weighted F1 score, and mean average precision (mAP). Since all measures, but mAP, require setting a threshold on the predictions, we choose a threshold value of 0.5 for all models and settings. Further details and definitions of the evaluation measures used in the study are given in Appendix A. We also provide additional performance details in terms of confusion matrices of each experiment, allowing for a more detailed (per class/label) analysis of model performance (reported in Appendix D).

## 4 Results

We present the results of a large-scale study comparing different DL models for multi-class (MCC) and multi-label classification (MLC) tasks from 22 datasets. To this end, we evaluate models from 10 architectures: AlexNet, VGG16, ResNet50, ResNet152, DenseNet162, EfficientNetB0, ConvNeXt, Vision Transformer (ViT), Swin Transformer (SwinT) and MLP Mixer. For each model architecture, we evaluate two variants: (i) models trained from scratch and (2) fine-tuned models previously trained on the ImageNet-1K dataset. We additionally assess the performance of models pre-trained using in-domain EO datasets. In the remainder, we outline and discuss the following:

- Performance of models trained from scratch with respect to the two types of tasks
- Benefits of pre-training models of different architectures and their effect in view of the dataset properties
- Models' ability to generalize on unseen in-domain datasets
- The choice of the pre-trained dataset and its effect on the performance of the downstream model
- The 'performance vs. cost of model training' trade-off between the considered modeling approaches
- Common issues that affect the models' predictive performance in the context of EO applications.

Detailed results of each experiment, with additional performance measures, are given in Appendices B, C and D.

#### 4.1 Training models from scratch

We begin by analyzing the performance of models trained from scratch, i.e., models initialized with random weights during training. Tables 4 and 5 present these results for the MCC and MLC tasks, respectively. Table 4 reports the accuracy (%) of the models learned from scratch for the 15 MCC datasets. It also reports the rank of the models, estimated based on their performance and averaged over the 15 datasets. The results show that, in general, convolutional architectures, especially the DenseNet, the EfficientNet, and the two ResNets, consistently perform well. This is even more evident for datasets such as PatternNet, RSI-CB256, and SAT6, where the DenseNet (and the other top-ranked models) lead to near-perfect results (accuracy greater than 99%). More specifically, DenseNet is the best-performing model in more than half of the tasks (9 out of 15) and achieves accuracy greater than 90% in 8 tasks. These performances are generally much lower for smaller datasets, such as WHU-RS19, Optimal31, UC Merced, SIRI-WHU, RSSCN7, and CLRS. However, the most challenging task is *So2SAT*, where EfficientNetB0 achieves the highest accuracy of 65.17%, while many of the models trail behind with a performance of 55-60%. These results are consistent with previous findings [35], suggesting clear signs of over-fitting, influenced by the quality and size of the images in the dataset. The two transformer architectures (SwinT and ViT), the MLP Mixer, and the latest ConvNeXt models are ranked at the bottom (only better than AlexNet), with lower, but, in many cases, still practically comparable performance to the leading DenseNets.

Next, we shift our focus to MLC tasks. Table 5 reports the mean average precision (%) of the models learned from scratch across the 7 MLC datasets. While DenseNets rank the best, they achieve the best result in only 1 out of 7 tasks. The second-ranked SwinT models achieve the best performance in 3 tasks with comparable performance in the remaining 4. Unlike the MCC tasks, the performance difference to other convolutional models (i.e., the two ResNets and the EfficientNetB0) here is much smaller. Moreover, most models were only able to achieve high performance (above 90%) on two tasks, *DFC15* and *MLRSNet*, with DenseNet and ResNet50 achieving the best results. However, this is an expected result, as MLC tasks are generally more challenging than MCC tasks. This can be attributed to two things in particular: First, in many cases, the semantic labels can be very similar, which makes many of the models struggle. Second, MLC datasets tend to have a more significant class/label imbalance, in

Table 4: Accuracy (%) of models trained from scratch on multi-class classification datasets. Bold indicates best performing model for a given dataset. We report the *average rank* of a model (lower is better), ranked based on the performance and averaged across the 15 datasets.

Dataset \ Model	AlexNet	VGG16	ResNet50	ResNet152	DenseNet161	EfficientNetB0	ViT	MLPMixer	ConvNeXt	SwinT
WHU-RS19	66.169	68.657	79.602	80.597	<b>80.597</b>	75.622	74.627	69.652	72.139	78.607
Optimal31	55.108	56.720	67.204	62.903	<b>71.237</b>	68.548	62.634	59.140	58.871	66.129
UC Merced	81.190	78.571	85.238	84.048	<b>86.190</b>	84.286	83.095	82.381	84.286	81.429
SIRI-WHU	83.750	84.792	<b>88.958</b>	88.750	86.667	86.042	86.250	82.5	84.167	85.833
RSSCN7	80.536	81.607	82.679	82.679	<b>87.321</b>	83.929	86.071	83.214	83.036	82.5
BCS	89.410	89.410	89.236	88.542	<b>90.799</b>	85.417	87.847	86.285	84.375	89.236
AID	81.350	81.950	89.050	89.9	<b>93.300</b>	90.050	79.350	71.750	81.1	87.700
CLRS	71.4	76.067	85.567	82.3	<b>86.167</b>	82.267	65.467	61.133	69.167	80
RSI-CB256	97.354	98.828	98.828	<b>99.152</b>	99.131	99.111	98.121	98.424	98.444	99.091
Eurosat	96.167	97.185	97	97.407	97.630	<b>97.796</b>	95.037	95.5	95.426	95.722
PatternNet	97.829	97.911	99.063	98.882	<b>99.243</b>	98.832	96.694	98.832	97.829	98.520
RESISC45	82.159	83.889	92.333	90.683	<b>93.460</b>	91.365	81.016	69.413	85.937	88.730
RSD46-WHU	86.032	88.625	90.549	89.944	92.211	90.612	86.466	81.253	88.693	91.806
So2Sat	56.511	62.271	59.587	61.477	55.428	<b>65.173</b>	55.333	53.580	60.154	57.128
SAT6	99.272	99.564	<b>100</b>	99.998	99.995	99.998	99.985	99.984	99.998	99.980
<i>Avg. Rank</i>	8.13	6.60	3.27	3.47	<b>2.00</b>	3.33	7.33	8.07	6.60	5.47

Table 5: Mean average precision (mAP %) of models trained from scratch on multi-label classification datasets. Bold indicates best performing model for a given dataset. We report the *average rank* of a model (lower is better), ranked based on the performance and averaged across the 7 datasets.

Dataset \ Model	AlexNet	VGG16	ResNet50	ResNet152	DenseNet161	EfficientNetB0	ViT	MLPMixer	ConvNeXt	SwinT
AID (mlc)	68.780	69.206	70.867	69.646	71.218	<b>72.889</b>	65.581	64.235	65.595	69.548
UC Merced (mlc)	75.516	76.797	79.867	73.657	85.414	79.874	<b>87.142</b>	75.677	72.271	81.071
DFC15	88.099	89.871	94.675	94.188	<b>95.848</b>	93.973	94.164	91.663	89.564	94.349
Planet UAS	60.282	60.682	64.192	64.956	64.738	63.868	59.414	58.550	61.277	<b>65.229</b>
MLRSNet	90.850	91.524	<b>95.259</b>	93.982	94.745	94.395	87.250	85.281	90.710	94.099
BigEarthNet 19	75.711	77.989	78.726	78.519	79.725	79.211	75.871	77.005	77.909	<b>80.586</b>
BigEarthNet 43	56.082	58.969	64.343	62.736	63.390	62.173	57.410	58.772	60.472	<b>67.487</b>
<i>Avg. Rank</i>	8.57	6.57	3.00	4.71	<b>2.14</b>	3.86	7.29	8.57	7.71	2.57

contrast to MCC datasets’ more uniform class distribution. In this context, the most challenging MLC tasks overall are *PlanetUAS* and *BigEarthNet43*, where the best performing SwinT models achieve mAP of 65.229% and 67.487%, respectively. Finally, similar to the previous MCC analysis, ViT, MLP Mixer, and ConvNeXt remain only better ranked than AlexNet. Nevertheless, their performance on these MLC tasks is much more competitive, for instance, in the case of ViT, which is the best model on the *UC Merced* task.

#### 4.2 The benefits of model pre-training

While training models from scratch leads to decent performance, in practice, leveraging pre-trained models can lead to significant performance improvements on image classification tasks [32], and in particular on tasks in EO domains [96].

This is also the general conclusion from our analysis. When using models that were first pre-trained on ImageNet-1K and then fine-tuned on the specific datasets, we found that: *Pre-trained models lead to substantial performance improvements compared to models trained from scratch*. Figure 2 illustrates this performance-improvement trend for different models across the 22 MCC and MLC tasks. We find that pre-training significantly improves the performance of all the evaluated models. Notably, we observe that the transformer models, based on either ViT or SwinT

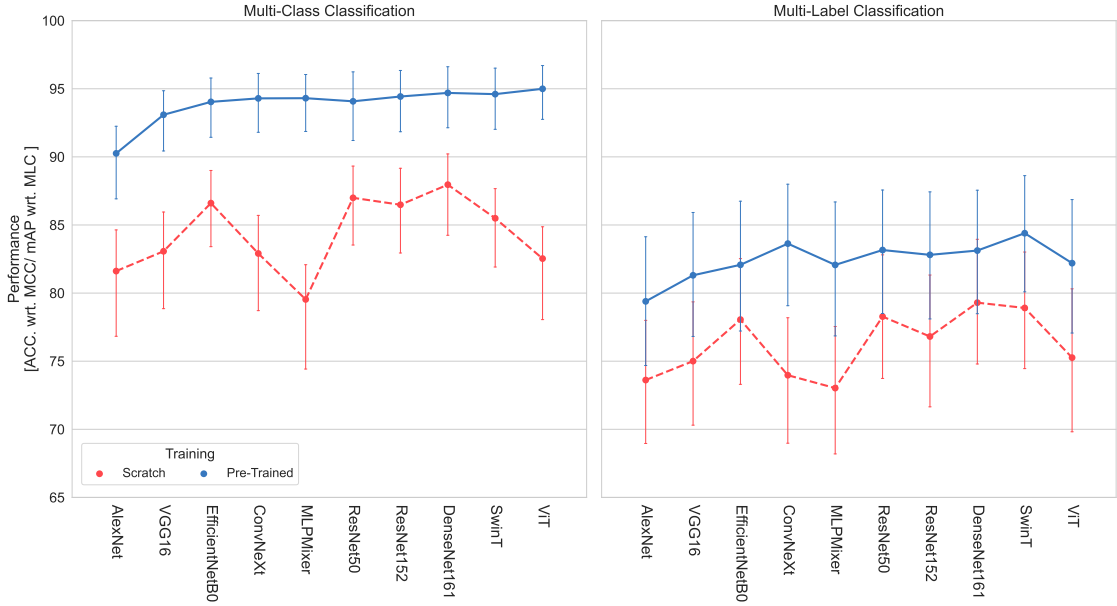


Figure 2: **Comparison of average performance improvement** of models from the 10 different architectures when trained from scratch (**red**) and employing pre-trained models (**blue**) across (**left**) MCC and (**right**) MLC datasets. Error bars indicate confidence interval of 68%. Models are ordered (worst to best) based on the average performance-rank of the pre-trained variants across all of the 22 datasets. Model pre-training leads to substantial performance improvements.

architectures, benefit the most from pre-training, followed by MLPmixer and ConvNeXt models. This is a significant improvement over the models trained from scratch. These results, especially for the case of ViT, are consistent with previously reported findings [39, 30].

Table 6: Accuracy (%) of models pre-trained on ImageNet-1K on multi-class classification datasets. Bold indicates best performing model for a given dataset. We report the *average rank* of a model (lower is better), ranked based on the performance and averaged across the 15 datasets.

Dataset\Model	AlexNet	VGG16	ResNet50	ResNet152	DenseNet161	EfficientNetB0	ViT	MLPMixer	ConvNeXt	SwinT
WHU-RS19	93.532	99.005	99.502	98.01	<b>100</b>	99.502	99.502	98.507	99.005	99.502
Optimal31	80.914	88.71	92.204	92.473	94.355	91.667	<b>94.624</b>	92.742	93.011	92.473
UC Merced	92.143	95.476	98.571	<b>98.810</b>	98.333	98.571	98.333	98.333	97.857	98.571
SIRI-WHU	92.292	93.958	95	<b>96.25</b>	95.625	95	95.625	95.208	<b>96.25</b>	95.625
RSSCN7	91.964	93.929	95	95	94.821	95.536	<b>95.893</b>	95.179	94.643	95.179
BCS	89.583	90.972	92.014	92.361	92.708	91.319	92.014	93.056	91.493	<b>93.403</b>
AID	92.9	96.1	96.55	97.2	97.25	96.25	<b>97.750</b>	96.7	96.95	97.4
CLRS	84.1	89.9	91.567	91.9	92.2	90.5	<b>93.200</b>	90.1	91.1	92.533
RSI-CB256	99.354	99.051	99.677	<b>99.859</b>	99.737	99.717	99.758	99.657	99.596	99.677
Eurosat	97.574	98.148	98.833	<b>99</b>	98.889	98.907	98.722	98.741	98.778	98.944
PatternNet	99.161	99.424	<b>99.737</b>	99.49	<b>99.737</b>	99.539	99.655	99.704	99.671	99.688
RESISC45	90.492	93.905	96.46	96.54	96.508	94.873	<b>97.079</b>	95.952	96.27	96.587
RSD46-WHU	90.646	92.422	94.158	94.404	<b>94.507</b>	93.387	94.238	93.673	93.627	93.536
So2Sat	59.203	65.375	61.903	65.169	65.756	65.801	<b>68.551</b>	67.066	66.169	65.950
SAT6	99.98	99.993	<b>100</b>	<b>100</b>	<b>100</b>	99.988	99.998	99.995	99.999	99.999
<i>Avg. Rank</i>	9.93	8.67	4.67	3.80	3.13	5.87	<b>3.07</b>	5.33	5.47	3.20

Tables 6 and 7 present the detailed results of these analyses for MCC and MLC tasks, respectively. Similar to the analyses in the previous section, we report model accuracy (%) in the case of MCC tasks and mean average precision (%) in the case of MLC tasks. We also report the rank of the models, averaged over the respective datasets. Consider-

Table 7: Mean average precision (mAP %) of models pre-trained on ImageNet-1K on multi-label classification datasets. Bold indicates best performing model for a given dataset. We report the *average rank* of a model (lower is better), ranked based on the performance and averaged across the 7 datasets.

Dataset \ Model	AlexNet	VGG16	ResNet50	ResNet152	DenseNet161	EfficientNetB0	ViT	MLPMixer	ConvNeXt	SwinT
AID (mlc)	75.906	79.893	80.758	80.942	81.708	78.002	81.539	80.879	<b>82.298</b>	82.254
UC Merced (mlc)	92.638	92.848	95.665	96.01	96.056	95.384	96.699	96.34	96.431	<b>96.831</b>
DFC15	94.057	96.566	97.662	97.6	97.529	96.787	97.617	97.941	97.994	<b>98.111</b>
Planet UAS	64.048	65.584	65.528	64.825	66.339	64.157	66.804	67.330	66.447	<b>67.837</b>
MLRSNet	93.399	94.633	96.272	96.432	96.306	95.391	96.41	95.049	95.807	<b>96.620</b>
BigEarthNet 19	77.147	78.418	79.983	79.776	79.686	80.221	77.31	77.288	80.283	<b>81.384</b>
BigEarthNet 43	58.554	61.205	66.256	64.066	64.229	64.589	58.997	59.648	66.166	<b>67.733</b>
<i>Avg. Rank</i>	10.00	7.86	5.14	5.43	5.00	6.86	4.86	5.71	3.00	<b>1.14</b>

ing MCC tasks (Table 6), most models achieve very good performance (accuracy over 90%) on 14 (out of 15) tasks, with (almost) perfect results in five of those. Notably, we observed significant performance improvements, compared to model counterparts trained from scratch, on smaller datasets (such as *WHU-RS19*, *Optimal31*, *UC Merced*, *SIRI-WHU*, *RSSCN7*, and *CLRS*), reaffirming the utility of transfer learning from large datasets in the context of EO image classification tasks. In terms of model architectures, the ViT ranks at the top among the model architectures, achieving the best performance in 6 out of 15 cases, followed by DenseNet161, SwinT, and ResNet152 with lower but comparable performance. Transformer architectures, and ViTs in particular, typically require large amounts of training data [39, 99] for learning robust, good performing models. As a result, using pre-trained models and fine-tuning them leads to substantial performance improvements, compared to training them from scratch. The performance of ViTs is further highlighted for the case of the challenging *So2SAT* task, where the ViT model leads to an accuracy of 68.55%, in contrast to the next ranked DenseNet and SwinT with an accuracy of 65.75% and 65.95%, respectively. In this specific case of *So2SAT*, we observed that over-fitting remains an issue, even for pre-trained models. Our further investigation of the train/validation loss trends showed that, regardless of the model at hand, with the training loss decreasing, the validation errors increase almost instantly (after 1-2 epochs) - a typical trend observed in over-fitting models (see Figure D.46 that illustrates such behavior in a ViT model). This, fortunately, is not the case for the remaining tasks, where we observed a decent performance overall. Most models, especially the top half ranked, achieved stable and mostly comparable performance.

The benefits of pre-training models also extend to MLC tasks (Table 7), in several cases with significant performance gains, compared to model counterparts trained from scratch. In particular, we found that pre-training can lead to minor improvements (1%-2%) on challenging tasks such as *PlanetUAS* and *BigEarthNet43* (mAP of 67.837% and 67.733% achieved by SwinTs); to more considerable improvements (up to 15%) in some cases such as *AID* and *UCMerced* (mAP of 82.298% and 96.83% obtained by ConvNeXt and SwinT, respectively). Also, in this case, we found that the transformer models benefited the most from pre-training. This is in line with studies[87, 40] that highlight the significance of pre-training to the generalization performance of these types of models. Notably, SwinT models ranked the best overall and achieved the best performance on 6 (out of the 7) tasks. They are followed by ViT and ConvNeXt, with comparable performance on most tasks.

### 4.3 Generalization capabilities to unseen data

We further investigate the generalization ability of the trained models by evaluating their performance across datasets not used during training. In particular, we present results from two evaluation settings: (1) performance measured on a holdout set compiled of test images with shared labels and (2) an exhaustive cross-dataset evaluation between pairs of datasets with overlapping labels. First, we analyze the predictive performance of all models when applied to the same holdout set with 3216 images sampled from the test splits from seven MCC datasets (*RESISC45*, *UC Merced*, *CLRS*, *PatternNet*, *AID*, *RSI-CB256* and *WHU-RS19*) using only images with labels shared among the seven datasets: 'Forest', 'Parking', 'River', 'Harbor', and 'Beach'. Figure C.1 (in Appendix C) presents further details of the distribution of images in the holdout set w.r.t. source datasets and labels. We evaluate and report the predictive performance of pre-trained models from all ten architectures. Note that here we only evaluate the models on the holdout set without additional fine-tuning. Table 8 reports the predictive performance assessed using accuracy (%) as an evaluation measure.

The results show that ViT models are able to generalize well to unseen images from other in-domain datasets. Namely, in many cases, ViT models perform better than the competitors, further supporting previous results regarding their performance on MCC tasks. The performance of ViTs is followed by models based on more recent architectures, such as SwinT, MLPMixer, and ConvNeXt, which show worse but, in many cases, practically comparable performance. With respect to specific datasets, our experiments show that models fine-tuned on the *CLRS* and *RESISC45* datasets were able to achieve much better performance than the others (with ViT models achieving 92.6% in the case of *CLRS*). We hypothesize that such performance may be related to the particular properties of these datasets: Both *CLRS* and *RESISC45* are multi-resolution datasets (containing images at different spatial resolutions) with a large number of diverse labels. However, this is not the case for models fine-tuned on *PatternNet* and *RSI-CB256*. While models trained and evaluated on these datasets separately show great performance (99% accuracy), this performance decreases significantly when evaluated on a holdout set (down to 66.79% and 65.2% for *RSI-CB256* and *PatternNet*, respectively). These results, along with results from models learned from scratch (Table 4), are indicative of both datasets being easily learned, producing models that are not able to generalize well to other unseen images and classification tasks.

In the second experimental setup, we employ the following pairwise evaluation scheme. We consider pairs of

Table 8: Accuracy (%) of models pre-trained on ImageNet-1K and fine-tuned on a specific source dataset and evaluated on the common test dataset with shared labels. Bold indicates best performing model for a given source dataset.

Dataset \ Model	AlexNet	VGG16	ResNet50	ResNet152	DenseNet161	EfficientNetB0	ViT	MLPMixer	ConvNeXt	SwinT
RESISC45	66.853	78.514	81.063	84.08	84.111	77.985	<b>86.007</b>	82.121	84.422	83.706
UC Merced	63.371	67.04	76.057	73.01	74.254	74.44	75.995	<b>79.478</b>	75.902	72.326
CLRS	80.037	83.427	89.801	88.557	89.024	86.07	<b>92.6</b>	89.646	89.303	90.299
PatternNet	43.501	52.332	56.965	54.54	56.716	60.044	64.739	62.687	59.391	<b>65.205</b>
AID	71.393	69.714	79.384	80.1	66.169	77.892	<b>83.862</b>	77.954	79.851	79.789
RSI-CB256	56.872	61.412	58.893	63.65	64.832	61.723	66.014	<b>66.791</b>	64.677	66.294
WHU-RS19	61.101	62.624	71.953	73.321	72.388	68.284	72.917	74.036	<b>74.876</b>	71.144
Avg. Rank	9.71	8.71	5.43	5.29	5.86	6.86	<b>2.14</b>	3.29	3.57	4.14

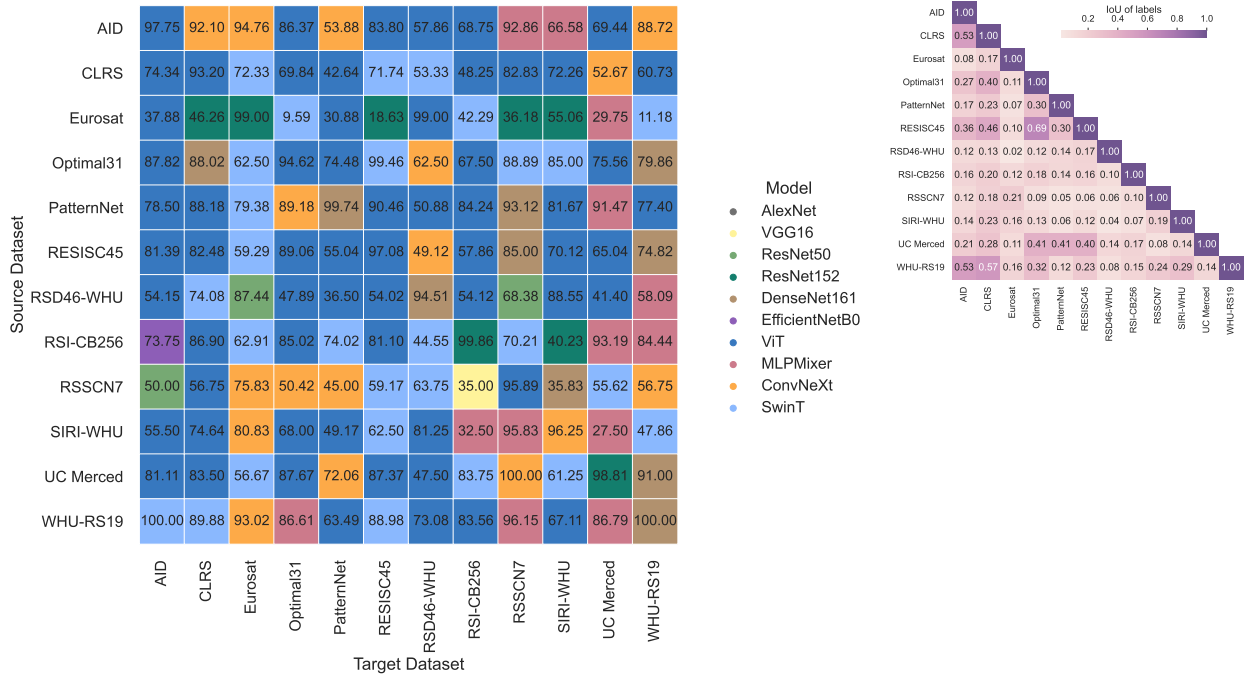


Figure 3: **Model generalization on multi-class classification tasks:** Comparison of the best performing pre-trained models (left) from the 10 different architectures (color-coded) in terms of accuracy (% acc. is indicated in each field); the models are fine-tuned on *source* dataset and evaluated on images with common/overlapping labels in *target* dataset. The heatmap (right) reports the label overlap between each pair of datasets, in terms of IoU. Transformer-based models, in particular the ViT models, perform the best when evaluated on other in-domain MCC datasets.

*source* and *target* datasets: We take pre-trained models that have been fine-tuned on a *source* dataset and evaluate them on test images from a *target* dataset. Note that we only *evaluate* the models on the target dataset without additional fine-tuning. We measure the performance only on a subset of images with shared labels between the source and target datasets. Therefore, for this experiment, we selected datasets with at least 0.15 IoU<sup>4</sup> overlap of labels with at least one other dataset. This resulted in pairs from 12 (out of 15) MCC datasets and 4 (out of 7) MLC datasets, yielding 256 comparisons of pre-trained models from each of the ten considered architectures. Figures 3 and 4 present the performance of the best model for each MCC and MLC comparison in terms of accuracy (%) and mAP (%), respectively. They also provide a summary of the overlap between each pair of datasets in terms of IoU. Detailed results of all comparisons, per architecture, are given in Appendix C.

The results support our earlier findings that the *transformer*-based models, in particular the ViT models (on MCC tasks) and the SwinT models (on MLC tasks), perform best when applied to other in-domain datasets. More specifically, when considering MCC tasks, the transformer-based models perform best in almost 2/3 of the comparisons, with the ViT models alone performing best in ~40% of them. ViTs are followed by SwinT, ConvNeXt, and MLP Mixer models that, in many cases, showed practically comparable performance. We observed that convolutional models such

<sup>4</sup>Intersection over Union (IoU), measures the overlap between two sets. Values range from 0 to 1, where 0 indicates no overlap and 1 indicates complete overlap between the sets

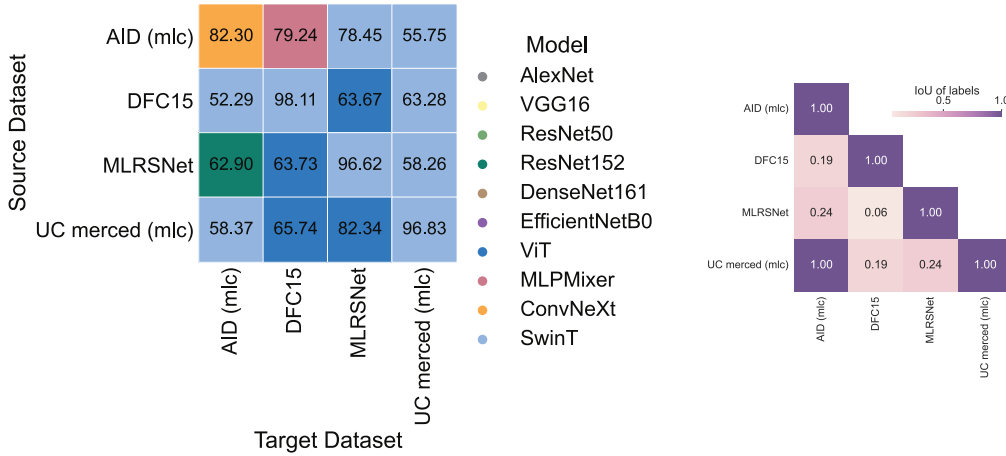


Figure 4: **Model generalization on multi-label classification tasks:** Comparison of the best performing pre-trained models (left) from the 10 different architectures (color-coded) in terms of **mean average precision** (% mAP is indicated in each field); the models are fine-tuned on *source* dataset and evaluated on images with common/overlapping labels in *target* dataset. The heatmap (right) reports the label overlap between each pair of datasets, in terms of IoU. In general, transformer-based models, in particular the SwinT models, lead to the best performance on MLC tasks.

as DenseNets, which exhibited good performance in our previous analyses (when evaluated on test images from the same dataset), generally lead to worse performance than models from more recent architectures. The dominance of the transformer-based models also extends to MLC tasks, with SwinT models producing the best overall performance, followed closely by ViT models. Note that these empirical results are also consistent with other studies [100, 99, 101], that highlight the robustness and good generalization capabilities of transformer-based models for general-domain images.

#### 4.4 Domain-adaptive transfer learning

Having demonstrated the practical benefits and generalization capabilities of using pre-trained models, we further investigate the impact of the pre-trained dataset on the performance of the downstream model. As we focus on particular domains of interest that leverage satellite imagery, we evaluate whether and how choosing more appropriate in-domain EO pre-training datasets (and strategies) affects downstream predictive performance. Our experimental setup aims to investigate two different strategies for such in-domain pre-training: (i) in-domain only, where models are pre-trained entirely on an EO dataset (ii) two-stage pre-training, where models are pre-trained on a combination of ImageNet-1K and an EO dataset. The former strategy is analogous to the ImageNet-1K pre-training strategy but uses a different EO dataset. In the second strategy, on the other hand, the models are first pre-trained on ImageNet-1K, followed by intermediate tuning on an in-domain EO dataset, before fine-tuning the models on the target EO dataset.

Rather than evaluating all architectures, in this set of experiments, we evaluate two types of architectures: a ViT and a DenseNet161, as representatives of transformer and convolutional architectures that have shown overall good performance in our previous experiments. Specifically, we analyze their performance on six tasks (3 MCC and 3 MLC) that proved somewhat challenging for these models: *CLRS*, *Optimal31*, *So2SAT*, *AID (mlc)*, *PlanetUAS*, and

Table 9: Comparison of pre-training strategies for (a) Vision Transformers (ViT) and (b) DenseNets161 using 4 in-domain EO datasets (SAT6, RSD46-WHU, MLRSNet, RESISC45) and ImageNet-1K. We report their performance on 3 multi-class and 3 multi-labels classification tasks, in terms of accuracy (% Acc.) and mean average precision (% mAP), respectively.

(a)

In-domain dataset	Pre-training strategy	Target dataset					
		CLRS [%Acc.]	Optimal31 [%Acc.]	So2Sat [%Acc.]	AID (mlc) [%mAP]	Planet UAS [%mAP]	BigEarthNet 19 [%mAP]
SAT6	In-domain only	60.767	58.065	54.672	62.2	59.538	74.618
	ImageNet-1K + In-domain	71.2	68.011	64.284	67.595	62.356	76.009
RSD46-WHU	In-domain only	72.267	75.269	57.859	71.209	61.015	75.529
	ImageNet-1K + In-domain	91.067	92.204	65.322	80.102	66.46	76.809
MLRSNet	In-domain only	71.7	77.688	54.746	72.915	60.985	74.827
	ImageNet-1K + In-domain	91.033	95.430	64.321	83.069	64.574	77.308
RESISC45	In-domain only	68.7	86.022	57.446	69.552	61.457	75.345
	ImageNet-1K + In-domain	92.533	98.925	66.876	82.888	66.654	76.682
/	ImageNet-1K only	93.2	94.624	68.551	81.539	66.804	77.31

(b)

In-domain dataset	Pre-training strategy	Target dataset					
		CLRS [%Acc.]	Optimal31 [%Acc.]	So2Sat [%Acc.]	AID (mlc) [%mAP]	Planet UAS [%mAP]	BigEarthNet 19 [%mAP]
SAT6	In-domain	65.467	55.914	58.455	59.363	59.419	76.745
	ImageNet-1K + In-domain	89.467	85.215	65.334	74.653	64.918	79.773
RSD46-WHU	In-domain	89.267	86.559	60.89	77.056	65.101	79.374
	ImageNet-1K + In-domain	91.8	93.280	65.152	82.339	66.161	79.867
MLRSNet	In-domain	89.7	92.742	61.03	80.144	64.53	79.646
	ImageNet-1K + In-domain	91.367	96.505	62.808	84.07	64.859	79.945
RESISC45	In-domain	86.433	93.011	60.009	73.199	63.532	78.309
	ImageNet-1K + In-domain	91.267	98.387	64.011	82.936	66.276	79.695
/	ImageNet-1K only	92.2	94.355	65.756	81.708	66.339	79.686

*BigEarthNet 19*. We select four different in-domain datasets for our pre-training: *SAT6*, *RSD46-WHU*, *MLRSNet* and *RESISC45*; based on the overall performance achieved in the previous analyses, their size (number of images), and their heterogeneity (in terms of semantic labels). Table 9 reports the results of these experiments.

Our general conclusion regarding pre-training remains: Pre-trained models based entirely on EO datasets can still outperform their counterparts trained from scratch. However, we find that the choice of the pre-training dataset has a significant impact on the downstream performance and is not necessarily related to the quality of the pre-training dataset (measured as stand-alone performance) or solely to its size. For instance, we found that models pre-trained entirely using *SAT6* (a dataset on which most models performed very well) performed much worse than the other pre-trained counterparts and, in some cases, even worse than models trained from scratch. This is not the case when pre-training models on *RSD46-WHU*, *MLRSNet*, and *RESISC45*, which led to better performance, compared to their counterparts trained from scratch (in both cases of ViT and DenseNets), albeit worse than models pre-trained on ImageNet-1K.

Importantly, we found that using a combined pre-training procedure, with ImageNet-1K followed by an in-domain dataset, can lead to improvements (up to 5%), especially when combined with *MLRSNet* or *RESISC45* datasets. This is specifically the case for *Optimal31* and *AID (mlc)*, where models from both ViT and DenseNet161 architectures were able to outperform their counterparts pre-trained only on ImageNet-1K. These results suggest that using datasets for

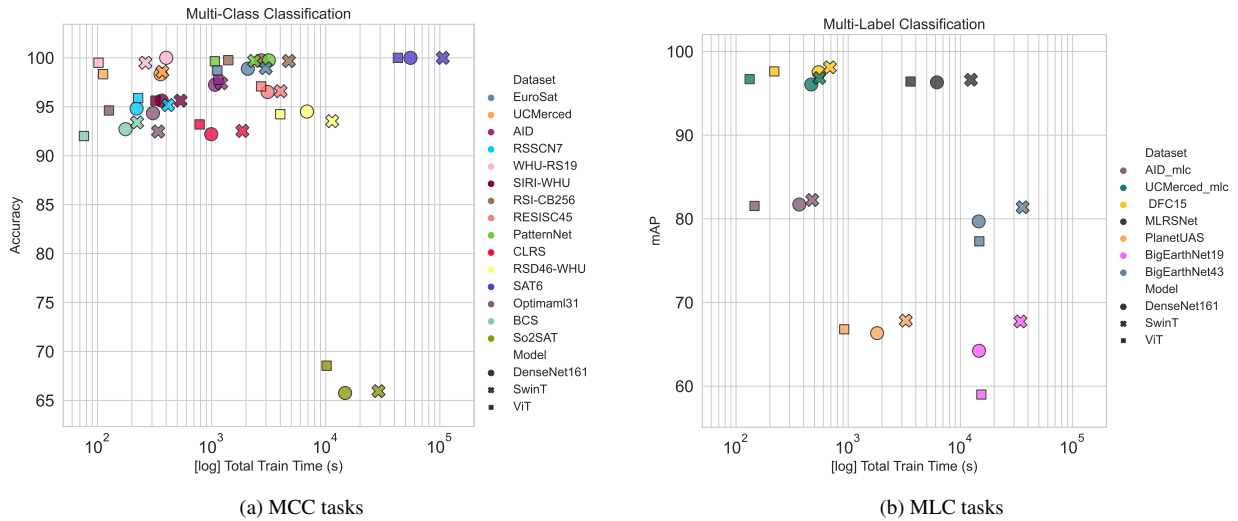


Figure 5: **Performance vs. total training time** comparison of the overall top-3 performing *pre-trained* model architectures, ViT, DenseNet161 and SwinT (denoted with different markers); evaluated on **(left)** MCC and **(right)** MLC datasets (color-coded). Performance is reported as accuracy (%) and mean average precision (mAP %) for MCC and MLC tasks, respectively. Note the log scale of the total training time (seconds).

intermediate fine-tuning that contain images at different resolutions with heterogeneous (but potentially semantically similar) labels, in addition to ImageNet-1K, can lead to performance improvements. However, in most cases, we did not observe neither practical nor significant benefits for using a combined pre-training procedure with an additional in-domain dataset that would justify the additional computational overhead for training such models.

#### 4.5 The 'performance vs. training cost' trade-off

Having established the performance of our evaluated models and demonstrated the clear benefits of using pre-trained models, we focus here on another line of comparison - the cost of model training. Recall from Section 2.2, and in particular Table 3, that we study model architectures that differ significantly in the number of learnable parameters. Typically, larger models require more computing resources and much more training time than smaller models. In our experimental setup, we train all models on the same computing infrastructure, under the same conditions, and with the same training/evaluation setup (in terms of hyperparameters and data partitioning). Therefore we can directly analyze the 'performance vs. training cost' (in terms of total training time) trade-off for each model variant from the ten different architectures (either pre-trained or trained from scratch) across the 22 datasets. This way, we can explicitly measure the benefits of each model and make further modeling decisions based on the performance of the models and the 'cost' of training them.

Figure 5 illustrates the trade-off for the top-3 best performing model architectures overall (as shown in Tables 6 and 7), DenseNet, ViT, and SwinT; applied to the 22 MCC and MLC tasks. While the performance analyses showed many similarities between these models, the difference between them in terms of training times is much more pronounced. In general, ViT requires less training time than both DenseNets and SwinTs. DenseNets have nearly a quarter of the



Figure 6: **Total training time** of pre-trained models for each of the (a) MCC and (b) MLC datasets. The training time of each model architecture (denoted with different colors) is depicted as a fraction (%) of the cumulative training time for each dataset. Furthermore, (c) and (d) illustrate the average time per epoch of each model variant on (c) MCC and (d) MLC tasks, comparing the (red) pre-trained model variants (from (a) and (b)) to their counterparts (blue) trained from scratch.

number of parameters of ViT but achieve almost half fewer FLOPS (floating-point operations per second) than them. For MCC tasks, ViT models generally result in comparable/better predictive performance than DenseNet models and, in many cases, require half the training time. SwinT models, on the other hand, are much more demanding. In almost all cases, training SwinT models takes up to 2-3 times longer than training ViTs and DenseNets. This is also true for MLC tasks, where SwinT models perform the best performance but at the cost of significant training time. These findings further support previous results [87], which point out that Swin transformers (the 'small' variant) have slower training and inference performance than Vision Transformers, which have significantly more parameters but achieve considerably more FLOPS. For an extended illustration of these trade-offs, covering all 10 model architectures, see Figure B.1 in the Appendix B.

We can further analyze these trends in training time trends for each model and dataset, as presented in Figure 6. In particular, Figure 6 illustrates the training (fine-tuning) times of each pre-trained model as a fraction of the cumulative training time of all models summed across all (a) multi-class and (b) multi-label datasets. This shows that, in many cases, ViT models can be trained almost twice as fast as the models of the other best-performing architectures, such as DenseNet and SwinT. The training cost of ViT models is similar to that of EfficientNetB0, ConvNeXt, and MLP Mixer, which are efficient but generally perform worse on these tasks. We can also observe that these variants of SwinT models are the slowest to train on all 22 tasks compared to the other architectures. This is also evident when comparing the time for each epoch (see Appendix B), with SwinT models taking twice longer to train compared to DenseNet161 models, the next slowest architecture. We also observed that fine-tuning pre-trained models almost halves the training time compared to training models from scratch, even though they take about the same time per epoch. Note, however,

that we have not accounted for the time required to pre-train each model, which certainly increases the overall training times significantly. This is generally expected behavior but may help in the design and planning of DL pipelines for similar EO. Additional results presenting models' training costs can be found in Appendix B.

#### 4.6 A closer look on several tasks

To better understand the performance of the learned models on the various MCC and MLC tasks, we examine the model decisions in detail, focusing on datasets (and classes) where the models tend to perform poorly. We hypothesize that these cases are related to several overarching issues that often affect the performance of the models:

- High inter-class similarity between images from different classes;
- Many EO image-classification tasks, which are formulated as MCC, are, in fact, MLC problems. In many cases, an image has a single label, but there are more than one classes/concepts present;
- Presence of abstract/complex/compound classes within the datasets, can cause many difficulties in detecting useful and consistent patterns;
- Absence of additional spatio-temporal data which captures the dynamics of land-cover changes

To investigate these issues, we simultaneously analyze the models' confusion matrices and visualizations of localized activation maps that highlight the distinguishing parts of the image responsible for the model decision. To generate such visualizations, we use Gradient-weighted Class Activation Mapping (GradCAM) [102], which is typically used to diagnose model predictions for various deep learning architectures [103], including Earth Observation applications [30, 104]. GradCAM uses the gradients of the target classes from the last convolutional layer and produces a coarse localization map highlighting important regions in the image for class prediction. In this set of analyses, we select several cases from the datasets considered datasets, especially those containing classes/land types for which the models perform poorly (based on the various evaluation scores, as reported in Appendix D), and calculate/visualize the corresponding GradCAM maps.

We start by investigating the inter-class similarities between images assigned to different classes. This is a common problem in practice in many similar EO applications, caused by the presence of visually similar (often indistinguishable) objects in an image. Figure 7 illustrates this problem using GradCAM activation maps of some sample images with their respective classes/labels from the different datasets.

Our qualitative analyses show that the predictive models are generally able to focus on the correct parts of the images (with distinguishable patterns) but cannot identify the correct object. This is the case, for example, when distinguishing between a 'church' and a 'palace' or a 'terrace' and a 'rectangular farmland', which are visually very similar but semantically different. As expected, the models also struggle with cases where the image labels are also semantically similar, such as in the distinction between 'railway' and 'railway station' or 'river' and 'harbor,' which even a human expert would have difficulty classifying. Similar cases can be further analyzed by examining the

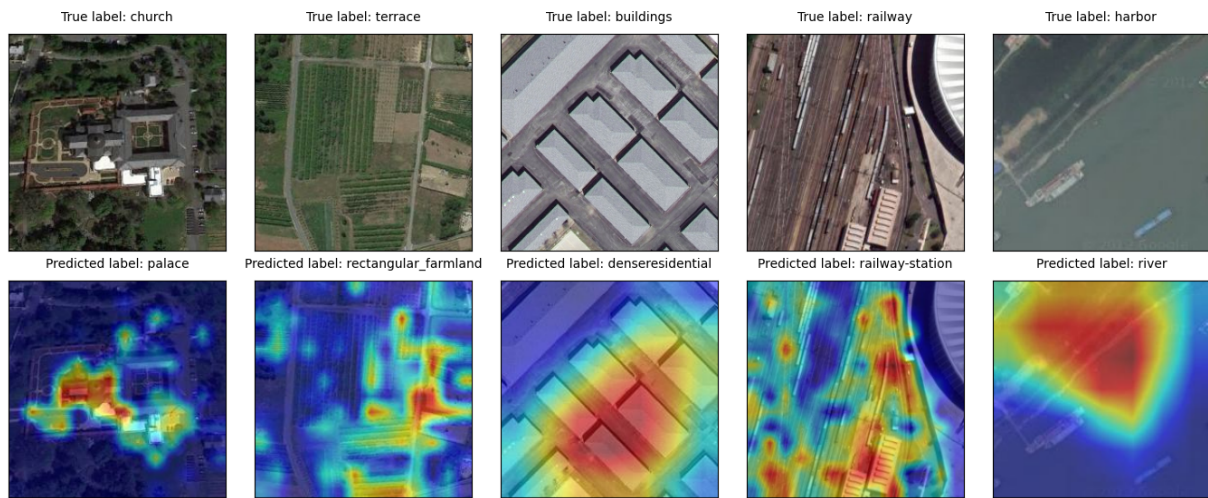


Figure 7: GradCAM visualizations calculated for example images with high inter-class similarity. The input images with their ground-truth label are shown in the first row, while the corresponding activation maps with predicted labels are shown below in the second row. The datasets for the images and the models used to predict the labels are as follows, from left to right: (1) Resisc45, ViT model (2) Resisc45, ViT model (3) UC Merced, ResNet152 model (4) CLRS, ViT model and (5) SIRI-WHU, ResNet152 model

confusion matrices. For example, the most challenging dataset, *So2Sat*, contains many such examples (see Figure D.45 in Appendix D.15), which are the reason for the poor overall performance of the models.

The second issue that we highlight is related to the fact that, in many cases, multiple land-cover classes/concepts are present in a single image, but the image itself is assigned to only one class - making it a multi-class instead of a multi-label problem. Figure 8 shows several activation maps illustrating this issue. For example, consider the image-pair on the far left: The image is labeled only as 'river', but we can also see an 'overpass' (a label also present in the dataset) that causes the model to make an 'incorrect' prediction, albeit with a probability of 0.54. Similar situations can be observed for the remaining images: Objects from other classes that are substantially present in an image are detected, thus confusing the models. This, however, shows that the models have been trained well and are performing as expected, but instead of outputting multiple labels (as in a typical MLC setting), they have to choose a single one - which can lead to errors and lower performance.

To evaluate the third issue, which relates to complex/compound classes, we examine samples with lower F1 scores. Complex/compound classes refer to classes that consist of objects with different physical properties and spatial distribution, making it very difficult to detect useful and consistent patterns. This is also true for abstract classes, where the semantic gap (in terms of labels) is challenging to overcome, which is typically the case when the features learned from the models differ from human interpretation.

Figure 9 illustrates these problems using the respective activation maps. In particular, in the case of *AID* (the two pairs of images on the far left), the model confuses 'school' with 'commercial', the latter being quite vague, for which the semantic gap is not easily dealt with. In the second case, the model has difficulty distinguishing between 'park' and

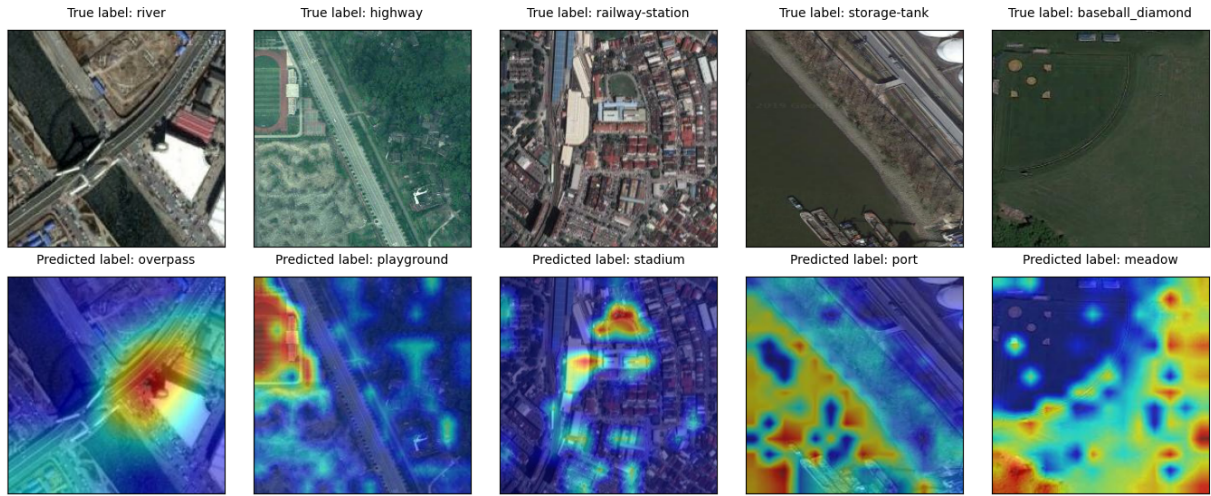


Figure 8: GradCAM visualizations that illustrate the MCC/MLC issues. The input images with their ground-truth label are shown in the first row, while the corresponding activation maps with predicted labels are shown below in the second row. The datasets for the images and the models used to predict the labels are as follows, from left to right: (1) Resisc45, ViT model (2) Resisc45, ViT model (3) UC Merced, ResNet152 model (4) CLRS, ViT model and (5) SIRI-WHU, ResNet152 model

'resort' (which is also evident in the confusion matrix in Figure D.9 in Appendix D.3). This could be because these classes consist of common objects but have different spatial distributions. Similar problems can be seen in the cases of *CLRS* and *SIRI-WHU* (the last three image pairs), where labels such as 'industrial' or 'meadow' are confused with labels such as 'commercial/residential/park', which are visually and semantically almost indistinguishable from the ground truth. Similar problems exist in MLC datasets, such as *BigEarthNet*, that contain multiple complex/compound classes. From the evaluation details (see Appendix D.17), we can see that complex/compound classes such as 'Complex cultivation patterns', 'Land principally occupied by agriculture, with significant areas of natural vegetation', and 'Industrial and commercial units' have lower F1 scores.

Finally, our analysis shows that for some tasks (such as *So2Sat*), one needs additional and more sophisticated (spatio-temporal) data to improve the performance of the predictive models. For example, the *So2Sat* dataset is very challenging, not only because of the high inter-class similarity but also because of the relatively low spatial resolution of the images. Images labeled 'Open high rise' or 'Compact low rise' are often confused with 'Open middle rise' or 'Lightweight low rise', respectively, which is hardly surprising without additional data that can capture such subtle and often subjective differences. Moreover, in the case of *BigEarthNet*, classes such as 'Permanent crops', 'Coastal wetlands', and 'Natural grassland and sparsely vegetated areas' require additional spatio-temporal data that capture the dynamics caused by frequent land cover changes, making the process of classification more reliable and thus more accurate.

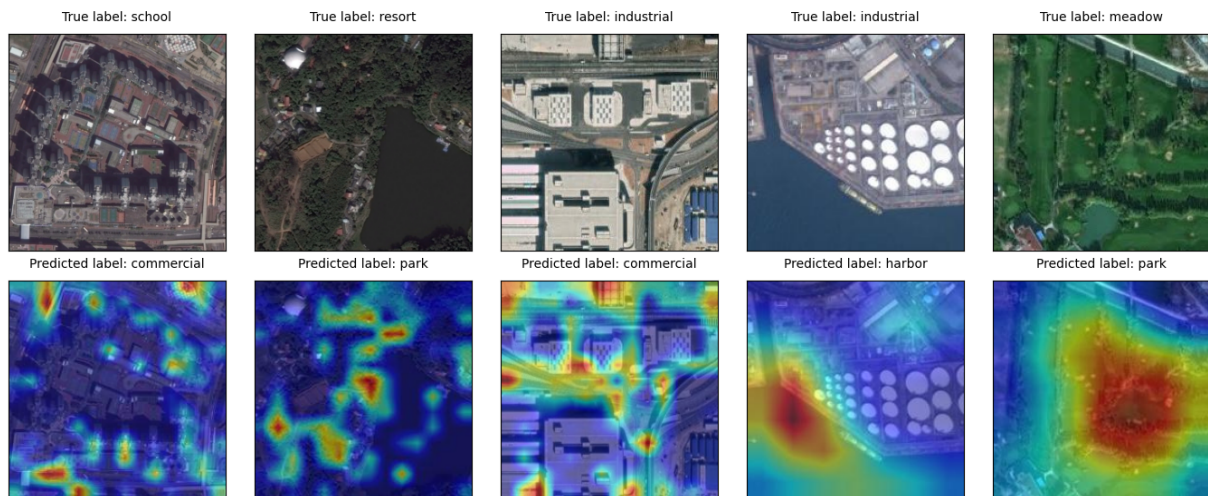


Figure 9: GradCAM visualizations for images with complex/compound classes. The input images with their ground-truth label are shown in the first row, while the corresponding activation maps with predicted labels are shown below in the second row. The datasets for the images and the models used to predict the labels are as follows, from left to right: (1) AID, ViT model (2) AID, ViT model (3) CLRS, ViT model (4) SIRI-WHU, ResNet152 model and (5) SIRI-WHU, ResNet152 model

## 5 Conclusions

We present a systematic review and evaluation of several modern DL architectures applied in Earth Observation. Specifically, we introduce *AiTLAS: Benchmark Arena* – an *open-source EO benchmark suite* and demonstrate its utility with a comprehensive comparative analysis of models from ten different state-of-the-art DL architectures, comparing them to a variety of multi-class and multi-label image classification tasks from 22 datasets. We compare models trained from scratch and pre-trained models under the same conditions and with the same hardware. We evaluate more than 500 models with different architectures and learning paradigms across tasks from 22 datasets with different sizes and properties. To our knowledge, the evaluation of these different setups (in terms of machine learning tasks, model setups, model architectures, and datasets) makes this the largest and most comprehensive empirical study of deep learning methods applied to EO datasets to date. All of the important details about the study design, the results, and the trained models are freely available. This will contribute to more systematic and rigorous experiments in future work and, more importantly, will enable better usability and faster development of novel approaches. We believe that both this study and the associated repository can serve as a starting point and a guiding design principle for evaluating and documenting machine learning approaches in the different domains of EO. More importantly, we hope that with further involvement from the community, *AiTLAS: Benchmark Arena* can become a reference point for further studies in this highly active research area.

More broadly, we believe that this work, along with the developed resources, will strongly impact the AI and EO research communities. First, such ready-to-use resources containing trained models, clear experimental designs, and detailed results will facilitate better adoption of sophisticated modeling approaches in the EO community - bringing

the EO and AI communities closer together. Second, it demonstrates the FAIRification process of AI4EO resources, i.e., making resources adhere to the FAIR principles (Findable, Accessible, Interoperable, and Reusable [105]). Finally, it contributes to the 'Green AI' initiative by saving additional computational overhead. Since all experimental details, especially the trained models, are publicly available – other experts and researchers can compare, reproduce, and reuse these resources - reducing the need to (repeatedly) run unnecessary experiments.

### **Reproducibility**

All the necessary details, in terms of the trained models, model parameters and implementations as well as details on all of the used datasets and their preprocessed versions are available at <https://github.com/biasvariancelabs/aitlas-arena>. All the models were trained/fine-tuned on NVIDIA A100-PCIE-40GB GPUs, running CUDA Version 11.5 ([www.nvidia.com/en-gb/data-center/a100/](http://www.nvidia.com/en-gb/data-center/a100/)). Note that, we do not host the datasets. To obtain them, please refer to each of the respective studies (referenced in Tables 1 and 2) or follow the links provided in our repository. The study was performed using the AiTLAS Toolbox [37], a library for exploratory and predictive analysis of satellite imagery pertaining to different remote-sensing tasks, available at <https://aitlas.bvlabs.ai>.

### **Acknowledgements**

We acknowledge the support of the European Space Agency ESA through the activity AiTLAS - AI4EO rapid prototyping environment. We thank Sofija Dimitrovska for her thoughtful feedback.

## References

- [1] A. Khan, A. Sohail, U. Zahoor, A. S. Qureshi, A survey of the recent architectures of deep convolutional neural networks, *Artificial Intelligence Review* 53 (2020) 5455–5516.
- [2] S. Khan, M. Naseer, M. Hayat, S. W. Zamir, F. S. Khan, M. Shah, Transformers in vision: A survey, *ACM Comput. Surv.* (2021). doi:10.1145/3505244.
- [3] J. E. Ball, D. T. Anderson, C. S. Chan Sr., Comprehensive survey of deep learning in remote sensing: theories, tools, and challenges for the community, *Journal of Applied Remote Sensing* 11 (2017) 1 – 54.
- [4] D. Tuia, F. Ratle, F. Pacifici, M. F. Kanevski, W. J. Emery, Active learning methods for remote sensing image classification, *IEEE Transactions on Geoscience and Remote Sensing* 47 (2009) 2218–2232. doi:10.1109/TGRS.2008.2010404.
- [5] M. Li, S. Zang, B. Zhang, S. Li, C. Wu, A review of remote sensing image classification techniques: the role of spatio-contextual information, *European Journal of Remote Sensing* 47 (2014) 389–411. doi:10.5721/EuJRS20144723.
- [6] T. Blaschke, Object based image analysis for remote sensing, *Isprs Journal of Photogrammetry and Remote Sensing* 65 (2010) 2–16.
- [7] T. Blaschke, J. Strobl, What’s wrong with pixels? some recent developments interfacing remote sensing and gis, in: *GIS – Zeitschrift für Geoinformationssysteme*, 2001.
- [8] G. Cheng, J. Han, X. Lu, Remote sensing image scene classification: Benchmark and state of the art, *Proceedings of the IEEE* 105 (2017) 1865–1883. doi:10.1109/JPROC.2017.2675998.
- [9] Y. Yang, S. Newsam, Bag-of-visual-words and spatial extensions for land-use classification, in: *Proceedings of the 18th SIGSPATIAL International Conference on Advances in Geographic Information Systems*, Association for Computing Machinery, 2010, p. 270–279.
- [10] D. Marmanis, M. Datcu, T. Esch, U. Stilla, Deep learning earth observation classification using imagenet pretrained networks, *IEEE Geoscience and Remote Sensing Letters* 13 (2016) 105–109. doi:10.1109/LGRS.2015.2499239.
- [11] H. Chen, V. Chandrasekar, H. Tan, R. Cifelli, Rainfall estimation from ground radar and trmm precipitation radar using hybrid deep neural networks, *Geophysical Research Letters* 46 (2019) 10669–10678. doi:https://doi.org/10.1029/2019GL084771.
- [12] J. Castillo-Navarro, B. Le Saux, A. Boulch, S. Lefèvre, Energy-based models in earth observation: From generation to semisupervised learning, *IEEE Transactions on Geoscience and Remote Sensing* 60 (2022) 1–11. doi:10.1109/TGRS.2021.3126428.
- [13] Y. Wang, C. M. Albrecht, N. A. A. Braham, L. Mou, X. X. Zhu, Self-supervised learning in remote sensing: A review, *CoRR* (2022). doi:10.48550/ARXIV.2206.13188.
- [14] M. Neumann, A. S. Pinto, X. Zhai, N. Houlsby, Training general representations for remote sensing using in-domain knowledge, in: *IGARSS 2020 - 2020 IEEE International Geoscience and Remote Sensing Symposium*, 2020, pp. 6730–6733. doi:10.1109/IGARSS39084.2020.9324501.
- [15] D. Ienco, R. Gaetano, C. Dupaquier, P. Maurel, Land cover classification via multitemporal spatial data by deep recurrent neural networks, *IEEE Geoscience and Remote Sensing Letters* 14 (2017) 1685–1689. doi:10.1109/LGRS.2017.2728698.
- [16] A. Chlingaryan, S. Sukkariéh, B. Whelan, Machine learning approaches for crop yield prediction and nitrogen status estimation in precision agriculture: A review, *Computers and Electronics in Agriculture* 151 (2018) 61–69. doi:https://doi.org/10.1016/j.compag.2018.05.012.
- [17] M. D. Johnson, W. W. Hsieh, A. J. Cannon, A. Davidson, F. Bédard, Crop yield forecasting on the canadian prairies by remotely sensed vegetation indices and machine learning methods, *Agricultural and Forest Meteorology* 218-219 (2016) 74–84. doi:https://doi.org/10.1016/j.agrformet.2015.11.003.
- [18] J. Xu, J. Yang, X. Xiong, H. Li, J. Huang, K. Ting, Y. Ying, T. Lin, Towards interpreting multi-temporal deep learning models in crop mapping, *Remote Sensing of Environment* 264 (2021) 112599. doi:https://doi.org/10.1016/j.rse.2021.112599.
- [19] B. Ayhan, C. Kwan, B. Budavari, L. Kwan, Y. Lu, D. Perez, J. Li, D. Skarlatos, M. Vlachos, Vegetation detection using deep learning and conventional methods, *Remote Sensing* 12 (2020). doi:10.3390/rs12152502.
- [20] Y.-H. Jo, D.-W. Kim, H. Kim, Chlorophyll concentration derived from microwave remote sensing measurements using artificial neural network algorithm, *Journal of Marine Science and Technology* 26 (2018). doi:10.6119/JMST.2018.02\_(1).0004.

- [21] H. Shirmard, E. Farahbakhsh, R. D. Müller, R. Chandra, A review of machine learning in processing remote sensing data for mineral exploration, *Remote Sensing of Environment* 268 (2022) 112750. doi:<https://doi.org/10.1016/j.rse.2021.112750>.
- [22] X. Zhang, Q. Zhang, G. Zhang, Z. Nie, Z. Gui, H. Que, A novel hybrid data-driven model for daily land surface temperature forecasting using long short-term memory neural network based on ensemble empirical mode decomposition, *International Journal of Environmental Research and Public Health* 15 (2018).
- [23] M. Sadeghi, A. A. Asanjan, M. Faridzad, P. Nguyen, K. Hsu, S. Sorooshian, D. Braithwaite, Persiann-cnn: Precipitation estimation from remotely sensed information using artificial neural networks–convolutional neural networks, *Journal of Hydrometeorology* 20 (2019) 2273–2289. doi:[10.1175/JHM-D-19-0110.1](https://doi.org/10.1175/JHM-D-19-0110.1).
- [24] N. Longbotham, C. Chaapel, L. Bleiler, C. Padwick, W. J. Emery, F. Pacifici, Very high resolution multiangle urban classification analysis, *IEEE Transactions on Geoscience and Remote Sensing* 50 (2012) 1155–1170. doi:[10.1109/TGRS.2011.2165548](https://doi.org/10.1109/TGRS.2011.2165548).
- [25] Z. Lv, T. Liu, J. A. Benediktsson, N. Falco, Land cover change detection techniques: Very-high-resolution optical images: A review, *IEEE Geoscience and Remote Sensing Magazine* 10 (2022) 44–63. doi:[10.1109/MGRS.2021.3088865](https://doi.org/10.1109/MGRS.2021.3088865).
- [26] B. Huang, B. Zhao, Y. Song, Urban land-use mapping using a deep convolutional neural network with high spatial resolution multispectral remote sensing imagery, *Remote Sensing of Environment* 214 (2018) 73–86. doi:<https://doi.org/10.1016/j.rse.2018.04.050>.
- [27] M. Somrak, S. Dzeroski, Z. Kokalj, Learning to classify structures in als-derived visualizations of ancient maya settlements with CNN, *Remote. Sens.* 12 (2020) 2215. doi:[10.3390/rs12142215](https://doi.org/10.3390/rs12142215).
- [28] G. Cheng, X. Xie, J. Han, L. Guo, G.-S. Xia, Remote sensing image scene classification meets deep learning: Challenges, methods, benchmarks, and opportunities, *IEEE Journal of Selected Topics in Applied Earth Observations and Remote Sensing* 13 (2020) 3735–3756. doi:[10.1109/JSTARS.2020.3005403](https://doi.org/10.1109/JSTARS.2020.3005403).
- [29] R. Schneider, M. Bonavita, A. Geer, R. Arcucci, P. Dueben, C. Vitolo, B. Le Saux, B. Demir, P.-P. Mathieu, Esa-ecmwf report on recent progress and research directions in machine learning for earth system observation and prediction, *npj Climate and Atmospheric Science* 5 (2022) 51. doi:[10.1038/s41612-022-00269-z](https://doi.org/10.1038/s41612-022-00269-z).
- [30] I. Papoutsis, N.-I. Bountos, A. Zavras, D. Michail, C. Tryfonopoulos, Efficient deep learning models for land cover image classification, *arXiv:2111.09451* (2022).
- [31] G.-S. Xia, J. Hu, F. Hu, B. Shi, X. Bai, Y. Zhong, L. Zhang, X. Lu, AID: A benchmark data set for performance evaluation of aerial scene classification, *IEEE Transactions on Geoscience and Remote Sensing* 55 (2017) 3965–3981.
- [32] X. Zhai, J. Puigcerver, A. Kolesnikov, P. Ruysen, C. Riquelme, M. Lucic, J. Djolonga, A. S. Pinto, M. Neumann, A. Dosovitskiy, L. Beyer, O. Bachem, M. Tschannen, M. Michalski, O. Bousquet, S. Gelly, N. Houlsby, A large-scale study of representation learning with the visual task adaptation benchmark, *arXiv:1910.04867* (2019).
- [33] L. Zhang, L. Zhang, B. Du, Deep learning for remote sensing data: A technical tutorial on the state of the art, *IEEE Geoscience and Remote Sensing Magazine* 4 (2016) 22–40. doi:[10.1109/MGRS.2016.2540798](https://doi.org/10.1109/MGRS.2016.2540798).
- [34] X. X. Zhu, D. Tuia, L. Mou, G.-S. Xia, L. Zhang, F. Xu, F. Fraundorfer, Deep learning in remote sensing: A comprehensive review and list of resources, *IEEE Geoscience and Remote Sensing Magazine* 5 (2017) 8–36. doi:[10.1109/MGRS.2017.2762307](https://doi.org/10.1109/MGRS.2017.2762307).
- [35] A. J. Stewart, C. Robinson, I. A. Corley, A. Ortiz, J. M. L. Ferres, A. Banerjee, Torchgeo: deep learning with geospatial data, *CoRR abs/2111.08872* (2021). *arXiv:2111.08872*.
- [36] G. Sumbul, A. de Wall, T. Kreuziger, F. Marcelino, H. Costa, P. Benevides, M. Caetano, B. Demir, V. Markl, BigEarthNet-MM: A large-scale, multimodal, multilabel benchmark archive for remote sensing image classification and retrieval [software and data sets], *IEEE Geoscience and Remote Sensing Magazine* 9 (2021) 174–180.
- [37] I. Dimitrovski, I. Kitanovski, P. Panov, N. Simidjievski, D. Kocev, Aitlas: Artificial intelligence toolbox for earth observation, *CoRR abs/2201.08789* (2022). *arXiv:2201.08789*.
- [38] A. Paszke, S. Gross, F. Massa, A. Lerer, J. Bradbury, G. Chanan, T. Killeen, Z. Lin, N. Gimelshein, L. Antiga, A. Desmaison, A. Kopf, E. Yang, Z. DeVito, M. Raison, A. Tejani, S. Chilamkurthy, B. Steiner, L. Fang, J. Bai, S. Chintala, Pytorch: An imperative style, high-performance deep learning library, in: *Advances in Neural Information Processing Systems* 32, Curran Associates, Inc., 2019, pp.

8024–8035.

- [39] A. Dosovitskiy, L. Beyer, A. Kolesnikov, D. Weissenborn, X. Zhai, T. Unterthiner, M. Dehghani, M. Minderer, G. Heigold, S. Gelly, et al., An image is worth 16x16 words: Transformers for image recognition at scale, *arXiv preprint arXiv:2010.11929* (2020).
- [40] Z. Liu, H. Hu, Y. Lin, Z. Yao, Z. Xie, Y. Wei, J. Ning, Y. Cao, Z. Zhang, L. Dong, F. Wei, B. Guo, Swin transformer v2: Scaling up capacity and resolution, in: *2022 IEEE/CVF Conference on Computer Vision and Pattern Recognition (CVPR)*, 2022, pp. 11999–12009. doi:10.1109/CVPR52688.2022.01170.
- [41] G. Tsoumakias, I. Katakis, Multi-label classification: An overview, *International Journal of Data Warehousing and Mining* 3 (2009) 1–13.
- [42] G.-S. Xia, W. Yang, J. Delon, Y. Gousseau, H. Sun, H. Maître, Structural high-resolution satellite image indexing, *International Archives of the Photogrammetry, Remote Sensing and Spatial Information Sciences - ISPRS Archives* 38 (2010).
- [43] P. Helber, B. Bischke, A. Dengel, D. Borth, Eurosat: A novel dataset and deep learning benchmark for land use and land cover classification, *IEEE Journal of Selected Topics in Applied Earth Observations and Remote Sensing* (2019).
- [44] W. Zhou, S. Newsam, C. Li, Z. Shao, Patternnet: A benchmark dataset for performance evaluation of remote sensing image retrieval, *ISPRS journal of photogrammetry and remote sensing* 145 (2018) 197–209.
- [45] H. Li, X. Dou, C. Tao, Z. Wu, J. Chen, J. Peng, M. Deng, L. Zhao, Rsi-cb: A large-scale remote sensing image classification benchmark using crowdsourced data, *Sensors* 20 (2020) 1594. doi:doi.org/10.3390/s20061594.
- [46] Q. Zou, L. Ni, T. Zhang, Q. Wang, Deep learning based feature selection for remote sensing scene classification, *IEEE Geoscience and Remote Sensing Letters* 12 (2015) 2321–2325. doi:10.1109/LGRS.2015.2475299.
- [47] S. Basu, S. Ganguly, S. Mukhopadhyay, R. DiBiano, M. Karki, R. Nemani, Deepsat: A learning framework for satellite imagery, in: *Proceedings of the 23rd SIGSPATIAL International Conference on Advances in Geographic Information Systems, SIGSPATIAL '15, Association for Computing Machinery*, 2015.
- [48] Q. Zhu, Y. Zhong, B. Zhao, G.-S. Xia, L. Zhang, Bag-of-visual-words scene classifier with local and global features for high spatial resolution remote sensing imagery, *IEEE Geoscience and Remote Sensing Letters* 13 (2016) 747–751.
- [49] H. Li, H. Jiang, X. Gu, J. Peng, W. Li, L. Hong, C. Tao, Clrs: Continual learning benchmark for remote sensing image scene classification, *Sensors* 20 (2020).
- [50] Y. Long, Y. Gong, Z. Xiao, Q. Liu, Accurate object localization in remote sensing images based on convolutional neural networks, *IEEE Transactions on Geoscience and Remote Sensing* 55 (2017) 2486–2498.
- [51] Q. Wang, S. Liu, J. Chanussot, X. Li, Scene classification with recurrent attention of vhr remote sensing images, *IEEE Transactions on Geoscience and Remote Sensing* 57 (2019) 1155–1167.
- [52] O. A. Penatti, K. Nogueira, J. A. Dos Santos, Do deep features generalize from everyday objects to remote sensing and aerial scenes domains?, in: *Proceedings of the IEEE conference on computer vision and pattern recognition workshops*, 2015, pp. 44–51.
- [53] X. X. Zhu, J. Hu, C. Qiu, Y. Shi, J. Kang, L. Mou, H. Bagheri, M. Haberle, Y. Hua, R. Huang, L. Hughes, H. Li, Y. Sun, G. Zhang, S. Han, M. Schmitt, Y. Wang, So2sat lcz42: A benchmark data set for the classification of global local climate zones [software and data sets], *IEEE Geoscience and Remote Sensing Magazine* 8 (2020) 76–89.
- [54] B. Chaudhuri, B. Demir, S. Chaudhuri, L. Bruzzone, Multilabel remote sensing image retrieval using a semisupervised graph-theoretic method, *IEEE Transactions on Geoscience and Remote Sensing* 56 (2018) 1144–1158.
- [55] X. Qi, P. Zhu, Y. Wang, L. Zhang, J. Peng, M. Wu, J. Chen, X. Zhao, N. Zang, P. T. Mathiopoulos, Mlrsnet: A multi-label high spatial resolution remote sensing dataset for semantic scene understanding, *ISPRS Journal of Photogrammetry and Remote Sensing* 169 (2020) 337–350.
- [56] Y. Hua, L. Mou, X. X. Zhu, Recurrently exploring class-wise attention in a hybrid convolutional and bidirectional LSTM network for multi-label aerial image classification, *ISPRS Journal of Photogrammetry and Remote Sensing* 149 (2019) 188–199.
- [57] Y. Hua, L. Mou, X. X. Zhu, Relation network for multilabel aerial image classification, *IEEE Transactions on Geoscience and Remote Sensing* 58 (2020) 4558–4572.
- [58] Kaggle, Planet: Understanding the amazon from space, 2022. URL: <https://www.kaggle.com/competitions/>

planet-understanding-the-amazon-from-space, last accessed 21 May 2022.

- [59] G. Sumbul, M. Charfuelan, B. Demir, V. Markl, Bigearthnet: A large-scale benchmark archive for remote sensing image understanding, *IGARSS 2019 - 2019 IEEE International Geoscience and Remote Sensing Symposium (2019)* 5901–5904.
- [60] A. Krizhevsky, I. Sutskever, G. E. Hinton, Imagenet classification with deep convolutional neural networks, *Advances in neural information processing systems* 25 (2012) 1097–1105.
- [61] K. Simonyan, A. Zisserman, Very deep convolutional networks for large-scale image recognition, *arXiv preprint arXiv:1409.1556* (2014).
- [62] K. He, X. Zhang, S. Ren, J. Sun, Deep residual learning for image recognition, in: *Proceedings of the IEEE conference on computer vision and pattern recognition*, 2016, pp. 770–778.
- [63] G. Huang, Z. Liu, L. Van Der Maaten, K. Q. Weinberger, Densely connected convolutional networks, in: *Proceedings of the IEEE conference on computer vision and pattern recognition*, 2017, pp. 4700–4708.
- [64] M. Tan, Q. Le, Efficientnet: Rethinking model scaling for convolutional neural networks, in: *International conference on machine learning*, PMLR, 2019, pp. 6105–6114.
- [65] Z. Liu, H. Mao, C.-Y. Wu, C. Feichtenhofer, T. Darrell, S. Xie, A convnet for the 2020s, *arXiv preprint arXiv:2201.03545* (2022).
- [66] I. O. Tolstikhin, N. Houlsby, A. Kolesnikov, L. Beyer, X. Zhai, T. Unterthiner, J. Yung, A. Steiner, D. Keysers, J. Uszkoreit, et al., Mlp-mixer: An all-mlp architecture for vision, *Advances in Neural Information Processing Systems* 34 (2021).
- [67] S. Marcel, Y. Rodriguez, Torchvision the machine-vision package of torch, in: *Proceedings of the 18th ACM international conference on Multimedia*, 2010, pp. 1485–1488.
- [68] R. Wightman, Pytorch image models, <https://github.com/rwightman/pytorch-image-models>, 2019. doi:10.5281/zenodo.4414861.
- [69] Q. Weng, Z. Mao, J. Lin, W. Guo, Land-use classification via extreme learning classifier based on deep convolutional features, *IEEE Geoscience and Remote Sensing Letters* 14 (2017) 704–708. doi:10.1109/LGRS.2017.2672643.
- [70] M. Castelluccio, G. Poggi, C. Sansone, L. Verdoliva, Land use classification in remote sensing images by convolutional neural networks, *CoRR* (2015). doi:10.48550/ARXIV.1508.00092.
- [71] X. Han, Y. Zhong, L. Cao, L. Zhang, Pre-trained alexnet architecture with pyramid pooling and supervision for high spatial resolution remote sensing image scene classification, *Remote Sensing* 9 (2017). doi:10.3390/rs9080848.
- [72] J. Kang, M. Körner, Y. Wang, H. Taubenböck, X. X. Zhu, Building instance classification using street view images, *ISPRS journal of photogrammetry and remote sensing* 145 (2018) 44–59.
- [73] F. Hu, G.-S. Xia, J. Hu, L. Zhang, Transferring deep convolutional neural networks for the scene classification of high-resolution remote sensing imagery, *Remote Sensing* 7 (2015) 14680–14707. doi:10.3390/rs71114680.
- [74] I. Goodfellow, Y. Bengio, A. Courville, *Deep Learning*, MIT Press, 2016. <http://www.deeplearningbook.org>.
- [75] S. Zagoruyko, N. Komodakis, Wide residual networks, *CoRR* (2016). doi:10.48550/ARXIV.1605.07146.
- [76] N. Audebert, B. Le Saux, S. Lefèvre, Beyond rgb: Very high resolution urban remote sensing with multimodal deep networks, *ISPRS Journal of Photogrammetry and Remote Sensing* 140 (2018) 20–32.
- [77] J. Zhang, C. Lu, X. Li, H.-J. Kim, J. Wang, A full convolutional network based on densenet for remote sensing scene classification, *Mathematical Biosciences and Engineering* 16 (2019) 3345–3367. doi:10.3934/mbe.2019167.
- [78] W. Tong, W. Chen, W. Han, X. Li, L. Wang, Channel-attention-based densenet network for remote sensing image scene classification, *IEEE Journal of Selected Topics in Applied Earth Observations and Remote Sensing* 13 (2020) 4121–4132. doi:10.1109/JSTARS.2020.3009352.
- [79] F. Chen, J. Y. Tsou, Drsnet: Novel architecture for small patch and low-resolution remote sensing image scene classification, *International Journal of Applied Earth Observation and Geoinformation* 104 (2021) 102577. doi:https://doi.org/10.1016/j.jag.2021.102577.
- [80] T.-Y. Lin, P. Dollár, R. Girshick, K. He, B. Hariharan, S. Belongie, Feature pyramid networks for object detection, in: *2017 IEEE Conference on Computer Vision and Pattern Recognition (CVPR)*, 2017, pp. 936–944. doi:10.1109/CVPR.2017.106.
- [81] S. Liu, C. He, H. Bai, Y. Zhang, J. Cheng, Light-weight attention semantic segmentation network for high-resolution remote sensing images, in: *IGARSS 2020-2020 IEEE International Geoscience and Remote Sensing Symposium, IEEE*, 2020, pp. 2595–2598.

- [82] Z. Tian, W. Wang, B. Tian, R. Zhan, J. Zhang, Resolution-aware network with attention mechanisms for remote sensing object detection., *ISPRS Annals of Photogrammetry, Remote Sensing & Spatial Information Sciences* 5 (2020).
- [83] H. Alhichri, A. S. Alswayed, Y. Bazi, N. Ammour, N. A. Alajlan, Classification of remote sensing images using efficientnet-b3 cnn model with attention, *IEEE Access* 9 (2021) 14078–14094. doi:10.1109/ACCESS.2021.3051085.
- [84] J. Devlin, M.-W. Chang, K. Lee, K. Toutanova, Bert: Pre-training of deep bidirectional transformers for language understanding, *arXiv preprint arXiv:1810.04805* (2018).
- [85] Y. Bazi, L. Bashmal, M. M. A. Rahhal, R. A. Dayil, N. A. Ajlan, Vision transformers for remote sensing image classification, *Remote Sensing* 13 (2021). doi:10.3390/rs13030516.
- [86] N. Gong, C. Zhang, H. Zhou, K. Zhang, Z. Wu, X. Zhang, Classification of hyperspectral images via improved cycle-mlp, *IET Computer Vision* 16 (2022) 468–478. doi:https://doi.org/10.1049/cvi2.12104.
- [87] Z. Liu, Y. Lin, Y. Cao, H. Hu, Y. Wei, Z. Zhang, S. Lin, B. Guo, Swin transformer: Hierarchical vision transformer using shifted windows, in: 2021 IEEE/CVF International Conference on Computer Vision (ICCV), 2021, pp. 9992–10002. doi:10.1109/ICCV48922.2021.00986.
- [88] L. Scheibenreif, J. Hanna, M. Mommert, D. Borth, Self-supervised vision transformers for land-cover segmentation and classification, in: 2022 IEEE/CVF Conference on Computer Vision and Pattern Recognition Workshops (CVPRW), 2022, pp. 1421–1430. doi:10.1109/CVPRW56347.2022.00148.
- [89] C. Zhang, L. Wang, S. Cheng, Y. Li, Swinsunet: Pure transformer network for remote sensing image change detection, *IEEE Transactions on Geoscience and Remote Sensing* 60 (2022) 1–13. doi:10.1109/TGRS.2022.3160007.
- [90] D. Wang, J. Zhang, B. Du, G.-S. Xia, D. Tao, An empirical study of remote sensing pretraining, *IEEE Transactions on Geoscience and Remote Sensing* (2022) 1–1. doi:10.1109/TGRS.2022.3176603.
- [91] Z. Xu, W. Zhang, T. Zhang, Z. Yang, J. Li, Efficient transformer for remote sensing image segmentation, *Remote Sensing* 13 (2021). doi:10.3390/rs13183585.
- [92] Z. Meng, F. Zhao, M. Liang, Ss-mlp: A novel spectral-spatial mlp architecture for hyperspectral image classification, *Remote Sensing* 13 (2021). doi:10.3390/rs13204060.
- [93] K. Sechidis, G. Tsoumakas, I. Vlahavas, On the stratification of multi-label data, in: *Proceedings of the 2011 European Conference on Machine Learning and Knowledge Discovery in Databases - Volume Part III*, Springer-Verlag, 2011, p. 145–158.
- [94] L. Liu, H. Jiang, P. He, W. Chen, X. Liu, J. Gao, J. Han, On the variance of the adaptive learning rate and beyond, in: *Proceedings of the Eighth International Conference on Learning Representations (ICLR 2020)*, 2020.
- [95] D. P. Kingma, J. Ba, Adam: A method for stochastic optimization, *arXiv preprint arXiv:1412.6980* (2014).
- [96] V. Risojevic, V. Stojnic, Do we still need ImageNet pre-training in remote sensing scene classification?, *arXiv abs/2111.03690* (2021). *arXiv:2111.03690*.
- [97] J. Yosinski, J. Clune, Y. Bengio, H. Lipson, How transferable are features in deep neural networks?, in: *Proceedings of the 27th International Conference on Neural Information Processing Systems - Volume 2*, 2014, p. 3320–3328.
- [98] S. Kornblith, J. Shlens, Q. V. Le, Do better imagenet models transfer better?, in: 2019 IEEE/CVF Conference on Computer Vision and Pattern Recognition (CVPR), 2019, pp. 2656–2666.
- [99] S. Paul, P.-Y. Chen, Vision transformers are robust learners, *Proceedings of the AAAI Conference on Artificial Intelligence* 36 (2022) 2071–2081.
- [100] S. Bhojanapalli, A. Chakrabarti, D. Glasner, D. Li, T. Unterthiner, A. Veit, Understanding robustness of transformers for image classification, in: 2021 IEEE/CVF International Conference on Computer Vision (ICCV), IEEE Computer Society, Los Alamitos, CA, USA, 2021, pp. 10211–10221.
- [101] C. Zhang, M. Zhang, S. Zhang, D. Jin, Q. feng Zhou, Z. Cai, H. Zhao, S. Yi, X. Liu, Z. Liu, Delving deep into the generalization of vision transformers under distribution shifts, 2022 IEEE/CVF Conference on Computer Vision and Pattern Recognition (CVPR) (2022) 7267–7276.
- [102] R. R. Selvaraju, M. Cogswell, A. Das, R. Vedantam, D. Parikh, D. Batra, Grad-cam: Visual explanations from deep networks via gradient-

- based localization, in: 2017 IEEE International Conference on Computer Vision (ICCV), 2017, pp. 618–626.
- [103] J. Gildenblat, contributors, Pytorch library for cam methods, <https://github.com/jacobgil/pytorch-grad-cam>, 2021.
- [104] J. Li, D. Lin, Y. Wang, G. Xu, Y. Zhang, C. Ding, Y. Zhou, Deep discriminative representation learning with attention map for scene classification, *Remote Sensing* 12 (2020).
- [105] M. D. Wilkinson, M. Dumontier, I. J. Aalbersberg, G. Appleton, M. Axton, A. Baak, N. Blomberg, J.-W. Boiten, L. B. da Silva Santos, P. E. Bourne, et al., The FAIR guiding principles for scientific data management and stewardship, *Scientific Data* 3 (2016) 1–9.

# Current Trends in Deep Learning for Earth Observation: An Open-source Benchmark Arena for Image Classification

*Ivica Dimitrovski, Ivan Kitanovski, Dragi Kocev, Nikola Simidjievski*

## Supplementary Material

### Table of Contents

---

<b>A</b>	<b>Evaluation metrics</b>	<b>1</b>
<b>B</b>	<b>Training Time Details</b>	<b>4</b>
<b>C</b>	<b>Extended results on model generalization performance</b>	<b>8</b>
C.1	Evaluation on a same holdout set . . . . .	8
C.2	Results from pairwise comparisons . . . . .	9
<b>D</b>	<b>Detailed data descriptions &amp; extended results per task</b>	<b>14</b>
D.1	UC Merced . . . . .	14
D.2	WHU-RS19 . . . . .	18
D.3	AID . . . . .	22
D.4	Eurosat . . . . .	26
D.5	PatternNet . . . . .	30
D.6	Resisc45 . . . . .	35
D.7	RSI-CB256 . . . . .	40
D.8	RSSCN7 . . . . .	44
D.9	SAT6 . . . . .	47
D.10	Siri-Whu . . . . .	50
D.11	CLRS . . . . .	53
D.12	RSD46-WHU . . . . .	57
D.13	Brazilian Coffee Scenes . . . . .	61
D.14	Optimal 31 . . . . .	64
D.15	So2Sat . . . . .	68
D.16	UC Merced multi-label . . . . .	72
D.17	BigEarthNet . . . . .	75
D.18	MLRSNet . . . . .	84
D.19	DFC15 . . . . .	88
D.20	Planet UAS . . . . .	91
D.21	AID multi-label . . . . .	95

---

## A Evaluation metrics

The predictive performance of machine learning models is typically assessed using different evaluation measures that capture different aspects of the models' behavior. Selecting the proper evaluation measures requires knowledge of the task and problem at hand. In order to have an unbiased and fair view of the performance, one needs to consider the models' performance along several measures and then compare their performance. In this study, we assess the performance of the models using a variety of different measures available for the machine learning tasks studied here: multi-class and multi-label classification.

**Multi-class classification** refers to the task where a sample can be assigned to exactly one class/label selected from a predefined set of possible classes/labels. Here, we overview several evaluation measures used for this task. Most widely used evaluation measure is *accuracy* due to its intuitive interpretation and straightforward calculation. It denotes the percentage of correctly labeled samples. *Precision* and *Recall* are defined for binary tasks (two classes, often called positive and negative class) by default. To extend the binary measures to multi-class classification tasks, we adopt the One-vs-Rest (One-vs-All) approach which converts a multi-class task into a series of binary tasks for each class/label in the target. Within this approach the sample from given class/label is treated as positive, and the samples from all the other classes/labels are treated as negative.

To calculate most of the evaluation measures, we need to define the following concepts: True Positives (TP), True Negatives (TN), False Positives (FP) and False Negatives (FN). These concepts combined together form the confusion matrix for the performance of a given model over a given dataset. The TP, TN, FP and FN are defined as follows:

- TP: the label is positive and the prediction is also positive
- TN: the label is negative and the prediction is also negative
- FP: the label is negative but the prediction is positive
- FN: the label is positive but the prediction is negative

*Precision* is then calculated as the fraction of correctly predicted positive observations from the total predicted positive observations:

$$Precision = \frac{TP}{TP+FP}$$

*Recall* is calculated as the fraction of correctly predicted positive observations from the available positive observations:

$$Recall = \frac{TP}{TP+FN}$$

*F1 score* is also a common evaluation measure used in machine learning tasks, basically it combines precision and recall through a weighted average. Therefore, this score takes both false positives and false negatives into account and is very useful, especially if we have an imbalanced class/label distribution. The F1 score can be calculated as:

$$F1 = 2 \cdot \frac{Precision \cdot Recall}{Precision + Recall}$$

These evaluation measures can then be aggregated across multiple classes using three strategies:

- *Macro averaging*: calculate the evaluation measures for each class/label separately and then average the individual values,
- *Micro averaging*: calculate the class wise confusion matrices and then aggregate the confusion matrices into a single one (i.e., add together the TP, FP, FN and FP values for each class). The aggregated confusion matrix is then used to calculate the values for the different evaluation measures, and
- *Weighted averaging*: based on macro averaging but using the frequency of the class/label as a weight in the average calculation.

Using these aggregation strategies, we then obtain macro-averaged, micro-averaged and weighted-averaged precision, recall and F1 score. Note that micro F1 score, micro precision and micro recall yield the same values as accuracy for the multi-class classification task. Taking into account this, for the multi-class classification tasks we report the following evaluation measures: Accuracy, Macro Precision, Weighted Precision, Macro Recall, Weighted Recall, Macro F1 score and Weighted F1 score.

**Multi-label classification** refers to the task where a sample can be assigned to multiple class/label from a predefined set of possible classes/labels. To transform the multi-label classification task to binary classification and apply the same metrics previously defined, we adopt the binary relevance method [41] that considers each label as an independent binary problem. In our case, in each node from the output layer, we use the sigmoid activation function to obtain a probability of the input image being labeled with each of the classes/labels. To use these probabilities to predict the classes/labels of the image, we need to define a threshold value. The model predicts whether an image contains the classes/labels with a probability that exceed the given threshold. The threshold value controls the rate of false positives v.s false negatives. Increasing the threshold reduces the number of false positives, whereas decreasing it reduces the number of false negatives. In our experiments, we use threshold value of 0.5. Taking into account this transformation, we can apply the formulas from above to calculate the same evaluation measures for multi-label classification tasks. While these evaluation measures are threshold dependent, we additionally use the *mean average precision* (mAP) - a threshold independent evaluation measure widely used in image classification tasks. mAP is calculated as the mean over the average precision values of the individual labels. Average precision summarizes a precision-recall curve as the weighted mean of the precision values obtained at each threshold, with the increase in recall from the previous threshold used as the weight:

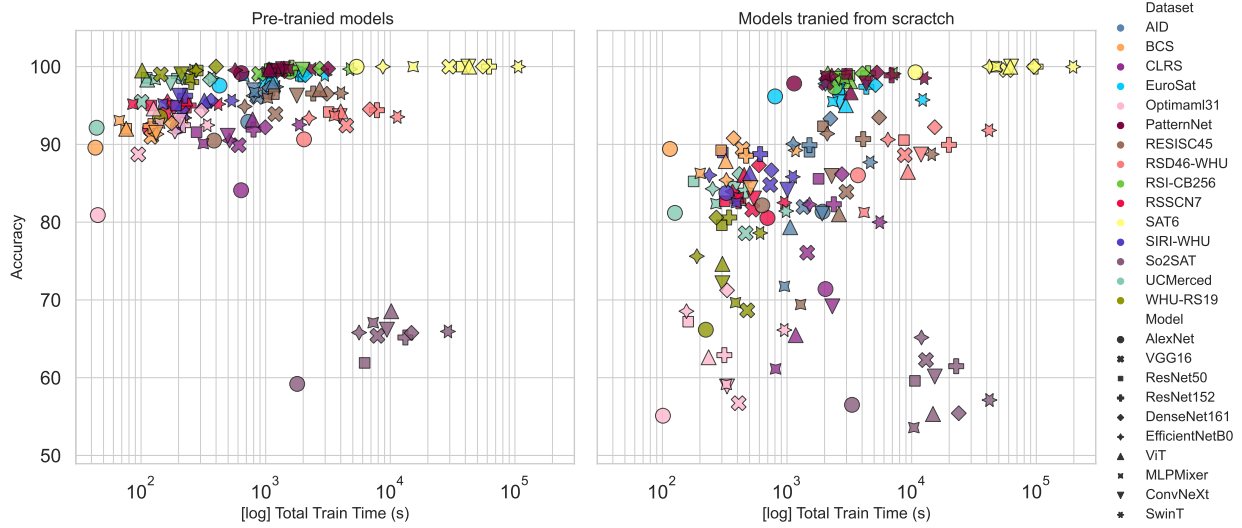
$$AP = \sum_n (R_n - R_{n-1})P_n$$

Where  $P_n$  and  $R_n$  are the precision and recall at the n-th threshold. It is a useful metric to compare how well models are ordering the predictions, without considering any specific decision threshold.

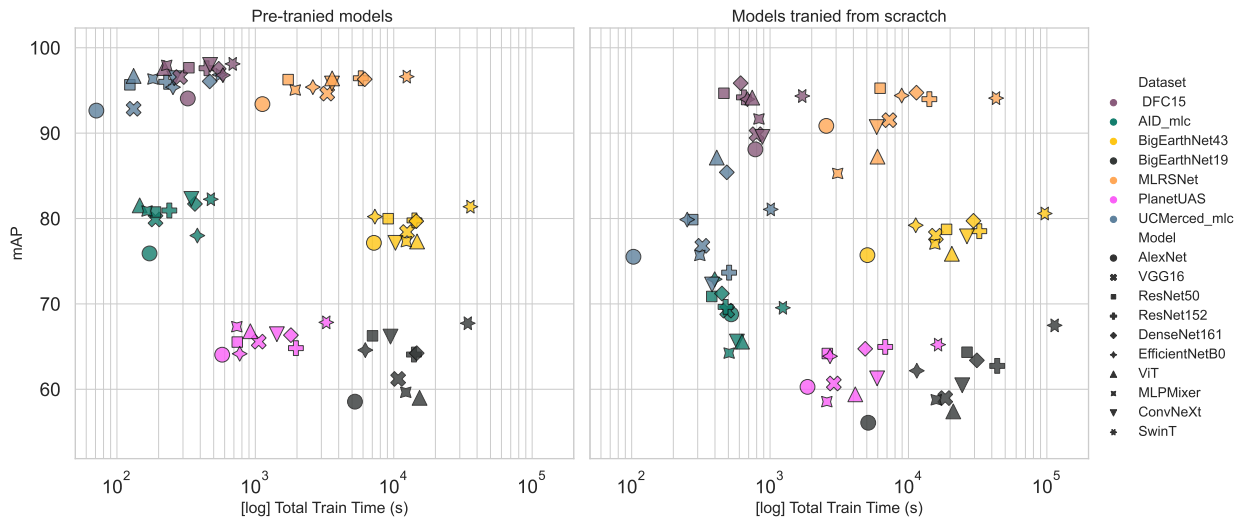
For the multi-label classification task, we report the following evaluation measures: Micro Precision, Macro Precision, Weighted Precision, Micro Recall, Macro Recall, Weighted Recall, Micro F1 score, Macro F1 score, Weighted F1 score and mean average precision (mAP). For all measures but mAP, that require a threshold on the predictions, we set it to 0.5 for all the models and settings.

For both tasks, we provide the means to perform even more detailed analysis of the performance by reporting the confusion matrices as a performance summary of the models. The confusion matrices provide detailed per class/label view of the models' performance.

## B Training Time Details



(a) Multi-Class classification tasks



(b) Multi-Label classification tasks

Figure B.1: **Performance vs. total training time** comparison of all model architectures (denoted with different markers); evaluated on **(top)** MCC and **(bottom)** MLC datasets (color-coded). We present both pretrained **(left)** and trained from scratch **(right)** variants. Performance is reported as accuracy (%) and mean average precision (mAP %) for MCC and MLC tasks, respectively. Note the log scale of the total training time (seconds)

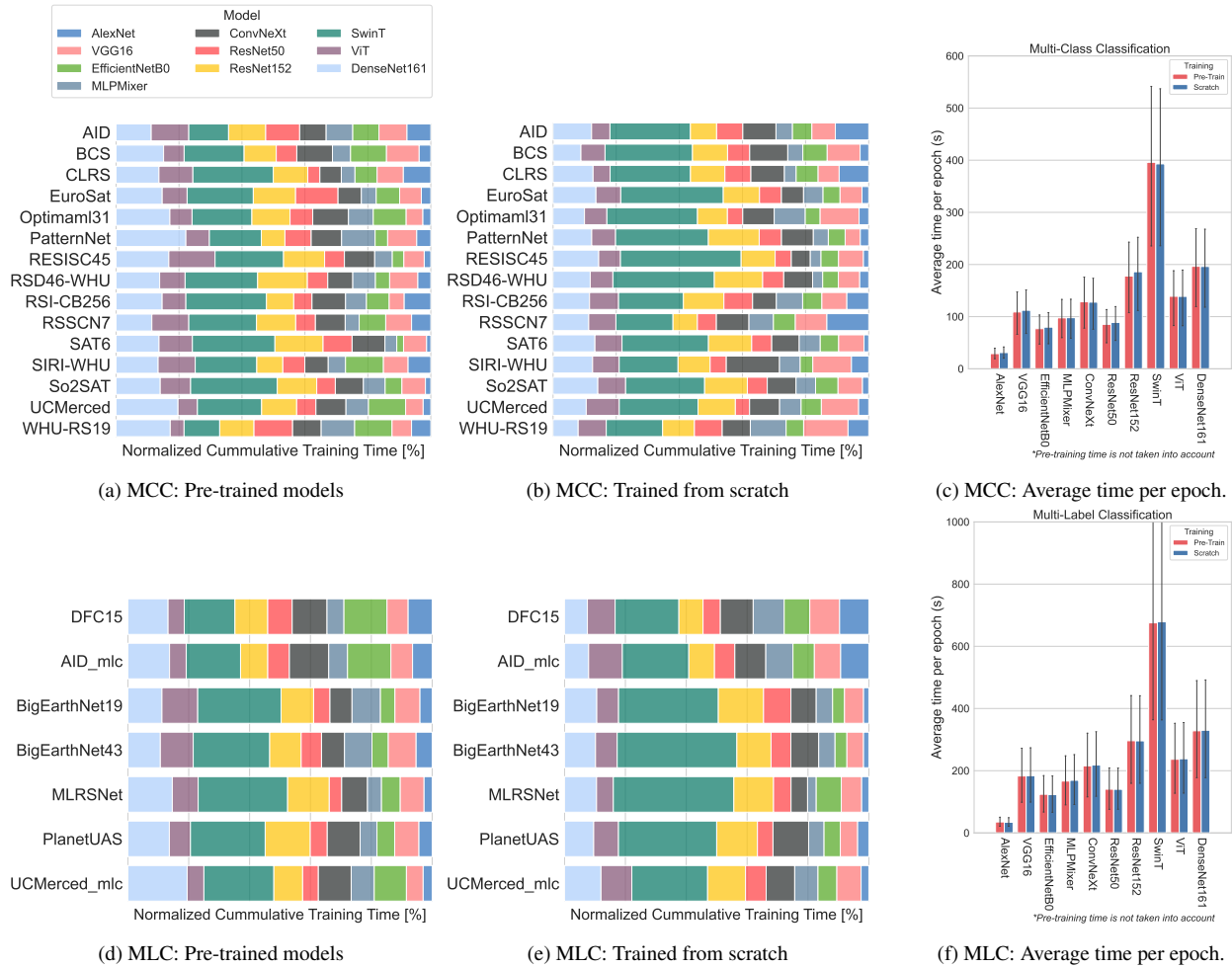


Figure B.2: **Training time** of models trained from scratch and pre-trained models for each of the (a,b) MCC and (d,e) MLC datasets. The training time of each model architecture (denoted with different colors) is depicted as a fraction (%) of the cumulative training time for each dataset. Furthermore, (c) and (f) illustrate the average time per epoch of each model variant on (c) MCC and (f) MLC tasks, comparing the (red) pre-trained model variants (from (a) and (b)) to their counterparts (blue) trained from scratch.

Table B.1: Training-time details for multi-class classification tasks.

	AlexNet		VGG16		ResNet50		ResNet152		DenseNet161		EfficientNetB0		ViT		MLPMixer		ComNeXt		SwinT		
	Pt.	Sc.	Pt.	Sc.	Pt.	Sc.	Pt.	Sc.	Pt.	Sc.	Pt.	Sc.	Pt.	Sc.	Pt.	Sc.	Pt.	Sc.			
Eurosat	Avg time/epoch (sec.)	8.88	8.02	33.69	33.62	26.56	26.45	56.21	61.12	62.5	23.47	23.49	30.41	31.45	40.38	40.03	124.17	122.44			
	Total training time (sec.)	426	802	977	2622	1912	2619	1904	4328	2078	5125	2032	1123	1056	2327	1050	2642	2980	12244		
	Best epoch	38	95	19	63	62	84	24	62	67	35	69	16	52	12	59	16	51	14	90	
UCMered	Avg time/epoch (sec.)	1.29	1.3	3.16	4.66	2.85	2.54	5.05	5.02	5.41	5.46	2.53	4	4.44	3.1	3.06	3.68	3.75	10.28	10.36	
	Total training time (sec.)	44	126	101	466	111	178	202	467	357	415	214	253	112	41.3	130	269	173	375	370	984
	Best epoch	24	82	22	85	29	55	30	78	56	61	77	93	18	78	32	73	37	92	26	80
AID	Avg time/epoch (sec.)	21.32	19.46	21.35	19.65	20.29	19.66	22.2	22.25	24.36	24.48	20	19.33	20.45	19.63	19.78	19.06	23.06	19.15	46.65	46.94
	Total training time (sec.)	725	1927	854	1356	1035	1514	1132	1513	1072	2228	800	1121	1145	1060	811	953	807	1915	1213	4647
	Best epoch	24	84	30	54	41	62	41	53	34	76	30	43	46	39	31	35	25	25	96	16
RSSCN7	Avg time/epoch (sec.)	3.19	6.97	4.68	6.74	3.9	3.76	7.09	6.9	7.59	8.5	3.79	3.65	5.54	5.52	4.3	4.08	5.23	5.43	13.42	13.78
	Total training time (sec.)	118	697	159	526	121	316	241	407	220	581	183	385	27	453	86	408	193	345	416	451
	Best epoch	27	88	24	68	21	69	24	44	19	55	33	93	31	67	10	100	23	87	21	54
WHU-RS19	Avg time/epoch (sec.)	2.78	2.53	3	4.79	2.85	3.85	4.02	4.29	4.04	4.04	2.76	189	102	303	247	386	211	303	263	608
	Total training time (sec.)	142	223	144	479	285	300	253	343	400	271	276	189	102	303	247	386	211	303	263	608
	Best epoch	41	73	38	96	96	63	53	65	89	52	100	53	20	73	77	89	56	90	34	86
SIRFAHU	Avg time/epoch (sec.)	4.28	3.54	4.98	7.32	4.66	3.81	6.65	6.54	7.3	7.49	3.61	5.37	5.08	4.55	3.92	5.64	11.99	11.87	12.1	11.13
	Total training time (sec.)	197	326	214	732	191	305	226	608	365	749	329	238	322	503	150	392	203	1007	534	1113
	Best epoch	36	77	33	93	31	65	24	78	40	94	62	51	50	84	23	98	26	69	35	77
RSI-CB256	Avg time/epoch (sec.)	34.84	34.99	34.04	34.9	33.69	36.39	51.9	51.86	56.6	56.75	33.5	26.5	41.18	41.08	35.29	29	40.35	36.93	113.14	113.6
	Total training time (sec.)	1568	2414	885	2757	1078	3166	1609	4472	2717	4029	1340	2123	1400	3204	1235	2900	1977	2622	4752	7157
	Best epoch	12	03	10	91	30	61	31	31	64	72	21	72	21	24	63	25	86	39	56	32
RESISC45	Avg time/epoch (sec.)	12.03	10.91	39.87	38.37	30.61	31.31	65.11	64.83	72.05	71.22	27.12	27.66	51.19	50.21	35.62	35.69	46.79	46.51	143.57	144.87
	Total training time (sec.)	385	633	1196	2993	1163	1941	2409	4084	3098	5484	678	2102	2713	2611	1033	1285	1778	2279	4020	14487
	Best epoch	22	43	20	63	28	47	27	48	33	62	15	61	43	37	19	21	28	34	18	85
PatternNet	Avg time/epoch (sec.)	15.17	13.75	37.74	37.47	29.1	35.65	62.94	60.05	68.87	71.08	25.86	27.54	48.5	49.05	33.8	34.54	45.93	45.06	138.59	138.59
	Total training time (sec.)	637	1141	1321	2061	1193	3030	1070	6905	3168	5260	569	2286	1067	3237	1521	2038	1378	4326	2357	12612
	Best epoch	32	68	25	40	31	70	7	88	36	59	12	68	12	51	33	44	20	81	7	76
CLRS	Avg time/epoch (sec.)	20.48	20.35	20.23	19.33	18.6	19.43	31.96	32.05	35.46	35.81	19.73	20.71	25.32	24.96	19.75	17.98	23.62	23.09	68.93	69.19
	Total training time (sec.)	635	2035	607	1450	279	1788	799	2373	993	2757	513	1512	785	1173	316	809	496	2309	1861	5535
	Best epoch	21	92	20	60	15	77	15	60	18	62	16	58	21	32	6	30	11	96	17	65
RSD46-WHU	Avg time/epoch (sec.)	58.03	58.84	158.32	162.89	123.27	127.53	269.45	272.7	297.7	301.16	111.55	113.93	210.37	211.93	148.25	148.42	196.2	194.93	599.42	588.25
	Total training time (sec.)	2031	3707	4433	8796	3205	8672	7814	19907	6847	15318	6446	3997	9325	3558	4149	3924	11891	11389	41766	41766
	Best epoch	25	48	18	39	16	53	19	58	13	36	10	40	9	29	14	12	10	46	9	56
SAT6	Avg time/epoch (sec.)	92.48	107.26	550.04	579.1	410.33	457.04	872.87	987.21	970.39	956.03	363	420.37	692.5	687.12	476.34	479.37	630.78	627.69	2403.62	1973.44
	Total training time (sec.)	5364	10726	29702	57910	37340	45704	61974	98721	55312	95603	8712	42037	42935	61841	15243	47937	42262	62769	106192	197344
	Best epoch	48	98	44	98	81	99	61	94	47	85	14	95	52	75	22	95	57	97	97	99
Optimam31	Avg time/epoch (sec.)	1.1	1.21	2.97	4.81	2.58	2.6	4.62	5.92	5.02	5.16	2.25	2.36	3.71	3.70	2.82	3.26	3.5	3.59	9.19	9.51
	Total training time (sec.)	45	101	95	409	129	165	217	314	306	330	187	156	206	235	141	326	203	330	340	951
	Best epoch	31	67	22	70	40	47	37	38	31	51	49	73	51	24	47	40	48	48	77	27
BCS	Avg time/epoch (sec.)	1.48	1.53	4.17	5.95	3.45	4.55	6.61	7.95	7.33	7.31	3.17	3.26	5.07	5.55	3.94	4.47	5.08	5.09	13.88	13.59
	Total training time (sec.)	43	115	121	440	76	296	119	469	176	373	133	326	76	322	67	201	132	509	222	1169
	Best epoch	19	60	19	59	12	50	18	44	14	36	32	98	5	43	7	30	16	95	6	71
SoSat	Avg time/epoch (sec.)	158.09	174.74	716.09	723.72	565.55	558.79	1200.64	1198.37	1324.1	1325.67	510.45	499.21	925.09	926.5	643.91	651.31	853.91	851.06	2636.45	2631.44
	Total training time (sec.)	1790	3320	7877	13027	6221	10617	13207	22769	14784	23862	5615	11981	10376	14824	7278	10421	9393	15319	29001	42103
	Best epoch	1	4	1	3	1	4	1	4	1	3	1	1	9	1	1	1	1	1	1	1

Table B.2: Training-time details for multi-Label classification tasks.

	AlexNet		VGG16		ResNet50		ResNet152		DenseNet161		EfficientNetB0		ConvNeXt		ViT		MLPMixer		SwinT		
	Pt.	Sc.	Pt.	Sc.	Pt.	Sc.	Pt.	Sc.	Pt.	Sc.	Pt.	Sc.	Pt.	Sc.	Pt.	Sc.	Pt.	Sc.	Pt.	Sc.	
AID	Avg time/epoch (sec.)	5.55	5.82	6.33	6.28	5.94	5.74	7.97	8.08	8.71	8.47	6.15	5.94	6.63	6.4	6.95	6.82	6.35	6.41	15.9	15.87
	Total training time (sec.)	172	524	190	490	379	239	477	366	449	381	398	345	576	146	627	165	506	477	1238	1238
	Best epoch	21	75	20	63	22	51	20	44	32	38	52	52	42	75	11	77	16	64	20	63
UCMerced	Avg time/epoch (sec.)	1.31	1.03	3.3	3.24	2.76	2.76	5.04	5.06	5.64	5.6	2.54	2.23	3.92	3.81	4.13	4.12	3.25	3.11	10.22	10.12
	Total training time (sec.)	71	103	132	324	124	276	227	506	468	487	254	252	259	381	132	412	182	311	552	1012
	Best epoch	44	91	30	99	35	99	35	86	73	72	98	99	56	100	22	95	46	99	44	99
DFC15	Avg time/epoch (sec.)	7.74	7.83	8.94	8.5	8.49	8.92	9.45	9.66	9.54	9.89	8.33	8.47	8.72	8.8	8.76	8.85	8.18	8.31	17.59	17.09
	Total training time (sec.)	325	783	286	799	331	464	444	647	544	613	583	686	471	880	219	743	229	831	686	1709
	Best epoch	32	99	22	79	29	37	37	52	47	47	60	66	44	91	15	69	18	100	29	95
MLRSNet	Avg time/epoch (sec.)	34.09	34.92	132.2	132.22	101.67	102.26	214.11	214.47	237.35	237.96	86.8	89.34	155.65	159.35	170.9	170.71	121.38	123.2	496.72	482.72
	Total training time (sec.)	1125	2549	3306	7272	1726	6238	5781	14155	6171	11422	2604	8934	3580	5896	3589	5975	1942	3080	12418	42962
	Best epoch	23	58	15	40	16	46	17	51	16	33	20	87	13	22	11	20	6	10	15	74
PlanetUAS	Avg time/epoch (sec.)	17.45	18.65	50.38	50.68	37	37.57	81.83	80.86	90.4	90.11	33.52	33.47	59.63	59.35	65.71	65.52	45.94	45.93	180.89	181.93
	Total training time (sec.)	576	1865	1058	2889	740	2592	1964	6792	1808	4866	771	2711	1431	5935	920	4128	735	2572	3256	16365
	Best epoch	23	87	11	42	10	54	14	69	10	39	13	66	14	90	4	48	6	41	8	75
BigEarthNet 19	Avg time/epoch (sec.)	90.43	84.18	537.9	544.28	413.24	409.87	874.56	878	976.93	982.63	366.35	364.13	631.67	645.51	698.5	709.86	488.68	500.77	1990	2011.29
	Total training time (sec.)	5245	5051	10758	15784	7025	18854	13993	32486	14654	29479	6228	11288	9475	26466	15367	20586	12217	15524	38820	96542
	Best epoch	48	45	10	14	7	31	6	22	5	15	7	16	5	26	12	14	15	16	8	33
BigEarthNet 43	Avg time/epoch (sec.)	89.85	86.78	542.3	542.24	414.18	413.89	881.69	875.2	969.67	975.34	365.4	359.16	642.81	643.66	702	702.53	492.84	495.88	2016	2031.64
	Total training time (sec.)	7188	5120	12473	18436	9112	26489	14107	43760	14545	31211	7308	11493	10285	24459	14742	21076	12321	15868	34272	113772
	Best epoch	70	44	13	19	12	49	6	35	5	17	10	17	6	23	11	15	15	17	7	41

## C Extended results on model generalization performance

### C.1 Evaluation on a same holdout set

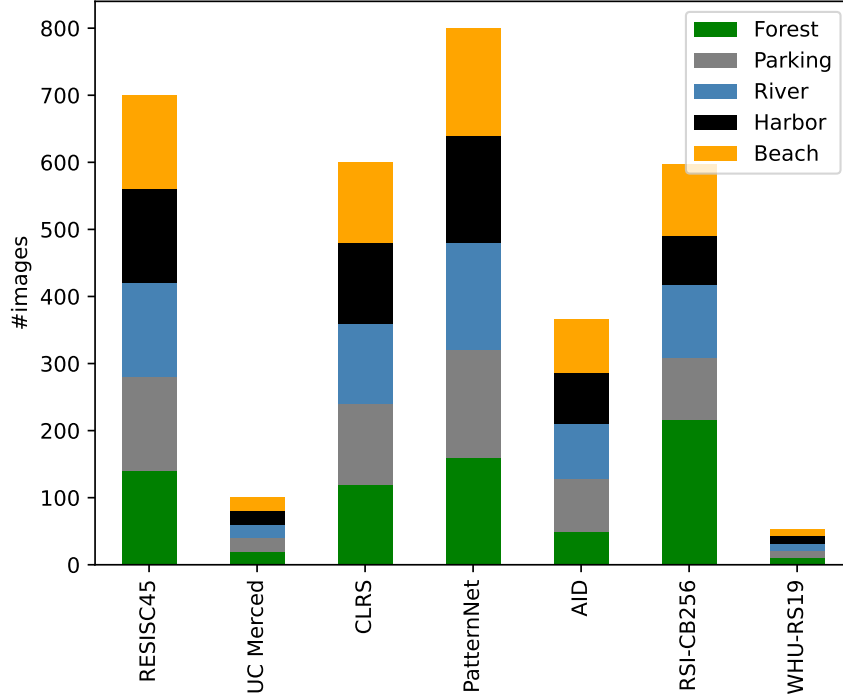


Figure C.1: Distribution of images in the holdout set w.r.t. source datasets and labels.

Table C.1: Accuracy (%) of models pre-trained on ImageNet-1K and fine-tuned on a specific source dataset and evaluated on the common test dataset with shared labels. Bold indicates best performing model for a given source dataset.

Dataset \ Model	AlexNet	VGG16	ResNet50	ResNet152	DenseNet161	EfficientNetB0	ViT	MLPMixer	ConvNeXt	SwinT
RESISC45	66.853	78.514	81.063	84.08	84.111	77.985	<b>86.007</b>	82.121	84.422	83.706
UC Merced	63.371	67.04	76.057	73.01	74.254	74.44	75.995	<b>79.478</b>	75.902	72.326
CLRS	80.037	83.427	89.801	88.557	89.024	86.07	<b>92.6</b>	89.646	89.303	90.299
PatternNet	43.501	52.332	56.965	54.54	56.716	60.044	64.739	62.687	59.391	<b>65.205</b>
AID	71.393	69.714	79.384	80.1	66.169	77.892	<b>83.862</b>	77.954	79.851	79.789
RSI-CB256	56.872	61.412	58.893	63.65	64.832	61.723	66.014	<b>66.791</b>	64.677	66.294
WHU-RS19	61.101	62.624	71.953	73.321	72.388	68.284	72.917	74.036	<b>74.876</b>	71.144
<i>Avg. Rank</i>	9.71	8.71	5.43	5.29	5.86	6.86	<b>2.14</b>	3.29	3.57	4.14

## C.2 Results from pairwise comparisons

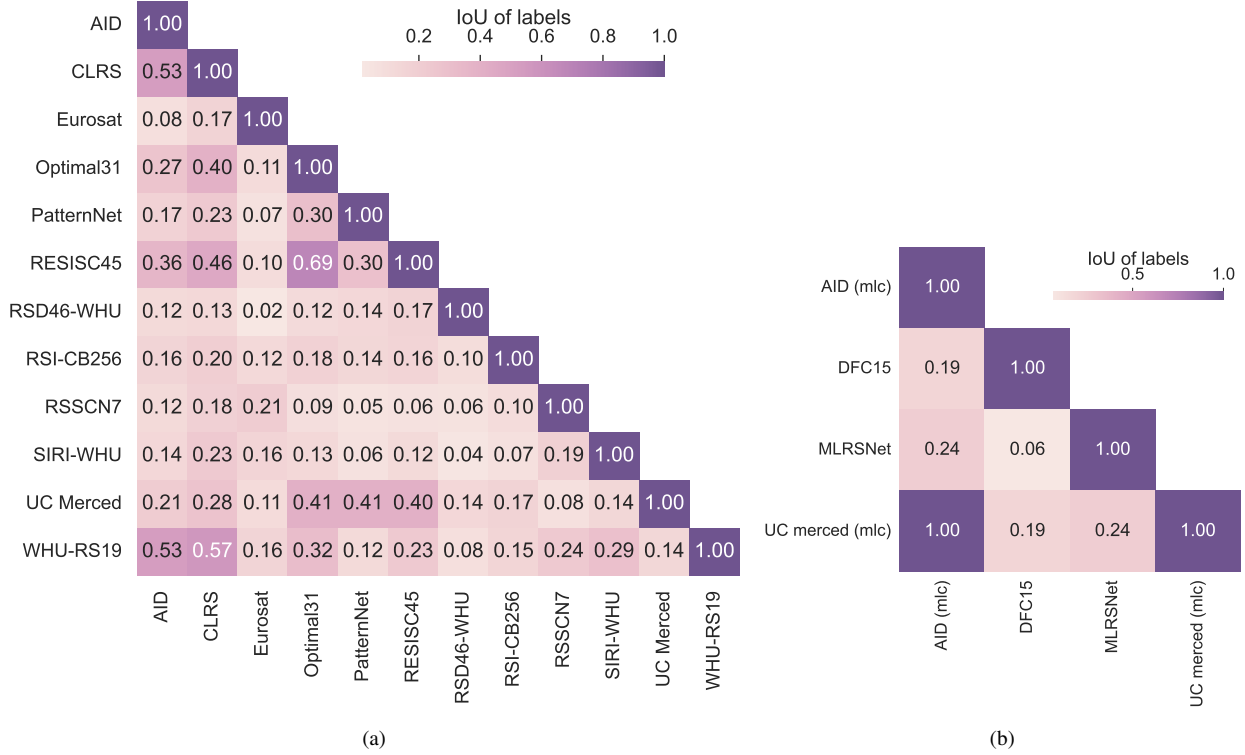


Figure C.2: Label overlap between each pair of datasets, in terms of Intersection over Union (IoU) for (a) MCC and (b) MLC datasets.

Table C.2: AlexNet on MCC tasks: Generalization performance in terms of accuracy (%) of ImageNet-1K pre-trained models, fine-tuned on *source* and evaluated on images with shared labels in *target* dataset.

Source \ Target dataset	RESISC45	UC Merced	CLRS	Optimal31	PatternNet	AID	RSI-CB256	WHU-RS19	SIRI-WHU	RSD46-WHU	Eurosat	SAT6	RSSCN7
RESISC45	90.492	57.368	49.053	96.505	76.217	70.802	57.793	67.717	43.333	30.377	0.704	0.0	39.167
UC Merced	51.729	92.143	37.583	62.222	74.522	50.94	75.182	56.604	9.375	20.656	0.438	0.57	46.875
CLRS	67.64	60.5	84.1	71.875	72.135	79.601	67.363	72.024	54.643	53.717	16.963	0.0	51.0
Optimal31	74.654	65.333	44.635	80.914	77.656	65.704	59.596	66.142	35.0	27.216	1.045	0.0	33.333
PatternNet	39.248	47.059	20.278	57.292	99.161	31.322	33.952	23.81	11.667	16.095	30.062	0.0	11.875
AID	67.107	57.778	54.298	78.846	62.125	92.9	57.5	98.333	27.5	37.144	1.312	7.437	45.0
RSI-CB256	45.13	70.0	32.833	50.833	71.319	50.469	99.354	61.644	29.167	36.944	29.821	10.597	16.25
WHU-RS19	54.702	74.0	42.396	60.417	63.125	72.968	64.938	93.532	26.429	42.055	0.0	0.0	48.25
SIRI-WHU	59.167	26.25	59.167	63.333	58.542	57.735	29.446	51.316	92.292	63.991	28.875	8.481	26.25
RSD46-WHU	35.714	35.625	44.896	54.167	44.062	49.643	38.433	59.615	60.0	90.646	97.0	2.379	48.75
Eurosat	24.286	15.0	39.667	27.083	37.083	25.714	37.092	46.512	67.5	26.108	97.574	0.017	57.083
SAT6	0.0	7.5	14.167	0.0	0.0	31.25	5.053	0.0	5.0	6.528	13.333	99.98	88.75
RSSCN7	73.095	70.0	59.833	69.444	68.125	75.357	43.833	84.615	92.5	45.268	2.529	0.032	91.964

Table C.3: VGG16 on MCC tasks: Generalization performance in terms of accuracy (%) of ImageNet-1K pre-trained models, fine-tuned on *source* and evaluated on images with shared labels in *target* dataset.

Source \ Target dataset	RESISC45	UC Merced	CLRS	Optimal31	PatternNet	AID	RSI-CB256	WHU-RS19	SIRI-WHU	RSD46-WHU	Eurosat	SAT6	RSSCN7
RESISC45	93.905	76.579	65.227	98.656	81.941	78.752	67.052	76.378	48.333	43.589	0.407	0.0	52.083
UC Merced	55.94	95.476	40.417	67.222	79.449	58.464	83.577	67.925	3.75	26.019	0.125	0.223	41.25
CLRS	76.615	68.0	89.9	81.771	75.781	86.273	73.392	82.143	66.429	65.137	14.259	0.012	52.75
Optimal31	79.378	71.333	53.229	88.71	80.977	67.09	59.091	63.78	50.5	36.299	6.0	0.0	37.917
PatternNet	45.263	55.588	29.306	61.458	99.424	41.379	52.293	31.746	25.0	23.98	29.0	0.0	26.25
AID	70.071	61.111	62.105	79.487	67.062	96.1	61.083	97.778	42.0	45.984	1.188	0.12	47.188
RSI-CB256	47.922	74.375	35.083	57.5	74.931	58.75	99.051	69.863	24.167	39.985	23.143	1.621	35.0
WHU-RS19	55.179	72.0	44.01	61.111	68.125	78.69	66.183	99.005	23.571	47.469	0.0	0.0	43.25
SIRI-WHU	53.452	11.25	61.429	68.333	36.667	56.906	27.988	61.842	93.958	74.734	30.375	18.881	25.833
RSD46-WHU	41.319	44.375	50.938	54.167	40.562	40.893	31.946	57.692	48.75	92.422	97.5	3.569	50.417
Eurosat	35.571	23.333	55.667	43.75	50.0	74.286	25.272	55.814	76.667	45.32	98.148	3.958	55.417
SAT6	81.429	37.5	52.083	58.333	100.0	63.393	7.979	90.909	0.0	18.62	0.167	99.993	31.25
RSSCN7	78.81	90.0	75.5	77.778	86.562	86.429	63.188	94.231	75.833	66.911	7.059	0.143	93.929

Table C.4: ResNet50 on MCC tasks: Generalization performance in terms of accuracy (%) of ImageNet-1K pre-trained models, fine-tuned on *source* and evaluated on images with shared labels in *target* dataset.

Source \ Target dataset	RESISC45	UC Merced	CLRS	Optimal31	PatternNet	AID	RSI-CB256	WHU-RS19	SIRI-WHU	RSD46-WHU	Eurosat	SAT6	RSSCN7
RESISC45	96.46	72.105	67.083	99.194	84.178	79.941	72.377	81.89	56.25	42.872	9.185	0.021	56.667
UC Merced	63.496	98.571	49.25	75.0	88.088	68.182	91.241	86.792	20.0	34.753	4.75	7.073	46.25
CLRS	80.435	73.5	91.567	86.979	85.573	88.574	79.984	87.5	71.071	67.582	33.407	0.427	51.25
Optimal31	86.636	73.333	63.906	92.204	87.07	82.91	75.337	77.953	60.0	37.291	5.955	2.806	43.333
PatternNet	46.128	54.412	27.847	65.104	99.737	39.224	64.847	44.444	17.5	23.73	29.938	0.0	26.25
AID	75.321	64.444	66.886	80.769	73.75	96.55	72.167	99.444	42.0	47.474	17.938	3.662	50.0
RSI-CB256	49.545	68.75	36.583	56.667	74.931	58.125	99.677	60.274	29.167	39.985	37.036	0.743	17.812
WHU-RS19	71.905	89.0	56.198	78.472	69.375	86.816	66.805	99.502	44.643	48.221	0.364	30.899	53.25
SIRI-WHU	55.0	20.0	60.476	61.667	42.083	52.762	27.697	55.263	95.0	71.901	47.562	41.35	22.917
RSD46-WHU	41.374	45.0	45.833	56.25	42.688	35.714	36.475	44.231	42.5	94.153	98.833	10.93	44.167
Eurosat	32.571	10.0	45.333	25.0	7.292	42.381	32.473	62.791	78.333	87.438	98.833	1.999	55.417
SAT6	0.714	7.5	17.083	8.333	0.0	37.5	5.053	0.0	0.0	7.196	0.167	100.0	68.75
RSSCN7	79.048	97.5	74.333	77.778	92.5	82.143	57.306	88.462	71.667	68.379	4.765	0.008	95.0

Table C.5: ResNet152 on MCC tasks: Generalization performance in terms of accuracy (%) of ImageNet-1K pre-trained models, fine-tuned on *source* and evaluated on images with shared labels in *target* dataset.

Source \ Target dataset	RESISC45	UC Merced	CLRS	Optimal31	PatternNet	AID	RSI-CB256	WHU-RS19	SIRI-WHU	RSD46-WHU	Eurosat	SAT6	RSSCN7
RESISC45	96.54	72.895	68.485	98.656	85.066	80.684	73.38	83.465	59.583	47.194	18.63	0.331	52.5
UC Merced	61.729	98.81	46.417	73.889	89.743	63.95	89.173	69.811	22.5	34.018	15.188	13.09	47.5
CLRS	81.553	70.0	91.933	84.896	80.469	88.42	79.984	85.119	70.0	71.065	46.259	2.62	51.75
Optimal31	87.972	72.667	65.99	92.473	86.797	82.217	82.071	78.74	56.5	38.252	6.273	18.893	42.5
PatternNet	51.053	49.412	33.681	63.542	99.49	35.776	61.463	28.571	30.0	30.013	24.875	0.0	15.0
AID	79.143	61.667	69.298	80.769	73.125	97.2	73.083	98.889	36.5	45.045	11.438	17.338	44.688
RSI-CB256	53.312	73.125	37.75	62.5	78.472	58.438	99.859	64.384	27.5	44.325	27.643	19.238	20.625
WHU-RS19	72.798	87.0	57.708	79.167	66.25	86.567	73.755	98.01	40.0	51.83	10.409	0.141	49.5
SIRI-WHU	66.19	50.0	67.262	73.333	74.375	66.298	40.233	57.895	96.25	84.061	55.062	18.092	27.083
RSD46-WHU	44.396	43.75	49.062	56.25	45.438	43.929	39.045	51.923	46.25	94.404	95.5	1.968	40.0
Eurosat	28.857	6.667	38.167	27.083	3.75	50.476	29.62	27.907	71.667	85.222	99.0	1.034	47.083
SAT6	0.0	10.0	26.25	0.0	0.0	46.429	19.681	0.0	15.0	6.825	2.833	100.0	68.75
RSSCN7	76.19	87.5	73.167	83.333	83.75	86.786	55.977	94.231	88.333	52.311	36.176	0.087	95.0

Table C.6: DenseNet161 on MCC tasks: Generalization performance in terms of accuracy (%) of ImageNet-1K pre-trained models, fine-tuned on *source* and evaluated on images with shared labels in *target* dataset.

Source \ Target dataset	RESISC45	UC Merced	CLRS	Optimal31	PatternNet	AID	RSI-CB256	WHU-RS19	SIRI-WHU	RSD46-WHU	Eurosat	SAT6	RSSCN7
RESISC45	96.508	75.0	69.015	98.925	87.862	78.975	76.543	81.89	60.0	49.385	10.111	29.235	56.25
UC Merced	63.271	98.333	50.917	73.889	87.059	68.025	92.214	75.472	16.875	31.995	12.25	5.067	55.0
CLRS	80.994	72.5	92.2	88.021	81.146	88.344	79.502	86.31	72.857	71.199	38.519	1.229	49.75
Optimal31	88.641	77.0	65.469	94.355	87.461	83.603	78.283	78.74	55.5	40.67	6.409	30.969	44.167
PatternNet	52.105	60.294	32.083	69.792	99.737	41.236	63.1	39.683	20.833	25.006	19.5	0.021	26.25
AID	66.25	39.444	45.175	76.923	58.75	88.85	49.083	93.333	24.5	26.295	3.125	20.976	38.125
RSI-CB256	52.208	68.75	41.75	55.833	72.292	63.125	99.737	71.233	30.833	45.03	39.464	0.145	23.75
WHU-RS19	74.821	91.0	59.167	79.861	69.167	87.396	69.295	100.0	45.0	53.233	1.591	0.007	55.5
SIRI-WHU	55.833	33.75	65.714	55.0	53.333	59.945	34.111	56.579	95.625	76.269	26.188	82.087	35.833
RSD46-WHU	41.758	44.375	49.271	50.0	41.25	47.5	36.353	53.846	38.75	94.507	96.0	0.711	48.75
Eurosat	5.857	1.667	20.5	0.0	5.417	2.381	39.402	25.581	57.5	76.601	98.889	0.2	30.417
SAT6	0.0	5.0	32.083	0.0	0.0	50.893	33.511	0.0	0.0	0.89	0.0	100.0	63.75
RSSCN7	85.0	97.5	80.5	80.556	93.125	91.429	59.013	92.308	81.667	63.316	11.941	0.921	94.821

Table C.7: EfficientNetB0 on MCC tasks: Generalization performance in terms of accuracy (%) of ImageNet-1K pre-trained models, fine-tuned on *source* and evaluated on images with shared labels in *target* dataset.

Source \ Target dataset	RESISC45	UC Merced	CLRS	Optimal31	PatternNet	AID	RSI-CB256	WHU-RS19	SIRI-WHU	RSD46-WHU	Eurosat	SAT6	RSSCN7
RESISC45	94.873	71.053	65.303	98.656	81.316	76.003	68.364	74.016	53.333	45.576	3.185	0.0	45.417
UC Merced	63.571	98.571	48.333	75.0	89.338	63.95	87.47	71.698	11.25	36.163	10.75	33.058	41.25
CLRS	80.373	71.0	90.5	83.333	82.604	87.807	76.206	82.738	68.929	67.716	11.37	0.541	56.5
Optimal31	86.06	74.333	64.583	91.667	85.469	78.984	74.327	72.441	61.0	41.538	4.864	0.804	35.0
PatternNet	50.338	58.824	35.833	69.271	99.539	42.529	65.611	49.206	17.5	25.732	22.75	1.17	34.375
AID	75.286	65.556	63.377	80.769	73.25	96.25	73.75	98.333	44.5	43.102	4.875	1.346	44.062
RSI-CB256	49.481	75.625	38.75	55.833	76.458	58.281	99.717	71.233	27.5	43.731	31.893	2.586	18.75
WHU-RS19	70.774	89.0	51.771	74.306	67.188	85.489	79.357	99.502	47.5	47.268	0.0	0.0	48.0
SIRI-WHU	61.548	40.0	60.833	65.0	65.625	52.21	36.735	55.263	95.0	74.262	11.188	4.447	25.833
RSD46-WHU	42.418	43.75	47.812	46.875	44.562	41.786	38.433	51.923	31.25	93.399	95.0	4.666	41.25
Eurosat	8.857	13.333	8.5	10.417	0.0	8.571	13.315	6.977	5.833	50.493	98.907	54.596	2.5
SAT6	6.429	10.0	5.417	8.333	1.875	12.5	13.298	0.0	0.0	7.196	0.0	99.988	30.0
RSSCN7	84.762	85.0	75.833	86.111	93.125	87.143	56.546	90.385	72.5	63.023	8.176	0.079	95.536

Table C.8: ViT on MCC tasks: Generalization performance in terms of accuracy (%) of ImageNet-1K pre-trained models, fine-tuned on *source* and evaluated on images with shared labels in *target* dataset.

Source \ Target dataset	RESISC45	UC Merced	CLRS	Optimal31	PatternNet	AID	RSI-CB256	WHU-RS19	SIRI-WHU	RSD46-WHU	Eurosat	SAT6	RSSCN7
RESISC45	97.079	87.368	71.553	98.118	90.461	83.804	81.096	88.189	62.5	54.015	15.519	5.992	51.667
UC Merced	65.038	98.333	51.333	75.556	89.007	69.436	88.2	83.019	25.625	41.404	24.375	28.516	41.875
CLRS	82.484	83.5	93.2	86.979	88.177	91.411	86.897	85.714	74.643	73.543	45.741	7.806	56.75
Optimal31	89.055	87.667	69.844	94.624	87.344	86.374	85.017	81.89	68.0	47.892	4.5	54.036	45.0
PatternNet	55.038	70.882	42.639	74.479	99.655	51.724	70.197	63.492	49.167	36.496	30.875	0.0	38.75
AID	81.393	81.111	74.342	87.821	78.5	97.75	70.083	98.333	55.5	54.145	37.875	33.276	46.562
RSI-CB256	57.857	81.25	48.25	67.5	84.236	68.75	99.758	83.562	27.5	54.117	33.821	11.852	27.812
WHU-RS19	66.369	81.0	60.729	77.083	77.396	87.313	71.473	99.502	43.214	56.391	5.455	23.313	52.0
SIRI-WHU	70.119	60.0	72.262	76.667	81.667	62.155	34.111	67.105	95.625	88.548	31.062	7.107	24.167
RSD46-WHU	47.637	47.5	52.708	60.417	50.875	57.857	43.819	73.077	81.25	94.238	99.0	10.62	51.25
Eurosat	51.857	48.333	70.167	56.25	58.958	93.333	55.435	83.721	77.5	70.936	98.722	2.132	62.5
SAT6	90.714	30.0	55.0	91.667	80.625	57.143	7.181	90.909	0.0	4.599	1.833	99.998	86.25
RSSCN7	81.429	85.0	82.833	83.333	90.625	90.0	69.829	86.538	45.0	65.297	20.412	56.78	95.893

Table C.9: MLP Mixer on MCC tasks: Generalization performance in terms of accuracy (%) of ImageNet-1K pre-trained models, fine-tuned on *source* and evaluated on images with shared labels in *target* dataset.

Source \ Target dataset	RESISC45	UC Merced	CLRS	Optimal31	PatternNet	AID	RSI-CB256	WHU-RS19	SIRI-WHU	RSD46-WHU	Eurosat	SAT6	RSSCN7
RESISC45	95.952	81.842	65.947	98.925	86.25	78.455	78.164	83.465	52.5	47.255	11.926	1.255	47.5
UC Merced	64.474	98.333	52.417	72.778	91.471	68.966	93.187	86.792	27.5	36.929	29.75	27.488	53.75
CLRS	80.373	67.0	90.1	83.333	80.365	88.42	80.305	84.524	69.286	68.252	34.37	3.88	49.25
Optimal31	87.12	74.667	65.938	92.742	86.797	82.679	80.303	86.614	64.0	39.678	8.364	6.486	41.667
PatternNet	52.481	68.529	39.792	67.708	99.704	51.868	67.686	49.206	48.333	29.662	26.312	0.233	24.375
AID	77.929	68.333	67.544	78.205	71.688	96.7	68.417	99.444	49.5	46.179	34.438	21.946	45.312
RSI-CB256	56.169	82.5	45.5	67.5	80.139	65.312	99.657	80.822	32.5	45.438	36.179	13.455	20.938
WHU-RS19	68.452	84.0	59.167	77.778	69.896	86.816	84.44	98.507	47.143	58.095	2.5	6.472	55.25
SIRI-WHU	67.262	38.75	72.024	80.0	77.292	66.575	34.694	65.789	95.208	82.999	40.25	0.978	33.333
RSD46-WHU	41.264	41.25	49.375	50.0	49.25	54.821	43.696	65.385	50.0	93.667	96.833	7.126	53.75
Eurosat	53.857	35.0	63.5	54.167	60.208	93.333	56.929	81.395	70.0	68.473	98.741	0.685	60.833
SAT6	97.143	50.0	55.833	100.0	100.0	61.607	6.117	90.909	0.0	9.125	0.0	99.995	77.5
RSSCN7	84.286	95.0	81.333	86.111	91.562	92.857	65.844	96.154	95.833	62.362	13.588	2.358	95.179

Table C.10: ConvNeXt on MCC tasks: Generalization performance in terms of accuracy (%) of ImageNet-1K pre-trained models, fine-tuned on *source* and evaluated on images with shared labels in *target* dataset.

Source \ Target dataset	RESISC45	UC Merced	CLRS	Optimal31	PatternNet	AID	RSI-CB256	WHU-RS19	SIRI-WHU	RSD46-WHU	Eurosat	SAT6	RSSCN7
RESISC45	96.27	82.895	71.136	98.656	90.099	81.798	78.318	81.89	56.25	52.253	11.444	0.049	55.0
UC Merced	64.436	97.857	52.667	72.778	91.066	66.928	91.971	73.585	18.125	38.737	5.438	2.732	50.625
CLRS	81.056	71.5	91.1	86.458	86.875	92.101	79.26	88.095	71.071	72.907	33.111	0.184	52.75
Optimal31	87.581	82.667	65.521	93.011	89.18	84.527	81.145	86.614	63.5	47.861	6.773	3.807	50.417
PatternNet	53.947	72.059	40.208	70.312	99.671	53.879	59.716	52.381	39.167	31.79	7.062	0.0	45.0
AID	76.143	63.889	68.158	82.051	73.812	96.95	71.583	99.444	51.5	52.85	21.375	18.89	42.188
RSI-CB256	53.701	82.5	42.75	60.833	79.028	66.094	99.596	76.712	25.0	50.408	27.786	14.977	29.688
WHU-RS19	63.75	80.0	53.958	70.139	76.354	88.723	70.539	99.005	38.571	51.579	0.0	0.0	56.75
SIRI-WHU	68.214	41.25	69.524	80.0	76.458	60.773	33.819	64.474	96.25	86.423	48.812	8.474	27.917
RSD46-WHU	49.121	46.875	51.562	62.5	48.125	47.321	39.168	55.769	62.5	93.627	97.333	7.778	51.25
Eurosat	56.286	55.0	69.167	54.167	64.792	94.762	48.641	93.023	80.833	39.655	98.778	0.479	75.833
SAT6	86.429	50.0	45.0	91.667	65.0	42.857	3.723	90.909	0.0	10.015	1.833	99.999	47.5
RSSCN7	82.857	100.0	80.833	83.333	89.375	88.929	63.188	94.231	68.333	59.501	8.118	1.953	94.643

Table C.11: SwinT on MCC tasks: Generalization performance in terms of accuracy (%) of ImageNet-1K pre-trained models, fine-tuned on *source* and evaluated on images with shared labels in *target* dataset.

Source \ Target dataset	RESISC45	UC Merced	CLRS	Optimal31	PatternNet	AID	RSI-CB256	WHU-RS19	SIRI-WHU	RSD46-WHU	Eurosat	SAT6	RSSCN7
RESISC45	96.587	86.316	71.742	99.462	88.355	82.987	79.398	88.976	62.5	50.942	11.704	4.357	59.167
UC Merced	60.714	98.571	46.0	72.778	89.779	64.734	88.2	60.377	10.0	40.239	11.875	51.12	55.625
CLRS	82.453	77.0	92.533	86.979	87.865	91.948	83.601	89.881	72.857	74.079	31.704	4.285	53.0
Optimal31	86.29	84.0	64.844	92.473	84.492	82.217	82.828	81.89	66.5	44.513	9.591	20.367	40.0
PatternNet	49.925	71.765	37.847	67.188	99.688	51.006	74.017	53.968	40.833	31.364	22.375	0.987	36.25
AID	79.286	74.444	71.579	83.974	76.312	97.4	72.0	100.0	50.5	51.133	27.875	20.957	47.188
RSI-CB256	55.519	83.75	44.333	61.667	78.472	67.812	99.677	83.562	30.0	46.254	42.286	13.953	27.812
WHU-RS19	66.667	75.0	52.5	75.694	77.083	84.577	58.506	99.502	47.857	50.727	11.182	0.0	56.25
SIRI-WHU	64.405	61.25	68.095	85.0	77.917	60.497	33.819	67.105	95.625	84.298	42.812	18.724	26.25
RSD46-WHU	45.604	45.625	53.333	52.083	45.938	51.25	44.553	59.615	43.75	93.536	94.833	6.06	63.75
Eurosat	59.286	56.667	72.333	62.5	79.375	92.857	62.908	79.07	78.333	80.542	98.944	5.963	56.667
SAT6	97.143	37.5	52.083	91.667	95.0	50.893	3.723	36.364	0.0	12.982	0.0	99.999	50.0
RSSCN7	82.381	97.5	80.333	88.889	88.125	88.214	70.209	90.385	91.667	56.713	19.647	0.016	95.179

Table C.12: AlexNet on MLC tasks: Generalization performance in terms of mean average precision (% mAP) of ImageNet-1K pre-trained models, fine-tuned on *source* and evaluated on images with shared labels in *target* dataset.

Source \ Target dataset	MLRSNet	AID (mlc)	UC merced (mlc)	DFC15
MLRSNet	93.399	74.226	74.63	39.901
AID (mlc)	53.989	75.908	43.061	35.914
UC merced (mlc)	45.323	46.986	92.638	37.287
DFC15	52.787	69.946	46.843	94.058

Table C.13: VGG16 on MLC tasks: Generalization performance in terms of mean average precision (% mAP) of ImageNet-1K pre-trained models, fine-tuned on *source* and evaluated on images with shared labels in *target* dataset.

Source \ Target dataset	MLRSNet	AID (mlc)	UC merced (mlc)	DFC15
MLRSNet	94.633	76.237	76.619	45.813
AID (mlc)	57.292	79.892	53.055	41.056
UC merced (mlc)	46.068	48.009	92.848	49.281
DFC15	51.959	71.354	58.691	96.565

Table C.14: ResNet50 on MLC tasks: Generalization performance in terms of mean average precision (% mAP) of ImageNet-1K pre-trained models, fine-tuned on *source* and evaluated on images with shared labels in *target* dataset.

Source \ Target dataset	MLRSNet	AID (mlc)	UC merced (mlc)	DFC15
MLRSNet	96.271	77.441	77.751	50.581
AID (mlc)	59.084	80.755	50.511	36.098
UC merced (mlc)	52.307	52.015	95.665	51.553
DFC15	48.23	67.506	55.907	97.664

Table C.15: ResNet152 on MLC tasks: Generalization performance in terms of mean average precision (% mAP) of ImageNet-1K pre-trained models, fine-tuned on *source* and evaluated on images with shared labels in *target* dataset.

Source \ Target dataset	MLRSNet	AID (mlc)	UC merced (mlc)	DFC15
MLRSNet	96.432	76.818	81.111	48.062
AID (mlc)	62.899	80.943	53.994	48.793
UC merced (mlc)	51.062	51.454	96.007	48.286
DFC15	53.242	73.216	56.132	97.606

Table C.16: DenseNet161 on MLC tasks: Generalization performance in terms of mean average precision (% mAP) of ImageNet-1K pre-trained models, fine-tuned on *source* and evaluated on images with shared labels in *target* dataset.

Source \ Target dataset	MLRSNet	AID (mlc)	UC merced (mlc)	DFC15
MLRSNet	96.306	77.359	80.212	52.007
AID (mlc)	62.522	81.709	55.913	43.452
UC merced (mlc)	55.494	54.165	96.057	52.486
DFC15	52.947	73.871	53.681	97.532

Table C.17: EfficientNetB0 on MLC tasks: Generalization performance in terms of mean average precision (% mAP) of ImageNet-1K pre-trained models, fine-tuned on *source* and evaluated on images with shared labels in *target* dataset.

Source \ Target dataset	MLRSNet	AID (mlc)	UC merced (mlc)	DFC15
MLRSNet	95.391	76.929	77.914	44.973
AID (mlc)	58.154	78.003	50.246	41.025
UC merced (mlc)	49.899	51.137	95.383	49.322
DFC15	46.145	67.706	45.535	96.784

Table C.18: ViT on MLC tasks: Generalization performance in terms of mean average precision (% mAP) of ImageNet-1K pre-trained models, fine-tuned on *source* and evaluated on images with shared labels in *target* dataset.

Source \ Target dataset	MLRSNet	AID (mlc)	UC merced (mlc)	DFC15
MLRSNet	96.408	77.141	82.344	63.666
AID (mlc)	62.51	81.541	52.498	49.896
UC merced (mlc)	57.166	52.044	96.699	63.075
DFC15	63.734	76.698	65.742	97.617

Table C.19: MLP Mixer on MLC tasks: Generalization performance in terms of mean average precision (% mAP) of ImageNet-1K pre-trained models, fine-tuned on *source* and evaluated on images with shared labels in *target* dataset.

Source \ Target dataset	MLRSNet	AID (mlc)	UC merced (mlc)	DFC15
MLRSNet	95.048	77.694	78.951	54.953
AID (mlc)	62.023	80.878	53.97	48.563
UC merced (mlc)	53.876	52.737	96.34	52.036
DFC15	55.864	79.241	58.727	97.941

Table C.20: ConvNeXt on MLC tasks: Generalization performance in terms of mean average precision (% mAP) of ImageNet-1K pre-trained models, fine-tuned on *source* and evaluated on images with shared labels in *target* dataset.

Source \ Target dataset	MLRSNet	AID (mlc)	UC merced (mlc)	DFC15
MLRSNet	95.807	76.333	80.243	56.256
AID (mlc)	62.766	82.298	57.133	42.201
UC merced (mlc)	56.192	53.227	96.43	50.419
DFC15	55.426	74.261	65.665	97.994

Table C.21: SwinT on MLC tasks: Generalization performance in terms of mean average precision (% mAP) of ImageNet-1K pre-trained models, fine-tuned on *source* and evaluated on images with shared labels in *target* dataset.

Source \ Target dataset	MLRSNet	AID (mlc)	UC merced (mlc)	DFC15
MLRSNet	96.62	78.452	81.812	59.951
AID (mlc)	61.463	82.254	58.374	52.293
UC merced (mlc)	58.263	55.748	96.831	63.277
DFC15	60.869	76.023	63.476	98.111

## D Detailed data descriptions & extended results per task

### D.1 UC Merced

The UC Merced dataset [9] consists of 2100 images divided into 21 land-use scene classes. Each class has 100 RGB aerial image which are 256x256 pixels and have a spatial resolution of 0.3m per pixel. The images were manually extracted from large images from the United States Geological Survey (USGS) National Map of the following US regions: Birmingham, Boston, Buffalo, Columbus, Dallas, Harrisburg, Houston, Jacksonville, Las Vegas, Los Angeles, Miami, Napa, New York, Reno, San Diego, Santa Barbara, Seattle, Tampa, Tucson, and Ventura. Samples from the datasets can be seen on Figure D.1.

The 21 classes are: agricultural, airplane, baseball diamond, beach, buildings, chaparral, dense residential, forest, freeway, golf course, harbor, intersection, medium density residential, mobile home park, overpass, parking lot, river, runway, sparse residential, storage tanks, and tennis courts. The authors have not set predefined train-test splits, so we have made such for our study (Figure D.2).

The detailed results for all pre-trained models are shown on Table D.1 and for all the models learned from scratch are presented on Table D.2. The best performing model is the pre-trained ResNet152. The results on a class level are show on Table D.3 along with a confusion matrix on Figure D.3.

Table D.1: Detailed results for pre-trained models on UCMerced

Model \ Metric	Accuracy	Macro Precision	Weighted Precision	Macro Recall	Weighted Recall	Macro F1 score	Weighted F1 score	Avg. time / epoch (sec.)	Total time (sec.)	Best epoch
AlexNet	92.14	92.24	92.24	92.14	92.14	92.03	92.03	1.29	44	24
VGG16	95.48	95.64	95.64	95.48	95.48	95.48	95.48	3.16	101	22
ResNet50	98.57	98.64	98.64	98.57	98.57	98.59	98.59	2.85	111	29
RestNet152	<b>98.81</b>	98.86	98.86	98.81	98.81	98.80	98.80	5.05	202	30
DenseNet161	98.33	98.40	98.40	98.33	98.33	98.34	98.34	5.41	357	56
EfficientNetB0	98.57	98.61	98.61	98.57	98.57	98.57	98.57	2.46	214	77
ConvNeXt	97.86	97.99	97.99	97.86	97.86	97.87	97.87	3.68	173	37
Vision Transformer	98.33	98.44	98.44	98.33	98.33	98.36	98.36	4.00	112	18
MLP Mixer	98.33	98.40	98.40	98.33	98.33	98.34	98.34	3.10	130	32
Swin Transformer	98.57	98.62	98.62	98.57	98.57	98.58	98.58	10.28	370	26

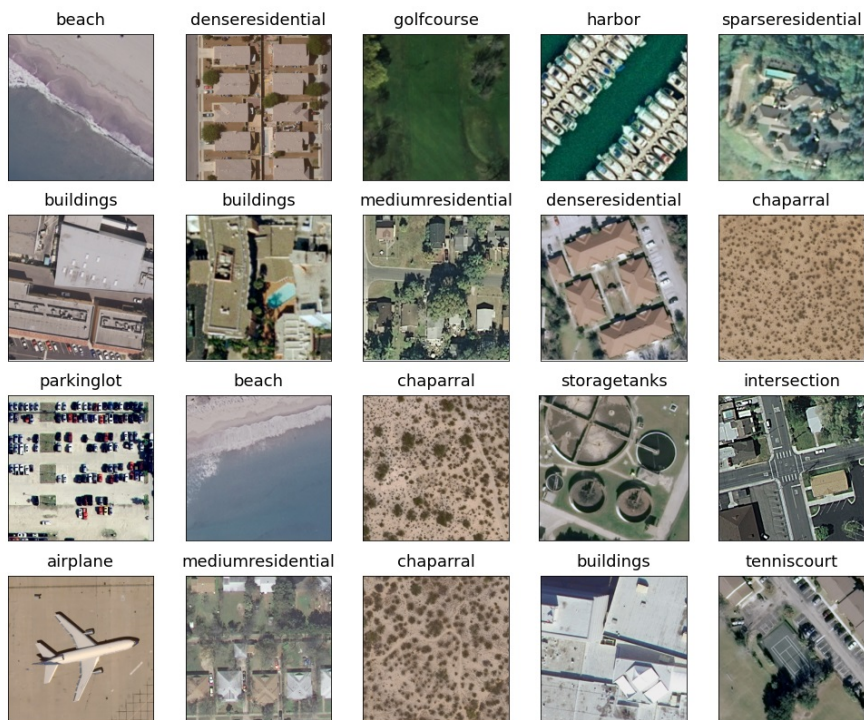


Figure D.1: Example images with labels from the UC Merced dataset.

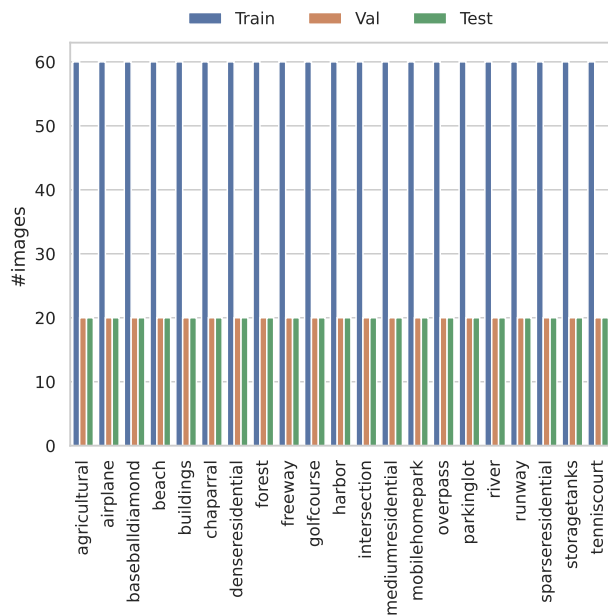


Figure D.2: Class distribution for the UC Merced dataset.

Table D.2: Detailed results for models trained from scratch on the UC Merced dataset.

Model \ Metric	Accuracy	Macro Precision	Weighted Precision	Macro Recall	Weighted Recall	Macro F1 score	Weighted F1 score	Avg. time / epoch (sec.)	Total time (sec.)	Best epoch
AlexNet	81.19	81.30	81.30	81.19	81.19	80.87	80.87	1.30	126	82
VGG16	78.57	78.96	78.96	78.57	78.57	78.30	78.30	4.66	466	85
ResNet50	85.24	85.20	85.20	85.24	85.24	84.75	84.75	2.54	178	55
ResNet152	84.05	84.02	84.02	84.05	84.05	83.68	83.68	5.02	467	78
DenseNet161	<b>86.19</b>	86.42	86.42	86.19	86.19	85.75	85.75	5.46	415	61
EfficientNetB0	84.29	85.27	85.27	84.29	84.29	84.16	84.16	2.53	253	93
ConvNeXt	84.29	84.51	84.51	84.29	84.29	84.14	84.14	3.75	375	92
Vision Transformer	83.10	83.64	83.64	83.10	83.10	82.76	82.76	4.44	413	78
MLP Mixer	82.38	82.12	82.12	82.38	82.38	82.01	82.01	3.06	269	73
Swin Transformer	81.43	81.74	81.74	81.43	81.43	81.14	81.14	10.36	984	80

Table D.3: Per class results for the pre-trained ResNet152 model on the UC Merced dataset.

Label	Precision	Recall	F1 score
agricultural	100.00	100.00	100.00
airplane	100.00	100.00	100.00
baseballdiamond	100.00	100.00	100.00
beach	100.00	100.00	100.00
buildings	94.74	90.00	92.31
chaparral	100.00	100.00	100.00
denserresidential	90.91	100.00	95.24
forest	100.00	100.00	100.00
freeway	100.00	100.00	100.00
golfcourse	100.00	100.00	100.00
harbor	100.00	100.00	100.00
intersection	100.00	100.00	100.00
mediumresidential	100.00	90.00	94.74
mobilehomepark	100.00	95.00	97.44
overpass	100.00	100.00	100.00
parkinglot	100.00	100.00	100.00
river	100.00	100.00	100.00
runway	100.00	100.00	100.00
sparseresidential	95.24	100.00	97.56
storagetanks	95.24	100.00	97.56
tenniscourt	100.00	100.00	100.00

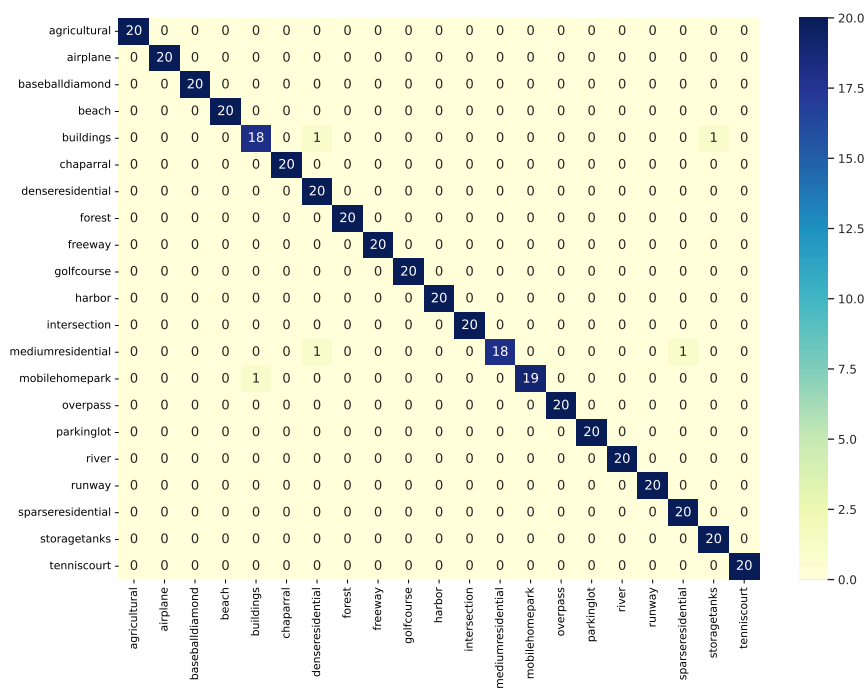


Figure D.3: Confusion matrix for the pre-trained ResNet152 model on the UC Merced dataset.

## D.2 WHU-RS19

WHU-RS19 is a set of satellite images exported from Google Earth, which provides high-resolution satellite images up to 0.5m and red, green and blue spectral bands [42]. It contains 19 classes of meaningful scenes in high-resolution satellite imagery, including: airport, beach, bridge, commercial area, desert, farmland, football field, forest, industrial area, meadow, mountain, park, parking lot, pond, port, railway station, residential area, river, and viaduct. For each class, there are about 50 samples with a total of 1005 images in the entire dataset. The data does not come with predefined train and test splits, so per standard we have made splits (Figure D.5).

The size of images is 600x600 pixel. The image samples of the same class are collected from different regions in satellite images of different resolutions and then might have different scales, orientations and illuminations. This makes the dataset challenging, however, the number of images is relatively small compared to the other datasets. Sample images from the dataset are shown in Figure D.4.

Detailed results for all pre-trained models are shown on Table D.4 and for all the models learned from scratch are presented on Table D.5. The best performing model is the pre-trained DenseNet161. The results on a class level are show on Table D.6 along with a confusion matrix on Figure D.6.

Table D.4: Detailed results for pre-trained models the WHU-RS19 dataset.

Model \ Metric	Accuracy	Macro Precision	Weighted Precision	Macro Recall	Weighted Recall	Macro F1 score	Weighted F1 score	Avg. time / epoch (sec.)	Total time (sec.)	Best epoch
AlexNet	93.53	94.44	94.30	93.63	93.53	93.73	93.59	2.78	142	41
VGG16	99.00	99.08	99.09	99.04	99.00	99.01	99.00	3.00	144	38
ResNet50	99.50	99.56	99.54	99.52	99.50	99.52	99.50	2.85	285	96
RestNet152	98.01	98.21	98.22	97.99	98.01	98.01	98.03	4.02	253	53
DenseNet161	<b>100.00</b>	100.00	100.00	100.00	100.00	100.00	100.00	4.04	400	89
EfficientNetB0	99.50	99.56	99.54	99.47	99.50	99.49	99.50	2.76	276	100
ConvNeXt	99.00	99.04	99.05	99.00	99.00	98.99	99.00	3.20	211	56
Vision Transformer	99.50	99.56	99.54	99.52	99.50	99.52	99.50	3.40	102	20
MLP Mixer	98.51	98.64	98.64	98.47	98.51	98.49	98.50	2.84	247	77
Swin Transformer	99.50	99.56	99.54	99.47	99.50	99.49	99.50	5.98	263	34

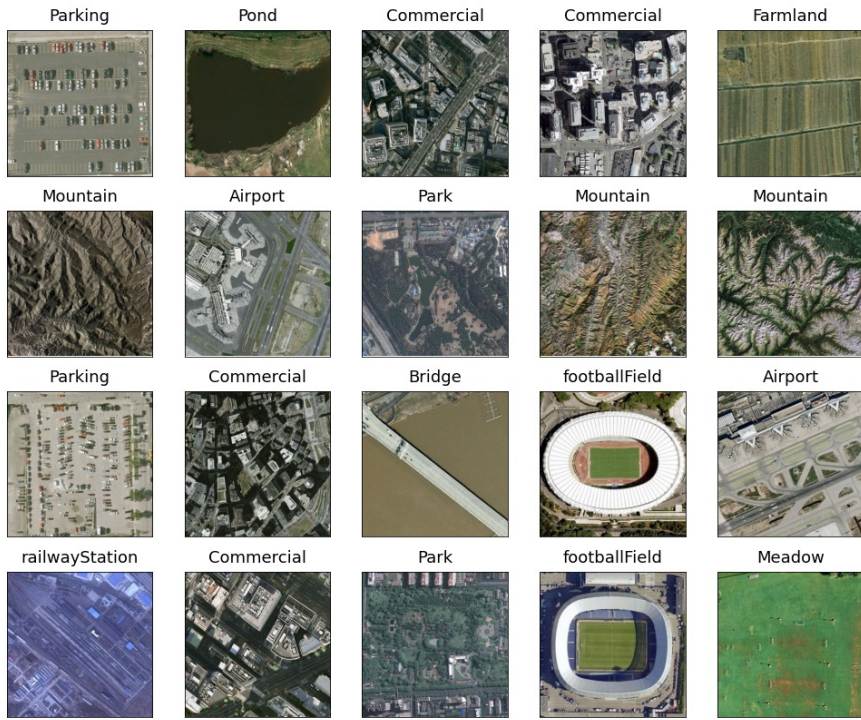


Figure D.4: Example images with labels from the WHU-RS19 dataset.

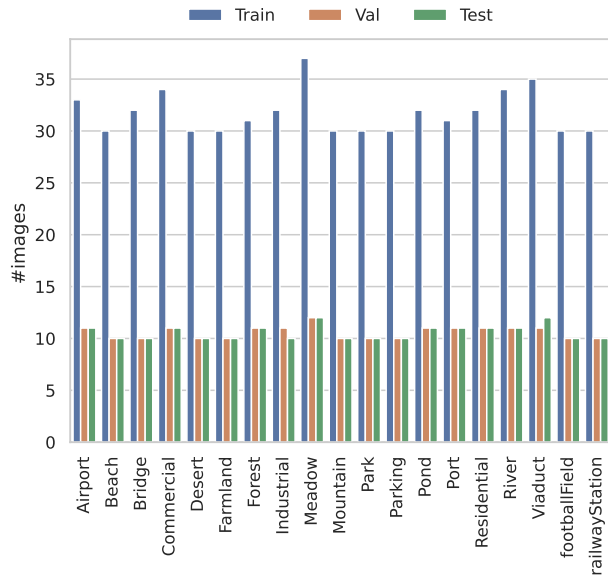


Figure D.5: Class distribution for the WHU-RS19 dataset.

Table D.5: Detailed results for models trained from scratch the WHU-RS19 dataset.

Model \ Metric	Accuracy	Macro Precision	Weighted Precision	Macro Recall	Weighted Recall	Macro F1 score	Weighted F1 score	Avg. time / epoch (sec.)	Total time (sec.)	Best epoch
AlexNet	66.17	67.93	67.68	66.28	66.17	66.53	66.36	2.53	223	73
VGG16	68.66	70.53	70.25	68.69	68.66	69.02	68.87	4.79	479	96
ResNet50	79.60	82.28	81.91	79.75	79.60	79.88	79.67	3.85	300	63
ResNet152	80.60	82.62	82.27	80.63	80.60	81.08	80.91	4.29	343	65
DenseNet161	<b>80.60</b>	82.75	82.44	80.59	80.60	80.75	80.60	4.04	271	52
EfficientNetB0	75.62	77.50	77.00	76.08	75.62	76.02	75.54	2.78	189	53
ConvNeXt	72.14	73.09	72.63	72.41	72.14	72.36	71.99	3.03	303	90
Vision Transformer	74.63	75.96	75.69	74.89	74.63	75.05	74.78	3.44	303	73
MLP Mixer	69.65	70.70	70.51	69.91	69.65	69.10	68.83	3.86	386	89
Swin Transformer	78.61	78.84	78.66	78.84	78.61	78.53	78.33	6.08	608	86

Table D.6: Per class results for the pre-trained DenseNet161 model on the WHU-RS19 dataset.

Label	Precision	Recall	F1 score
Airport	100.00	100.00	100.00
Beach	100.00	100.00	100.00
Bridge	100.00	100.00	100.00
Commercial	100.00	100.00	100.00
Desert	100.00	100.00	100.00
Farmland	100.00	100.00	100.00
footballField	100.00	100.00	100.00
Forest	100.00	100.00	100.00
Industrial	100.00	100.00	100.00
Meadow	100.00	100.00	100.00
Mountain	100.00	100.00	100.00
Park	100.00	100.00	100.00
Parking	100.00	100.00	100.00
Pond	100.00	100.00	100.00
Port	100.00	100.00	100.00
railwayStation	100.00	100.00	100.00
Residential	100.00	100.00	100.00
River	100.00	100.00	100.00
Viaduct	100.00	100.00	100.00

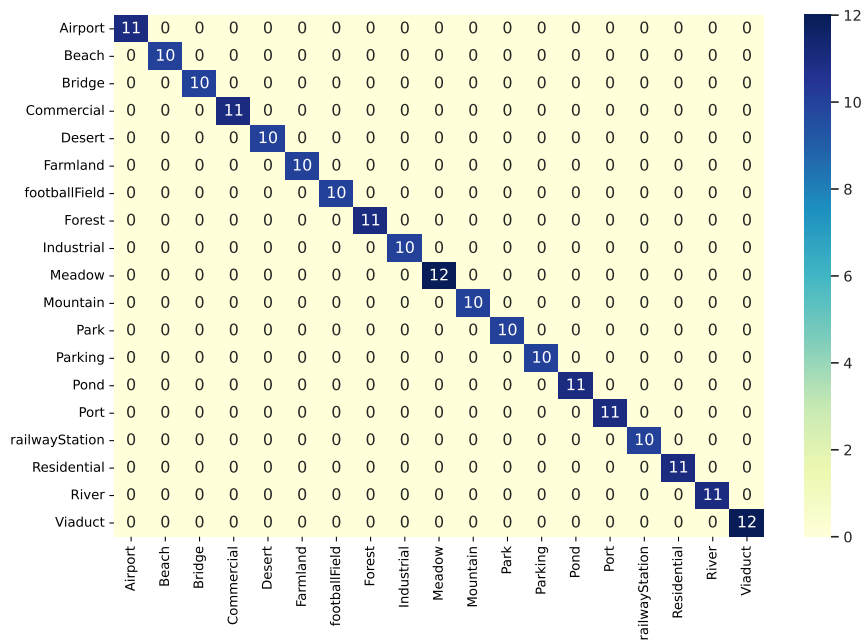


Figure D.6: Confusion matrix for the pre-trained DenseNet161 model on the WHU-RS19 dataset.

### D.3 AID

Aerial Image Dataset (AID) is a large-scale aerial image dataset generated by collecting sample images from Google Earth imagery. The goal of AID is to advance the state-of-the-art in scene classification of remote sensing images. For creating AID, more than ten thousands aerial scene images have been collected and annotated. It consists of 10000 RGB images with 600x600 pixels resolution (Figure D.7). The dataset is made up of the following 30 classes (aerial scene types): airport, bare land, baseball field, beach, bridge, center, church, commercial, dense residential, desert, farmland, forest, industrial, meadow, medium residential, mountain, park, parking, playground, pond, port, railway station, resort, river, school, sparse residential, square, stadium, storage tanks and viaduct.

All the images were labeled by the specialists in the field of remote sensing image interpretation. All samples from each class are chosen from different countries and regions around the world, but mainly in China, USA, England, France, Italy, Japan, Germany etc. They are extracted at different time and seasons under different image conditions. Although, all images have a 600x600 pixels resolution, their spatial resolution varies from 8 to 0.5 meters.

The dataset has no predefined train-test splits, so for properly conducting the study we have made train, test and validation splits. The distribution of the splits is presented on Figure D.8. Detailed results for all pre-trained models are shown on Table D.7 and for all the models learned from scratch are presented on Table D.8. The best performing model is the pre-trained ViT model. The results on a class level are show on Table D.9 along with a confusion matrix on Figure D.9.

Table D.7: Detailed results for pre-trained models on the AID dataset.

Model \ Metric	Accuracy	Macro Precision	Weighted Precision	Macro Recall	Weighted Recall	Macro F1 score	Weighted F1 score	Avg. time / epoch (sec.)	Total time (sec.)	Best epoch
AlexNet	92.90	92.90	92.94	92.65	92.90	92.72	92.87	21.32	725	24
VGG16	96.10	95.95	96.11	95.91	96.10	95.90	96.08	21.35	854	30
ResNet50	96.55	96.48	96.56	96.26	96.55	96.30	96.50	20.29	1035	41
RestNet152	97.20	97.14	97.24	97.07	97.20	97.08	97.19	22.20	1132	41
DenseNet161	97.25	97.25	97.30	97.10	97.25	97.12	97.23	24.36	1072	34
EfficientNetB0	96.25	96.24	96.26	96.15	96.25	96.16	96.23	20.00	800	30
ConvNeXt	96.95	96.95	96.97	96.81	96.95	96.85	96.93	23.06	807	25
Vision Transformer	<b>97.75</b>	97.56	97.76	97.53	97.75	97.52	97.73	20.45	1145	46
MLP Mixer	96.70	96.58	96.74	96.52	96.70	96.51	96.69	19.78	811	31
Swin Transformer	97.40	97.43	97.41	97.26	97.40	97.32	97.38	46.65	1213	16



Figure D.7: Example images with labels from the AID dataset.

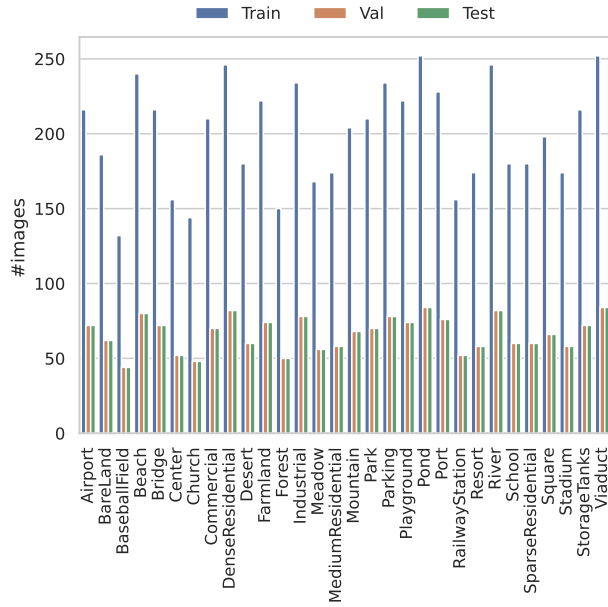


Figure D.8: Class distribution for the AID dataset.

Table D.8: Detailed results for models trained from scratch on the AID dataset.

Model \ Metric	Accuracy	Macro Precision	Weighted Precision	Macro Recall	Weighted Recall	Macro F1 score	Weighted F1 score	Avg. time / epoch (sec.)	Total time (sec.)	Best epoch
AlexNet	81.35	81.23	81.32	81.14	81.35	81.07	81.23	19.46	1927	84
VGG16	81.95	81.80	82.04	81.52	81.95	81.50	81.84	19.65	1356	54
ResNet50	89.05	89.09	89.23	88.82	89.05	88.85	89.04	19.66	1514	62
ResNet152	89.90	90.08	90.09	89.60	89.90	89.73	89.88	22.25	1513	53
DenseNet161	<b>93.30</b>	93.32	93.42	93.13	93.30	93.17	93.30	24.48	2228	76
EfficientNetB0	90.05	90.19	90.32	89.88	90.05	89.92	90.08	19.33	1121	43
ConvNeXt	81.10	81.51	81.18	80.87	81.10	81.03	80.98	19.15	1915	96
Vision Transformer	79.35	79.27	79.27	79.51	79.35	79.30	79.21	19.63	1060	39
MLP Mixer	71.75	72.02	71.87	72.01	71.75	71.73	71.52	19.06	953	35
Swin Transformer	87.70	87.96	87.85	87.62	87.70	87.66	87.66	46.94	4647	84

Table D.9: Per class results for the pre-trained Vision Transformer on the AID dataset.

Label	Precision	Recall	F1 score
Airport	98.61	98.61	98.61
BareLand	98.41	100.00	99.20
BaseballField	97.78	100.00	98.88
Beach	100.00	100.00	100.00
Bridge	100.00	100.00	100.00
Center	87.72	96.15	91.74
Church	93.48	89.58	91.49
Commercial	95.71	95.71	95.71
DenseResidential	98.80	100.00	99.39
Desert	100.00	100.00	100.00
Farmland	100.00	100.00	100.00
Forest	100.00	100.00	100.00
Industrial	94.94	96.15	95.54
Meadow	100.00	100.00	100.00
MediumResidential	98.28	98.28	98.28
Mountain	100.00	100.00	100.00
Park	94.44	97.14	95.77
Parking	100.00	100.00	100.00
Playground	98.63	97.30	97.96
Pond	98.81	98.81	98.81
Port	97.44	100.00	98.70
RailwayStation	96.23	98.08	97.14
Resort	94.12	82.76	88.07
River	98.80	100.00	99.39
School	91.38	88.33	89.83
SparseResidential	98.36	100.00	99.17
Square	98.44	95.45	96.92
Stadium	96.49	94.83	95.65
StorageTanks	100.00	100.00	100.00
Viaduct	100.00	98.81	99.40

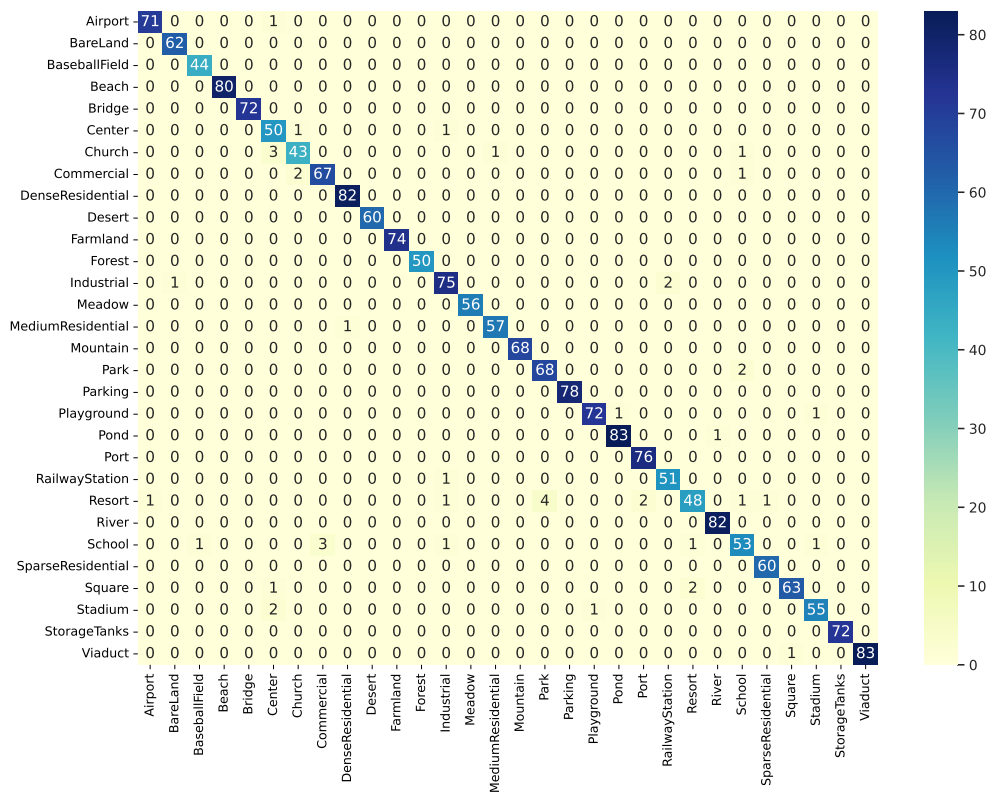


Figure D.9: Confusion matrix for the pre-trained Vision Transformer model on the AID dataset.

#### D.4 Eurosat

EuroSAT [43] is a land use and land cover classification dataset based on Sentinel-2 satellite images covering 13 spectral bands and consisting out of 10 classes with in total 27000 labeled and geo-referenced images. The dataset provides RGB and multi-spectral (MS) version of the data. The spectral bands and their respective spatial resolutions are presented on Table D.10. The 10 image classes are the following: Annual Crop, Forest, Herbaceous Vegetation, Highway, Industrial, Pasture, Permanent Crop, Residential, River, Sea/Lake. Some samples from the dataset are presented on Figure D.10. The class distribution of our train, test and validation splits are provided on Figure D.11.

Detailed results for all pre-trained models are shown on Table D.11 and for all the models learned from scratch are presented on Table D.12. The best performing model is the pre-trained ResNet152 model. The results on a class level are show on Table D.13 along with a confusion matrix on Figure D.12.



Figure D.10: Example images with labels from the Eurosat dataset.

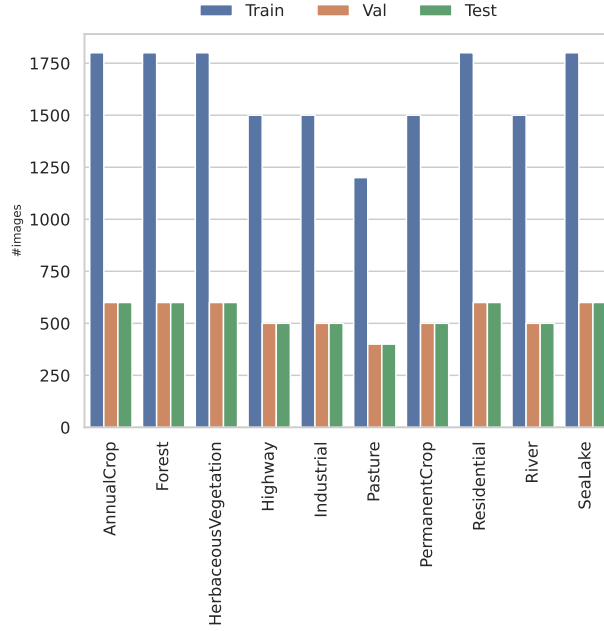


Figure D.11: Class distribution for the Eurosat dataset.

Table D.10: Eurosat bands and spatial resolutions.

<b>Band</b>	<b>Spatial resolution <math>m</math></b>
B01 - Aerosols	60
B02 - Blue	10
B03 - Green	10
B04 - Red	10
B05 - Red edge 1	20
B06 - Red edge 2	20
B07 - Red edge 3	20
B08 - NIR	10
B08A - Red edge 4	20
B09 - Water vapor	60
B10 - Cirrus	60
B11 - SWIR 1	20
B12 - SWIR 2	20

Table D.11: Detailed results for pre-trained models on the Eurosat dataset.

Model \ Metric	Accuracy	Macro Precision	Weighted Precision	Macro Recall	Weighted Recall	Macro F1 score	Weighted F1 score	Avg. time / epoch (sec.)	Total time (sec.)	Best epoch
AlexNet	97.57	97.48	97.58	97.48	97.57	97.48	97.57	8.88	426	38
VGG16	98.15	98.14	98.15	98.06	98.15	98.09	98.15	33.69	977	19
ResNet50	98.83	98.82	98.83	98.77	98.83	98.79	98.83	26.56	1912	62
ResNet152	<b>99.00</b>	99.00	99.00	98.96	99.00	98.98	99.00	56.00	1904	24
DenseNet161	98.89	98.88	98.89	98.82	98.89	98.85	98.89	61.12	2078	24
EfficientNetB0	98.91	98.91	98.91	98.86	98.91	98.88	98.91	23.47	1056	35
ConvNeXt	98.78	98.76	98.78	98.75	98.78	98.75	98.78	40.38	1050	16
Vision Transformer	98.72	98.71	98.73	98.64	98.72	98.68	98.72	43.19	1123	16
MLP Mixer	98.74	98.73	98.74	98.65	98.74	98.68	98.74	30.41	669	12
Swin Transformer	98.94	98.94	98.95	98.89	98.94	98.91	98.94	124.17	2980	14

Table D.12: Detailed results for models trained from scratch on the Eurosat dataset.

Model \ Metric	Accuracy	Macro Precision	Weighted Precision	Macro Recall	Weighted Recall	Macro F1 score	Weighted F1 score	Avg. time / epoch (sec.)	Total time (sec.)	Best epoch
AlexNet	96.17	96.02	96.18	96.10	96.17	96.06	96.17	8.02	802	95
VGG16	97.19	97.17	97.19	97.04	97.19	97.10	97.18	33.62	2622	63
ResNet50	97.00	96.93	97.01	96.85	97.00	96.88	97.00	26.45	2619	84
ResNet152	97.41	97.36	97.41	97.27	97.41	97.31	97.40	56.21	4328	62
DenseNet161	97.63	97.57	97.64	97.51	97.63	97.54	97.63	62.50	5125	67
EfficientNetB0	<b>97.80</b>	97.76	97.80	97.72	97.80	97.74	97.79	24.19	2032	69
ConvNeXt	95.43	95.25	95.44	95.29	95.43	95.27	95.43	40.03	2642	51
Vision Transformer	95.04	94.86	95.02	94.80	95.04	94.82	95.02	44.22	2963	52
MLP Mixer	95.50	95.29	95.50	95.35	95.50	95.31	95.49	31.45	2327	59
Swin Transformer	95.72	95.78	95.78	95.45	95.72	95.58	95.72	122.44	12244	90

Table D.13: Per class results for the pre-trained ResNet152 model on the Eurosat dataset.

Label	Precision	Recall	F1 score
Annual Crop	98.66	98.33	98.50
Forest	99.17	99.50	99.33
Herbaceous Vegetation	98.01	98.67	98.34
Highway	99.20	98.80	99.00
Industrial	99.40	99.00	99.20
Pasture	98.74	98.25	98.50
Permanent Crop	98.59	97.60	98.09
Residential	99.50	100.00	99.75
River	99.20	99.60	99.40
Sea Lake	99.50	99.83	99.67

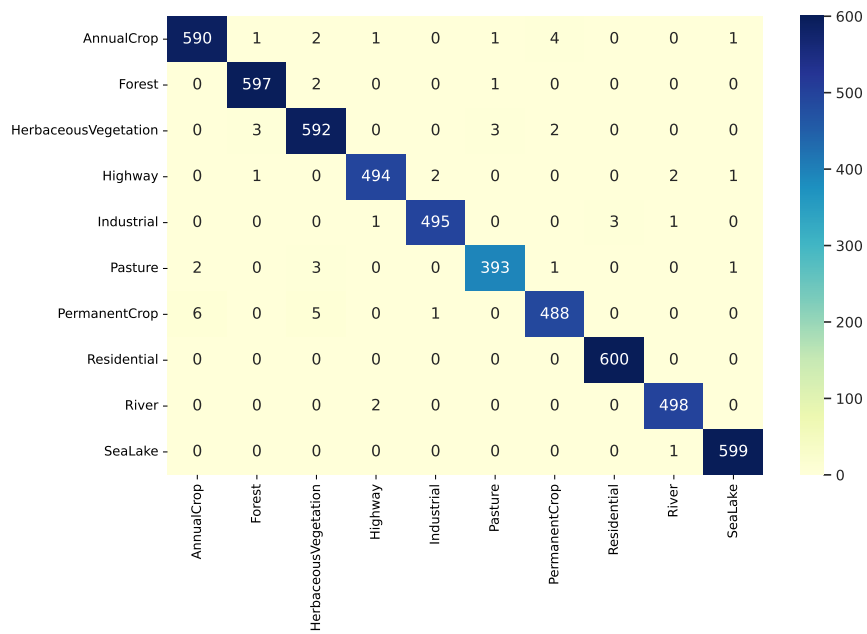


Figure D.12: Confusion matrix for the pre-trained ResNet152 model on the Eurosat dataset.

### D.5 PatternNet

PatternNet is a large-scale remote sensing dataset that was collected specifically for Remote sensing image retrieval. It contains 38 classes: airplane, baseball field, basketball court, beach, bridge, cemetery, chaparral, christmas tree farm, closed road, coastal mansion, crosswalk, dense residential, ferry terminal, football field, forest, freeway, golf course, harbor, intersection, mobile home park, nursing home, oil gas field, oil well, overpass, parking lot, parking space, railway, river, runway, runway marking, shipping yard, solar panel, sparse residential, storage tank, swimming pool, tennis court, transformer station and wastewater treatment plant. There are a total of 38 classes with 800 images of size 256×256 pixels for each class. The class distribution of the train, test and validation splits we generated is presented on Figure D.14, since the dataset does not have predefined ones.

PatternNet dataset has the following main characteristics: It’s the largest publicly available dataset specifically designed for remote sensing image retrieval. It has a higher spatial resolution, so that the classes of interest constitute a larger portion of the image. It has high inter-class similarity and high intra-class diversity. Some sample images are shown on Figure D.13.

Detailed results for all pre-trained models are shown on Table D.14 and for all the models learned from scratch are presented on Table D.15. The best performing models are the pre-trained DenseNet161 and ResNet50 models. The results on a class level are show on Table D.16 along with a confusion matrix on Figure D.15.

Table D.14: Detailed results for pre-trained models on the PatternNet dataset.

Model \ Metric	Accuracy	Macro Precision	Weighted Precision	Macro Recall	Weighted Recall	Macro F1 score	Weighted F1 score	Avg. time / epoch (sec.)	Total time (sec.)	Best epoch
AlexNet	99.16	99.17	99.17	99.16	99.16	99.16	99.16	15.17	637	32
VGG16	99.42	99.43	99.43	99.42	99.42	99.42	99.42	37.74	1321	25
ResNet50	<b>99.74</b>	99.74	99.74	99.74	99.74	99.74	99.74	29.10	1193	31
RestNet152	99.49	99.49	99.49	99.49	99.49	99.49	99.49	62.94	1070	7
DenseNet161	<b>99.74</b>	99.74	99.74	99.74	99.74	99.74	99.74	68.87	3168	36
EfficientNetB0	99.54	99.54	99.54	99.54	99.54	99.54	99.54	25.86	569	12
ConvNeXt	99.67	99.67	99.67	99.67	99.67	99.67	99.67	45.93	1378	20
Vision Transformer	99.65	99.66	99.66	99.65	99.65	99.65	99.65	48.50	1067	12
MLP Mixer	99.70	99.71	99.71	99.70	99.70	99.70	99.70	33.80	1521	35
Swin Transformer	99.69	99.69	99.69	99.69	99.69	99.69	99.69	138.65	2357	7

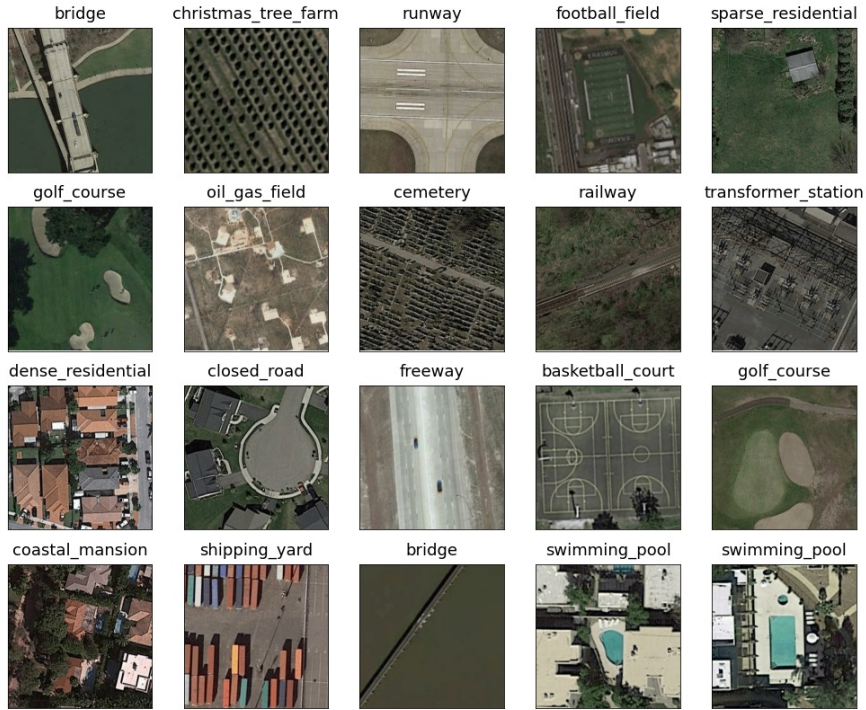


Figure D.13: Example images with labels from the PatternNet dataset.

Table D.15: Detailed results for models trained from scratch on the PatternNet dataset.

Model \ Metric	Accuracy	Macro Precision	Weighted Precision	Macro Recall	Weighted Recall	Macro F1 score	Weighted F1 score	Avg. time / epoch (sec.)	Total time (sec.)	Best epoch
AlexNet	97.83	97.83	97.83	97.83	97.83	97.82	97.82	13.75	1141	68
VGG16	97.91	97.93	97.93	97.91	97.91	97.91	97.91	37.47	2061	40
ResNet50	99.06	99.07	99.07	99.06	99.06	99.06	99.06	35.65	3030	70
ResNet152	98.88	98.89	98.89	98.88	98.88	98.88	98.88	69.05	6905	88
DenseNet161	<b>99.24</b>	99.25	99.25	99.24	99.24	99.24	99.24	71.08	5260	59
EfficientNetB0	98.83	98.84	98.84	98.83	98.83	98.83	98.83	27.54	2286	68
ConvNeXt	97.83	97.83	97.83	97.83	97.83	97.82	97.82	45.06	4326	81
Vision Transformer	96.69	96.69	96.69	96.69	96.69	96.68	96.68	49.05	3237	51
MLP Mixer	98.83	98.84	98.84	98.83	98.83	98.83	98.83	34.54	2038	44
Swin Transformer	98.52	98.53	98.53	98.52	98.52	98.52	98.52	138.59	12612	76

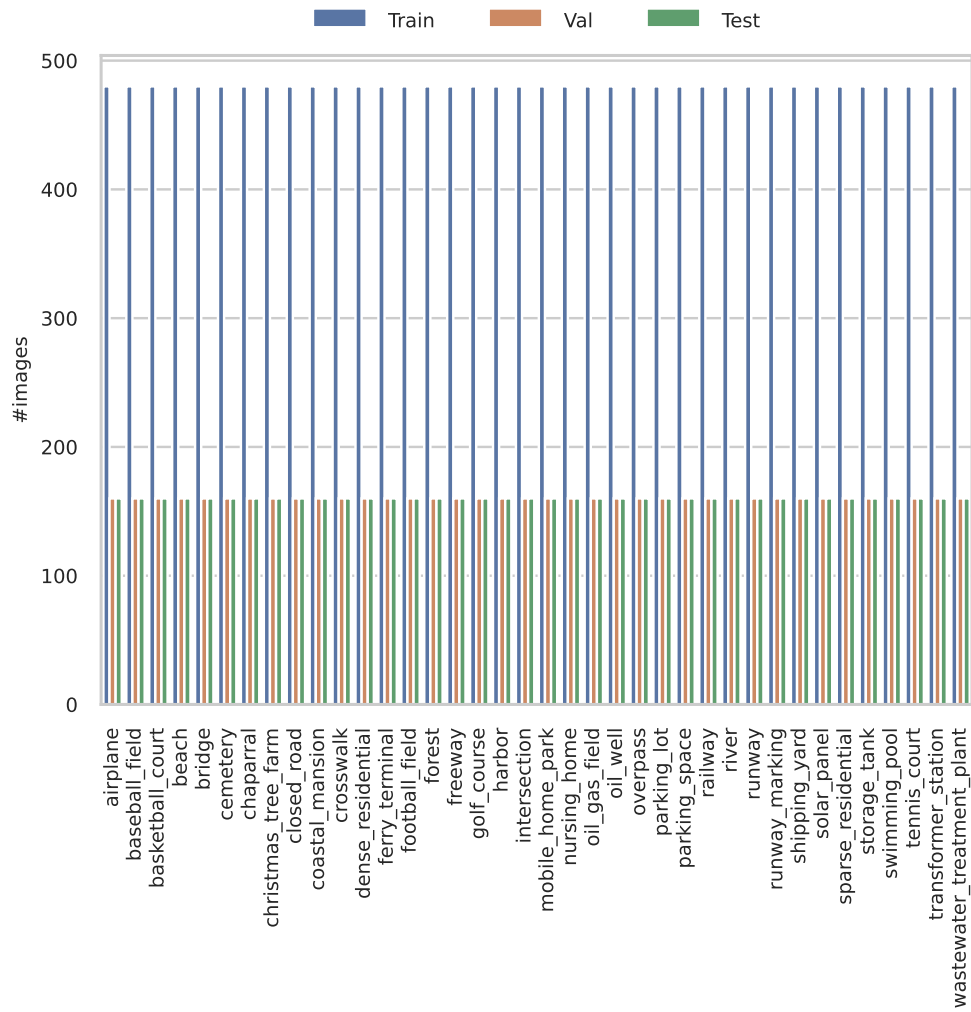


Figure D.14: Class distribution for the PatternNet dataset.

Table D.16: Per class results for the pre-trained DenseNet161 model on the PatternNet dataset.

Label	Precision	Recall	F1 score
airplane	100.00	100.00	100.00
baseball field	100.00	100.00	100.00
basketball court	99.37	98.75	99.06
beach	100.00	100.00	100.00
bridge	98.77	100.00	99.38
cemetery	100.00	100.00	100.00
chaparral	100.00	100.00	100.00
christmas tree farm	100.00	100.00	100.00
closed_road	99.38	100.00	99.69
coastal_mansion	98.73	97.50	98.11
crosswalk	100.00	100.00	100.00
dense_residential	100.00	100.00	100.00
ferry terminal	100.00	98.75	99.37
football field	100.00	100.00	100.00
forest	100.00	100.00	100.00
freeway	100.00	100.00	100.00
golf course	100.00	100.00	100.00
harbor	100.00	100.00	100.00
intersection	99.38	100.00	99.69
mobile home park	100.00	100.00	100.00
nursing home	100.00	99.38	99.69
oil gas field	100.00	100.00	100.00
oil well	100.00	100.00	100.00
overpass	100.00	100.00	100.00
parking lot	100.00	100.00	100.00
parking space	100.00	100.00	100.00
railway	100.00	100.00	100.00
river	100.00	100.00	100.00
runway	100.00	99.38	99.69
runway marking	99.38	100.00	99.69
shipping yard	100.00	100.00	100.00
solar panel	100.00	100.00	100.00
sparse residential	96.91	98.13	97.52
storage tank	99.38	99.38	99.38
swimming pool	100.00	100.00	100.00
tennis court	100.00	99.38	99.69
transformer station	99.38	100.00	99.69
wastewater treatment plant	99.38	99.38	99.38

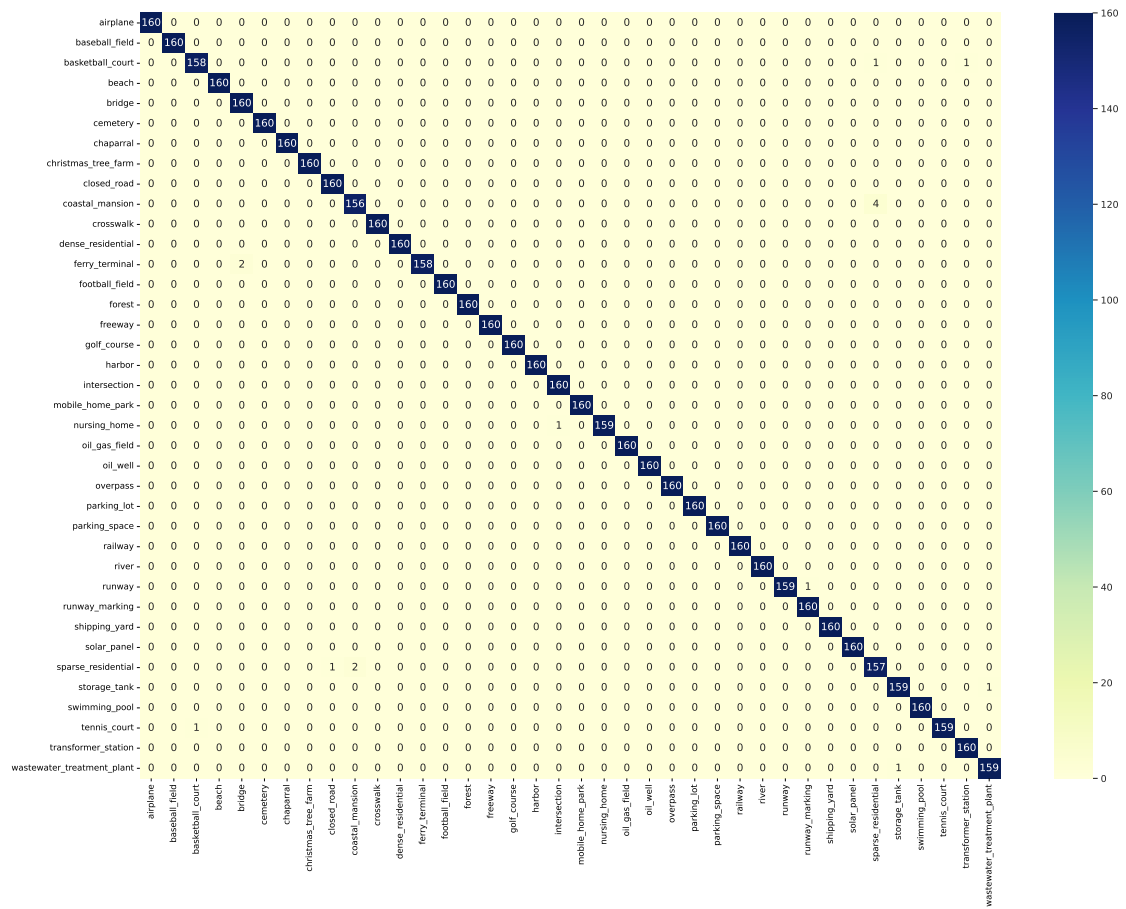


Figure D.15: Confusion matrix for the pre-trained DenseNet161 model on the PatternNet dataset.

#### D.6 *Resisc45*

RESISC45 [8] dataset is a publicly available benchmark for Remote Sensing Image Scene Classification (RESISC), created by Northwestern Polytechnical University (NWPU). This dataset contains 31500 images, covering 45 scene classes with 700 images in each class. The 45 scene classes are as follows: airplane, airport, baseball diamond, basketball court, beach, bridge, chaparral, church, circular farmland, cloud, commercial area, dense residential, desert, forest, freeway, golf course, ground track field, harbor, industrial area, intersection, island, lake, meadow, medium residential, mobile home park, mountain, overpass, palace, parking lot, railway, railway station, rectangular farmland, river, roundabout, runway, sea ice, ship, snowberg, sparse residential, stadium, storage tank, tennis court, terrace, thermal power station, and wetland. Accordingly, these classes contain a variety of spatial patterns, some homogeneous with respect to texture, some homogeneous with respect to color, others not homogeneous at all.

The images are with a size of 256x256 pixels in the RGB color space. The spatial resolution varies from about 30m to 0.2m per pixel for most of the scene classes except for the classes of island, lake, mountain, and snowberg that have lower spatial resolutions. The 31500 images cover more than 100 countries and regions all over the world, including developing, transition, and highly developed economies (Figure D.16). Our generated train, test and validation splits distribution is show on Figure D.17.

Detailed results for all pre-trained models are shown on Table D.17 and for all the models learned from scratch are presented on Table D.18. The best performing model is the pre-trained Vision Transformer model. The results on a class level are show on Table D.19 along with a confusion matrix on Figure D.18.

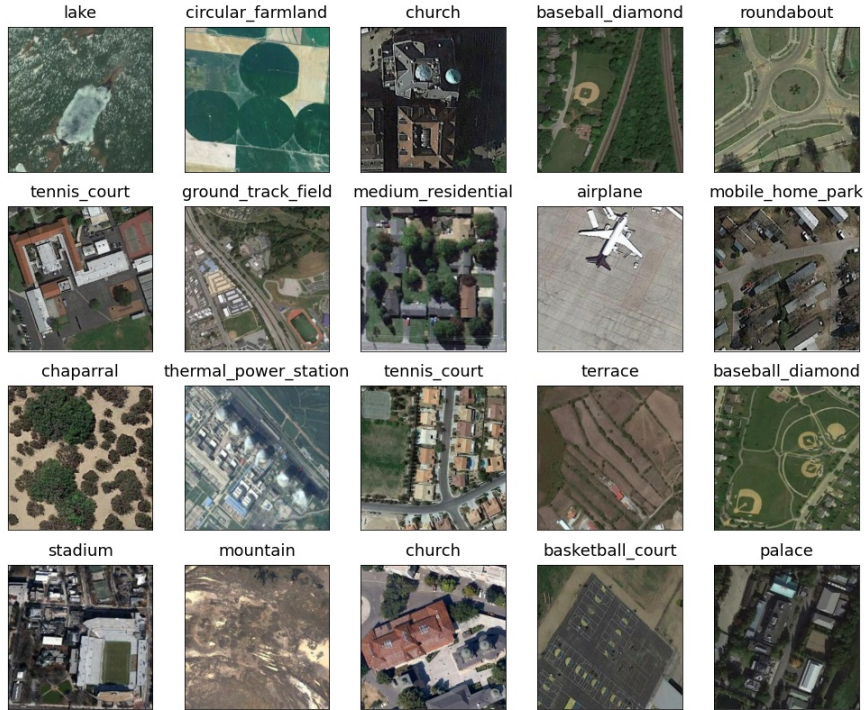


Figure D.16: Example images with labels from the Resisc45 dataset.

Table D.17: Detailed results for pre-trained models on the Resisc45 dataset.

Model \ Metric	Accuracy	Macro Precision	Weighted Precision	Macro Recall	Weighted Recall	Macro F1 score	Weighted F1 score	Avg. time / epoch (sec.)	Total time (sec.)	Best epoch
AlexNet	90.49	90.56	90.56	90.49	90.49	90.49	90.49	12.03	385	22
VGG16	93.90	93.91	93.91	93.90	93.90	93.89	93.89	39.87	1196	20
ResNet50	96.46	96.50	96.50	96.46	96.46	96.46	96.46	30.61	1163	28
ResNet152	96.54	96.57	96.57	96.54	96.54	96.54	96.54	65.11	2409	27
DenseNet161	96.51	96.53	96.53	96.51	96.51	96.51	96.51	72.05	3098	33
EfficientNetB0	94.87	94.93	94.93	94.87	94.87	94.88	94.88	27.12	678	15
ConvNeXt	96.27	96.28	96.28	96.27	96.27	96.26	96.26	46.79	1778	28
Vision Transformer	<b>97.08</b>	97.10	97.10	97.08	97.08	97.07	97.07	51.19	2713	43
MLP Mixer	95.95	95.99	95.99	95.95	95.95	95.96	95.96	35.62	1033	19
Swin Transformer	96.59	96.60	96.60	96.59	96.59	96.58	96.58	143.57	4020	18

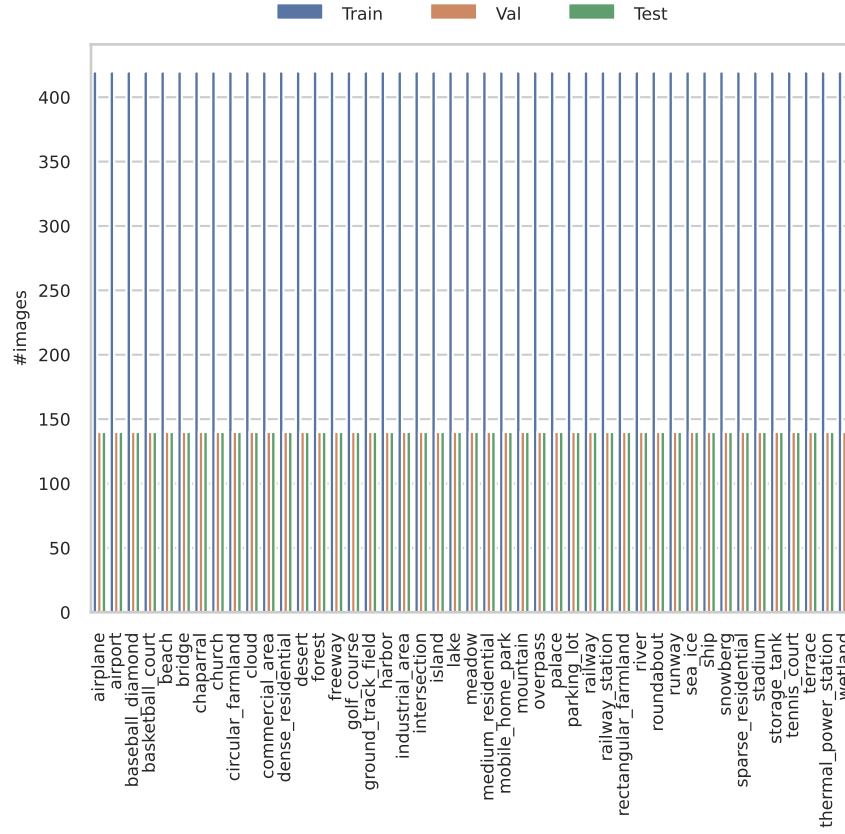


Figure D.17: Class distribution for the Resisc45 dataset.

Table D.18: Detailed results for models trained from scratch on the Resisc45 dataset.

Model \ Metric	Accuracy	Macro Precision	Weighted Precision	Macro Recall	Weighted Recall	Macro F1 score	Weighted F1 score	Avg. time / epoch (sec.)	Total time (sec.)	Best epoch
AlexNet	82.16	82.29	82.29	82.16	82.16	82.10	82.10	10.91	633	43
VGG16	83.89	84.00	84.00	83.89	83.89	83.84	83.84	38.37	2993	63
ResNet50	92.33	92.40	92.40	92.33	92.33	92.33	92.33	31.31	1941	47
ResNet152	90.68	90.79	90.79	90.68	90.68	90.69	90.69	64.83	4084	48
DenseNet161	<b>93.46</b>	93.50	93.50	93.46	93.46	93.46	93.46	71.22	5484	62
EfficientNetB0	91.37	91.47	91.47	91.37	91.37	91.38	91.38	27.66	2102	61
ConvNeXt	85.94	86.30	86.30	85.94	85.94	86.05	86.05	46.51	2279	34
Vision Transformer	81.02	81.18	81.18	81.02	81.02	80.98	80.98	50.21	2611	37
MLP Mixer	69.41	69.67	69.67	69.41	69.41	69.22	69.22	35.69	1285	21
Swin Transformer	88.73	88.82	88.82	88.73	88.73	88.71	88.71	144.87	14487	85

Table D.19: Per class results for the pre-trained Vision Transformer model on the Resisc45 dataset,

Label	Precision	Recall	F1 score
airplane	99.28	98.57	98.92
airport	95.89	100.00	97.90
baseball_diamond	97.89	99.29	98.58
basketball_court	97.22	100.00	98.59
beach	98.59	100.00	99.29
bridge	97.87	98.57	98.22
chaparral	97.90	100.00	98.94
church	90.85	92.14	91.49
circular_farmland	98.59	100.00	99.29
cloud	100.00	99.29	99.64
commercial_area	95.07	96.43	95.74
dense_residential	94.20	92.86	93.53
desert	97.86	97.86	97.86
forest	97.79	95.00	96.38
freeway	99.27	97.14	98.19
golf_course	98.58	99.29	98.93
ground_track_field	100.00	99.29	99.64
harbor	100.00	100.00	100.00
industrial_area	94.96	94.29	94.62
intersection	97.86	97.86	97.86
island	98.59	100.00	99.29
lake	93.75	96.43	95.07
meadow	95.00	95.00	95.00
medium_residential	91.61	93.57	92.58
mobile_home_park	97.22	100.00	98.59
mountain	95.74	96.43	96.09
overpass	99.25	94.29	96.70
palace	91.91	89.29	90.58
parking_lot	99.28	98.57	98.92
railway	93.84	97.86	95.80
railway_station	96.30	92.86	94.55
rectangular_farmland	91.95	97.86	94.81
river	99.24	92.86	95.94
roundabout	99.29	100.00	99.64
runway	100.00	95.71	97.81
sea_ice	100.00	98.57	99.28
ship	97.22	100.00	98.59
snowberg	98.59	100.00	99.29
sparse_residential	96.43	96.43	96.43
stadium	97.90	100.00	98.94
storage_tank	98.56	97.86	98.21
tennis_court	98.54	96.43	97.47
terrace	96.21	90.71	93.38
thermal_power_station	96.45	97.14	96.80
wetland	97.01	92.86	94.89



D.7 RSI-CB256

RSI-CB256 [45] is a large scale remote sensing image classification benchmark via crowd-source data such as Open Street Map (OSM) data, ground objects in remote sensing images etc. It contains 35 categories and more than 24000 images with a size of 256x256 pixels (Figure D.19). A strict object category system according to the national standard of land-use classification in China and the hierarchical grading mechanism of ImageNet-1K has been established. Using crowd-source data as a supervisor facilitates machine self-learning through the Internet. The class distribution of the train, test and validation splits is presented in Figure D.20.

Detailed results for all pre-trained models are shown on Table D.20 and for all the models learned from scratch are presented on Table D.21. The best performing model is the pre-trained ResNet152 model. The results on a class level are show on Table D.22 along with a confusion matrix on Figure D.21.

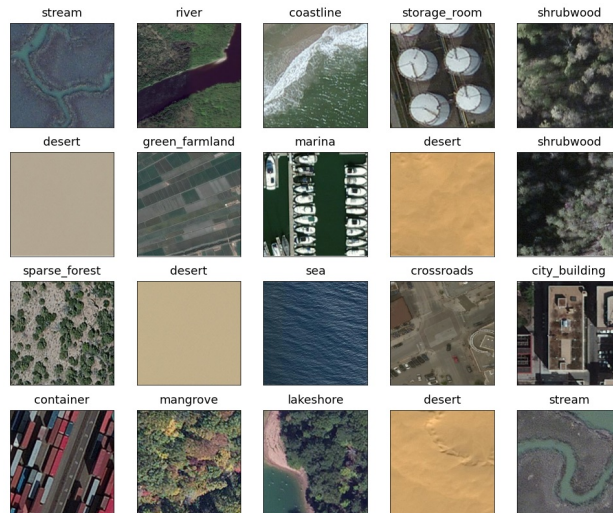


Figure D.19: Example images with labels from the RSI-CB256 dataset.

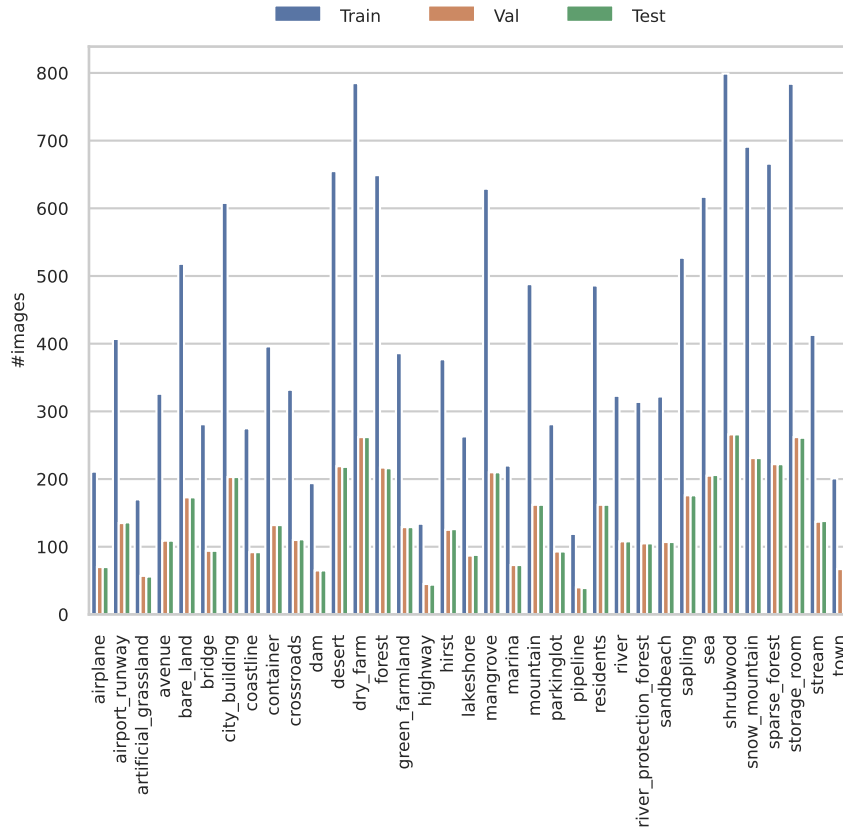


Figure D.20: Class distribution for the RSI-CB526 dataset.

Table D.20: Detailed results for pre-trained models on the RSI-CB256 dataset.

Model \ Metric	Accuracy	Macro Precision	Weighted Precision	Macro Recall	Weighted Recall	Macro F1 score	Weighted F1 score	Avg. time / epoch (sec.)	Total time (sec.)	Best epoch
AlexNet	99.35	99.13	99.36	99.06	99.35	99.09	99.35	34.84	1568	35
VGG16	99.05	98.93	99.07	98.75	99.05	98.83	99.05	34.04	885	16
ResNet50	99.68	99.53	99.68	99.54	99.68	99.53	99.68	33.69	1078	22
ResNet152	<b>99.86</b>	99.85	99.86	99.82	99.86	99.83	99.86	51.90	1609	21
DenseNet161	99.74	99.68	99.74	99.64	99.74	99.66	99.74	56.60	2717	38
EfficientNetB0	99.72	99.63	99.72	99.65	99.72	99.64	99.72	33.50	1340	30
ConvNeXt	99.60	99.50	99.60	99.55	99.60	99.52	99.60	40.35	1977	39
Vision Transformer	99.76	99.75	99.76	99.71	99.76	99.73	99.76	41.18	1400	24
MLP Mixer	99.66	99.54	99.66	99.61	99.66	99.57	99.66	35.29	1235	25
Swin Transformer	99.68	99.54	99.68	99.62	99.68	99.57	99.68	113.14	4752	32

Table D.21: Detailed results for models trained from scratch on the RSI-CB256 dataset.

Model \ Metric	Accuracy	Macro Precision	Weighted Precision	Macro Recall	Weighted Recall	Macro F1 score	Weighted F1 score	Avg. time / epoch (sec.)	Total time (sec.)	Best epoch
AlexNet	97.35	96.55	97.39	96.54	97.35	96.51	97.35	34.99	2414	54
VGG16	98.83	98.51	98.84	98.36	98.83	98.43	98.83	34.90	2757	64
ResNet50	98.83	98.51	98.84	98.36	98.83	98.43	98.83	36.39	3166	72
ResNet152	<b>99.15</b>	98.98	99.15	98.81	99.15	98.89	99.15	51.86	4472	72
DenseNet161	99.13	98.80	99.13	98.71	99.13	98.75	99.13	56.75	4029	56
EfficientNetB0	99.11	98.85	99.12	98.91	99.11	98.87	99.11	26.50	2123	71
ConvNeXt	98.44	97.75	98.45	97.74	98.44	97.73	98.44	36.93	2622	56
Vision Transformer	98.12	97.52	98.13	97.12	98.12	97.31	98.12	41.08	3204	63
MLP Mixer	98.42	97.81	98.43	97.80	98.42	97.79	98.42	29.00	2900	86
Swin Transformer	99.09	98.83	99.09	98.70	99.09	98.76	99.09	113.60	7157	48

Table D.22: Per class results for the pre-trained ResNet152 model on the RSI-CB256 dataset.

Label	Precision	Recall	F1 score
airplane	100.00	100.00	100.00
airport_runway	100.00	100.00	100.00
artificial_grassland	100.00	100.00	100.00
avenue	100.00	99.08	99.54
bare_land	98.30	100.00	99.14
bridge	98.95	100.00	99.47
city_building	100.00	100.00	100.00
coastline	100.00	98.91	99.45
container	100.00	99.24	99.62
crossroads	99.11	100.00	99.55
dam	100.00	100.00	100.00
desert	100.00	98.62	99.31
dry_farm	100.00	100.00	100.00
forest	100.00	100.00	100.00
green_farmland	100.00	100.00	100.00
highway	100.00	97.73	98.85
hirst	100.00	100.00	100.00
lakeshore	100.00	100.00	100.00
mangrove	100.00	100.00	100.00
marina	100.00	100.00	100.00
mountain	100.00	100.00	100.00
parkinglot	98.94	100.00	99.47
pipeline	100.00	100.00	100.00
residents	100.00	100.00	100.00
river	100.00	100.00	100.00
river_protection_forest	100.00	100.00	100.00
sandbeach	100.00	100.00	100.00
sapling	100.00	100.00	100.00
sea	99.52	100.00	99.76
shrubwood	100.00	100.00	100.00
snow_mountain	100.00	100.00	100.00
sparse_forest	100.00	100.00	100.00
storage_room	100.00	100.00	100.00
stream	100.00	100.00	100.00
town	100.00	100.00	100.00

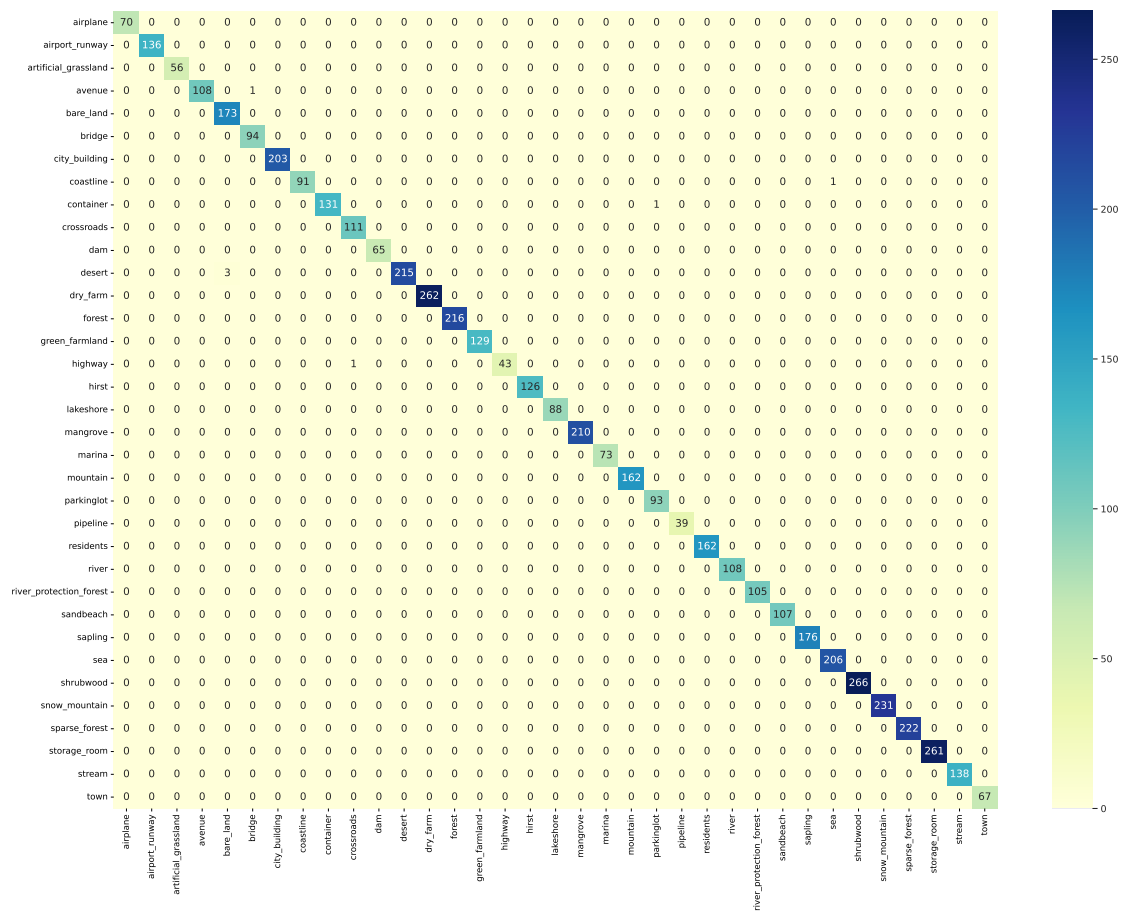


Figure D.21: Confusion matrix for the pre-trained ResNet152 model on the RSI-CB256 dataset.

### D.8 RSSCN7

RSSCN7 [46] is a scene classification dataset. The images are obtained from Google Earth. This dataset was collected for academic research. It contains a total of 2800 remote sensing images, which are organized into 7 scene classes: grass land, forest, farm land, parking lot, residential region, industrial region, and river/lake (Figure D.22). For each, class there are 400 RGB images that are cropped on four different scales with 100 images per scale. Each image has a 400x400 pixels size. The main challenge of this dataset is the scale variations of the images. The class distribution over the train, test and validation splits is presented on Figure D.23.

Detailed results for all pre-trained models are shown on Table D.23 and for all the models learned from scratch are presented on Table D.24. The best performing model is the pre-trained Vision Transformer model. The results on a class level are show on Table D.25 along with a confusion matrix on Figure D.24.

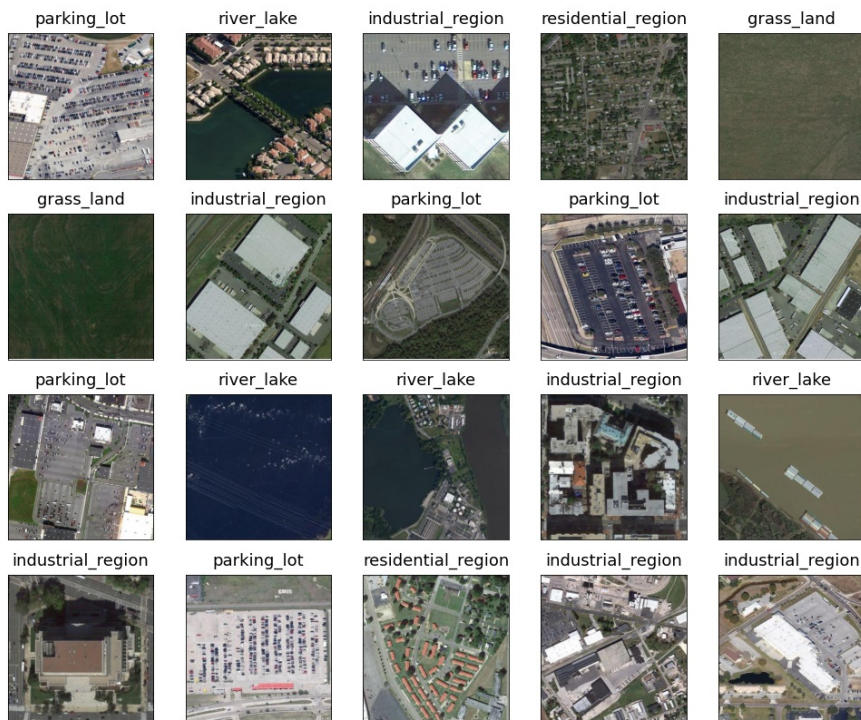


Figure D.22: Example images with labels from the RSSCN7 dataset.

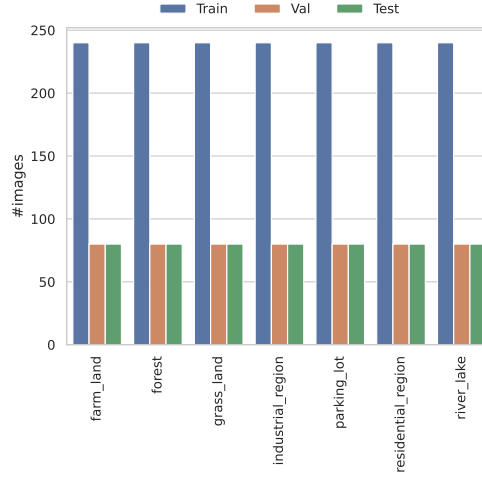


Figure D.23: Class distribution for the RSSCN7 dataset.

Table D.23: Detailed results for pre-trained models on the RSSCN7 dataset.

Model \ Metric	Accuracy	Macro Precision	Weighted Precision	Macro Recall	Weighted Recall	Macro F1 score	Weighted F1 score	Avg. time / epoch (sec.)	Total time (sec.)	Best epoch
AlexNet	91.96	92.05	92.05	91.96	91.96	91.92	91.92	3.19	118	27
VGG16	93.93	93.95	93.95	93.93	93.93	93.90	93.90	4.68	159	24
ResNet50	95.00	95.08	95.08	95.00	95.00	94.99	94.99	3.90	121	21
ResNet152	95.00	95.07	95.07	95.00	95.00	95.01	95.01	7.09	241	24
DenseNet161	94.82	94.83	94.83	94.82	94.82	94.82	94.82	7.59	220	19
EfficientNetB0	95.54	95.56	95.56	95.54	95.54	95.54	95.54	3.79	163	33
ConvNeXt	94.64	94.76	94.76	94.64	94.64	94.61	94.61	5.23	183	25
Vision Transformer	<b>95.89</b>	95.95	95.95	95.89	95.89	95.91	95.91	5.54	227	31
MLP Mixer	95.18	95.23	95.23	95.18	95.18	95.17	95.17	4.30	86	10
Swin Transformer	95.18	95.23	95.23	95.18	95.18	95.18	95.18	13.42	416	21

Table D.24: Detailed results for models trained from scratch on the RSSCN7 dataset.

Model \ Metric	Accuracy	Macro Precision	Weighted Precision	Macro Recall	Weighted Recall	Macro F1 score	Weighted F1 score	Avg. time / epoch (sec.)	Total time (sec.)	Best epoch
AlexNet	80.54	80.64	80.64	80.54	80.54	80.45	80.45	6.97	697	85
VGG16	81.61	81.50	81.50	81.61	81.61	81.41	81.41	6.74	526	63
ResNet50	82.68	82.65	82.65	82.68	82.68	82.41	82.41	3.76	316	69
ResNet152	82.68	82.65	82.65	82.68	82.68	82.41	82.41	6.90	407	44
DenseNet161	<b>87.32</b>	87.55	87.55	87.32	87.32	87.38	87.38	8.50	595	55
EfficientNetB0	83.93	84.03	84.03	83.93	83.93	83.87	83.87	3.65	365	93
ConvNeXt	83.04	82.84	82.84	83.04	83.04	82.90	82.90	5.43	543	87
Vision Transformer	86.07	86.17	86.17	86.07	86.07	86.00	86.00	5.52	453	67
MLP Mixer	83.21	83.29	83.29	83.21	83.21	83.17	83.17	4.08	408	100
Swin Transformer	82.50	82.59	82.59	82.50	82.50	82.50	82.50	13.78	951	54

Table D.25: Per class results for the pre-trained Vision Transformer model on the RSSCN7 dataset.

Label	Precision	Recall	F1 score
farm_land	97.40	93.75	95.54
forest	100.00	98.75	99.37
grass_land	91.57	95.00	93.25
industrial_region	92.59	93.75	93.17
parking_lot	94.94	93.75	94.34
residential_region	100.00	98.75	99.37
river_lake	95.12	97.50	96.30

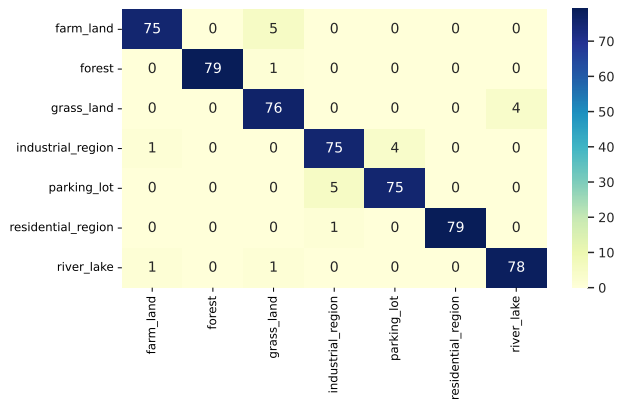


Figure D.24: Confusion matrix for the pre-trained Vision Transformer model on the RSSCN7 dataset.

### D.9 SAT6

SAT-6 [47] consists of a total of 405000 image patches each of size 28x28 and covering 6 land cover classes - barren land, trees, grassland, roads, buildings and water bodies (Figure D.25). The authors of the dataset selected 324000 images for the training dataset and 81000 were selected as testing dataset. Additionally we have selected 20% of the images from the train dataset to create the validation split. The training and test datasets were selected from disjoint National Agriculture Imagery Program (NAIP) tiles. The specifications for the various land cover classes of SAT-6 were adopted from those used in the National Land Cover Data (NLCD) algorithm. The class distribution of the train, test and validation splits is presented on Figure D.25.

Detailed results for all pre-trained models are shown on Table D.26 and for all the models learned from scratch are presented on Table D.27. All pre-trained model obtained excellent result on the dataset with ResNet50, ResNet152, DenseNet161, ConvNeXt, Vision Transformer, MLP-Mixer and Swin Transformer achieving 100 % accuracy. The results on a class level are show on Table D.28 along with a confusion matrix on Figure D.27 for the DenseNet161 model.

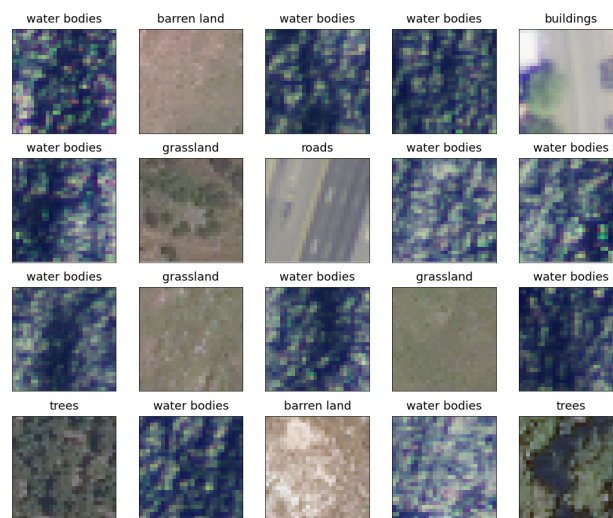


Figure D.25: Example images with labels from the SAT6 dataset.

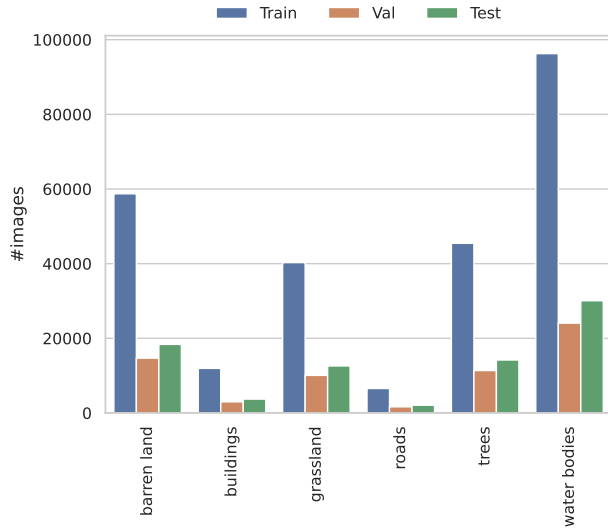


Figure D.26: Class distribution for the SAT6 dataset.

Table D.26: Detailed results for pre-trained models on the SAT6 dataset.

Model \ Metric	Accuracy	Macro Precision	Weighted Precision	Macro Recall	Weighted Recall	Macro F1 score	Weighted F1 score	Avg. time / epoch (sec.)	Total time (sec.)	Best epoch
AlexNet	99.98	99.98	99.98	99.97	99.98	99.97	99.98	92.48	5364	48
VGG16	99.99	99.99	99.99	99.99	99.99	99.99	99.99	550.04	29702	44
ResNet50	100.00	100.00	100.00	100.00	100.00	100.00	100.00	410.33	37340	81
ResNet152	100.00	100.00	100.00	100.00	100.00	100.00	100.00	872.87	61974	61
DenseNet161	100.00	100.00	100.00	100.00	100.00	100.00	100.00	970.39	55312	47
EfficientNetB0	99.99	99.99	99.99	99.99	99.99	99.99	99.99	363.00	8712	14
ConvNeXt	100.00	100.00	100.00	99.99	100.00	100.00	100.00	630.78	42262	57
Vision Transformer	100.00	100.00	100.00	100.00	100.00	100.00	100.00	692.50	42935	52
MLP Mixer	100.00	100.00	100.00	100.00	100.00	100.00	100.00	476.34	15243	22
Swin Transformer	100.00	100.00	100.00	100.00	100.00	100.00	100.00	2,003.62	106192	43

Table D.27: Detailed results for models trained from scratch on the SAT6 dataset.

Model \ Metric	Accuracy	Macro Precision	Weighted Precision	Macro Recall	Weighted Recall	Macro F1 score	Weighted F1 score	Avg. time / epoch (sec.)	Total time (sec.)	Best epoch
AlexNet	99.27	98.67	99.27	98.65	99.27	98.66	99.27	107.26	10726	98
VGG16	99.56	99.42	99.56	99.42	99.56	99.42	99.56	579.10	57910	98
ResNet50	100.00	100.00	100.00	100.00	100.00	100.00	100.00	457.04	45704	99
ResNet152	100.00	100.00	100.00	100.00	100.00	100.00	100.00	987.21	98721	94
DenseNet161	100.00	100.00	100.00	100.00	100.00	100.00	100.00	956.03	95603	85
EfficientNetB0	100.00	100.00	100.00	100.00	100.00	100.00	100.00	420.37	42037	95
ConvNeXt	100.00	100.00	100.00	100.00	100.00	100.00	100.00	627.69	62769	97
Vision Transformer	99.99	99.98	99.99	99.98	99.99	99.98	99.99	687.12	61841	75
MLP Mixer	99.98	99.98	99.98	99.96	99.98	99.97	99.98	479.37	47937	95
Swin Transformer	99.98	99.96	99.98	99.97	99.98	99.97	99.98	1,973.44	197344	99

Table D.28: Per class results for the pre-trained DenseNet model on the SAT6 dataset.

Label	Precision	Recall	F1 score
buildings	100.00	100.00	100.00
barren land	100.00	100.00	100.00
trees	100.00	100.00	100.00
grassland	100.00	100.00	100.00
roads	100.00	100.00	100.00
water bodies	100.00	100.00	100.00

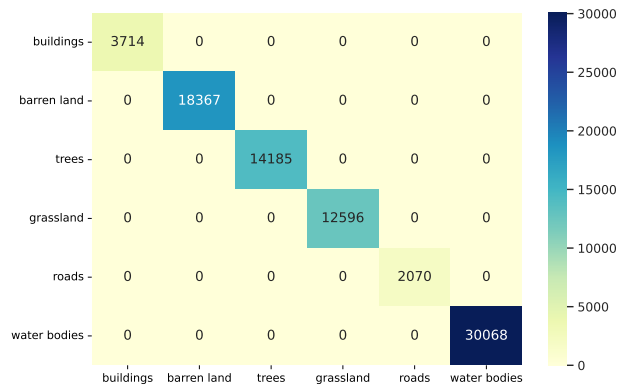


Figure D.27: Confusion matrix for the pre-trained DenseNet161 model on the SAT6 dataset.

D.10 Siri-Whu

The SIRI-WHU [48] is a scene classification dataset comprised of 2400 images organized into 12 classes. Each class contains 200 images with a 2m spatial resolution and a size of 200×200 pixels (Figure D.28). It was collected from Google Earth (Google Inc.) by the Intelligent Data Extraction and Analysis of Remote Sensing (RS\_IDEA) Group in Wuhan University. The 12 land-use classes contain agriculture, commercial, harbor, idle land, industrial, meadow, overpass, park, pond, residential, river, and water. This dataset mainly covers urban areas in China, which means it lack diversity and is less challenging. The class distribution is presented on Figure D.29.

Detailed results for all pre-trained models are shown on Table D.29 and for all the models learned from scratch are presented on Table D.30. The best performing model is the pre-trained ResNet152 model. The results on a class level are show on Table D.31 along with a confusion matrix on Figure D.30.

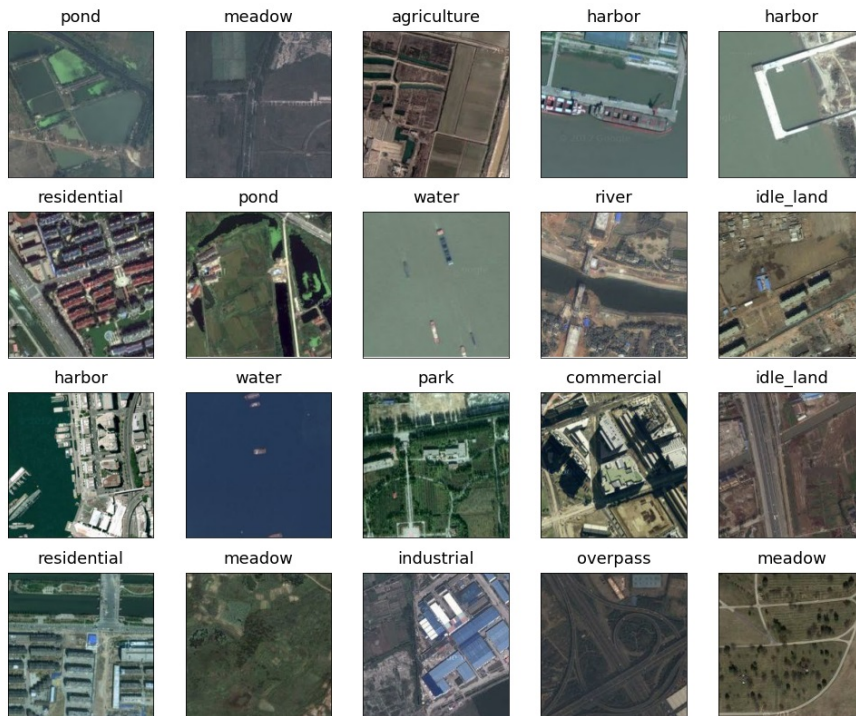


Figure D.28: Example images with labels from the SIRI-WHU dataset.

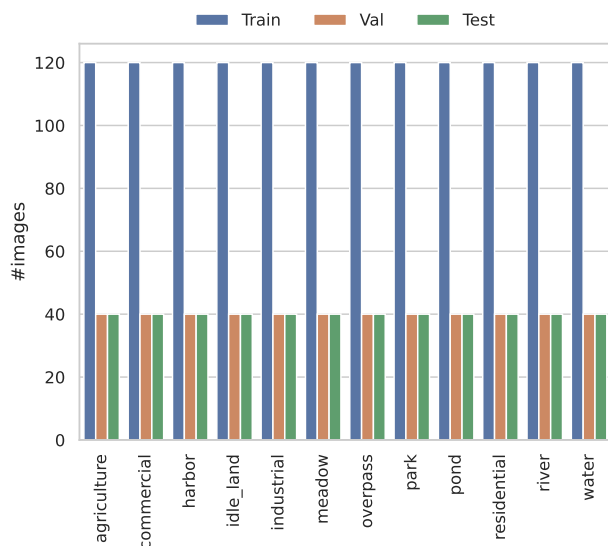


Figure D.29: Class distribution for the SIRI-WHU dataset.

Table D.29: Detailed results for pre-trained models on the SIRI-WHU dataset.

Model \ Metric	Accuracy	Macro Precision	Weighted Precision	Macro Recall	Weighted Recall	Macro F1 score	Weighted F1 score	Avg. time / epoch (sec.)	Total time (sec.)	Best epoch
AlexNet	92.29	92.64	92.64	92.29	92.29	92.31	92.31	4.28	197	36
VGG16	93.96	94.08	94.08	93.96	93.96	93.96	93.96	4.98	214	33
ResNet50	95.00	95.12	95.12	95.00	95.00	95.01	95.01	4.66	191	31
RestNet152	<b>96.25</b>	96.27	96.27	96.25	96.25	96.24	96.24	6.65	226	24
DenseNet161	95.63	95.64	95.64	95.63	95.63	95.61	95.61	7.30	365	40
EfficientNetB0	95.00	95.09	95.09	95.00	95.00	95.01	95.01	4.57	329	62
ConvNeXt	96.25	96.34	96.34	96.25	96.25	96.24	96.24	5.64	203	26
Vision Transformer	95.63	95.73	95.73	95.63	95.62	95.63	95.63	5.37	322	50
MLP Mixer	95.21	95.36	95.36	95.21	95.21	95.23	95.23	4.55	150	23
Swin Transformer	95.63	95.60	95.60	95.63	95.62	95.57	95.57	11.87	534	35

Table D.30: Detailed results for models trained from scratch on the SIRI-WHU dataset.

Model \ Metric	Accuracy	Macro Precision	Weighted Precision	Macro Recall	Weighted Recall	Macro F1 score	Weighted F1 score	Avg. time / epoch (sec.)	Total time (sec.)	Best epoch
AlexNet	83.75	83.83	83.83	83.75	83.75	83.66	83.66	3.54	326	77
VGG16	84.79	85.05	85.05	84.79	84.79	84.70	84.70	7.32	732	93
ResNet50	<b>88.96</b>	89.14	89.14	88.96	88.96	88.94	88.94	3.81	305	65
ResNet152	88.75	88.67	88.67	88.75	88.75	88.62	88.62	6.54	608	78
DenseNet161	86.67	87.38	87.38	86.67	86.67	86.56	86.56	7.49	749	94
EfficientNetB0	86.04	86.23	86.23	86.04	86.04	85.94	85.94	3.61	238	51
ConvNeXt	84.17	84.32	84.32	84.17	84.17	84.09	84.09	11.99	1007	69
Vision Transformer	86.25	86.31	86.31	86.25	86.25	86.14	86.14	5.08	503	84
MLP Mixer	82.50	82.40	82.40	82.50	82.50	82.34	82.34	3.92	392	98
Swin Transformer	85.83	86.02	86.02	85.83	85.83	85.62	85.62	12.10	1113	77

Table D.31: Per class results for the pre-trained ResNet152 model on the SIRI-WHU dataset.

Label	Precision	Recall	F1 score
agriculture	100.00	100.00	100.00
commercial	100.00	97.50	98.73
harbor	90.48	95.00	92.68
idle_land	97.50	97.50	97.50
industrial	100.00	97.50	98.73
meadow	92.11	87.50	89.74
overpass	95.24	100.00	97.56
park	92.31	90.00	91.14
pond	100.00	100.00	100.00
residential	97.56	100.00	98.77
river	92.50	92.50	92.50
water	97.50	97.50	97.50

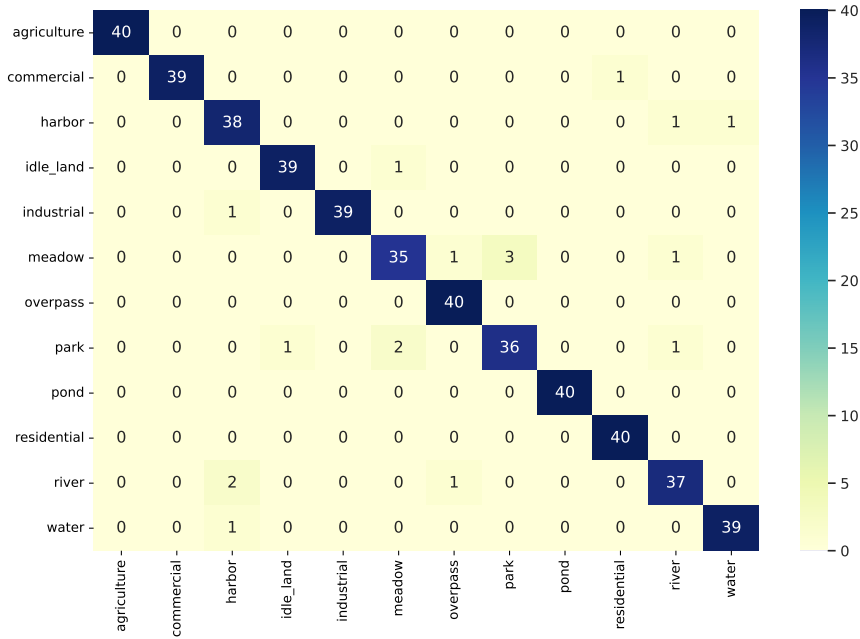


Figure D.30: Confusion matrix for the pre-trained ResNet152 model on the SIRI-WHU dataset.

### D.11 CLRS

This dataset [49] is a database designed for the task named Continual/Lifelong learning for remote sensing image scene classification. The proposed CLRS dataset consists of 15000 remote sensing images divided into 25 scene classes covering over 100 countries (Figure D.31). The images have a spatial resolution between 0.26 8.85 meters. The data is acquired from multiple sources such as: Google Earth, Bing Map, Google Map, and Tianditu. The class distribution of the train, test and validation splits is presented on Figure D.32.

Detailed results for all pre-trained models are shown on Table D.32 and for all the models learned from scratch are presented on Table D.33. The best performing model is the pre-trained Vision Transformer model. The results on a class level are show on Table D.34 along with a confusion matrix on Figure D.33.

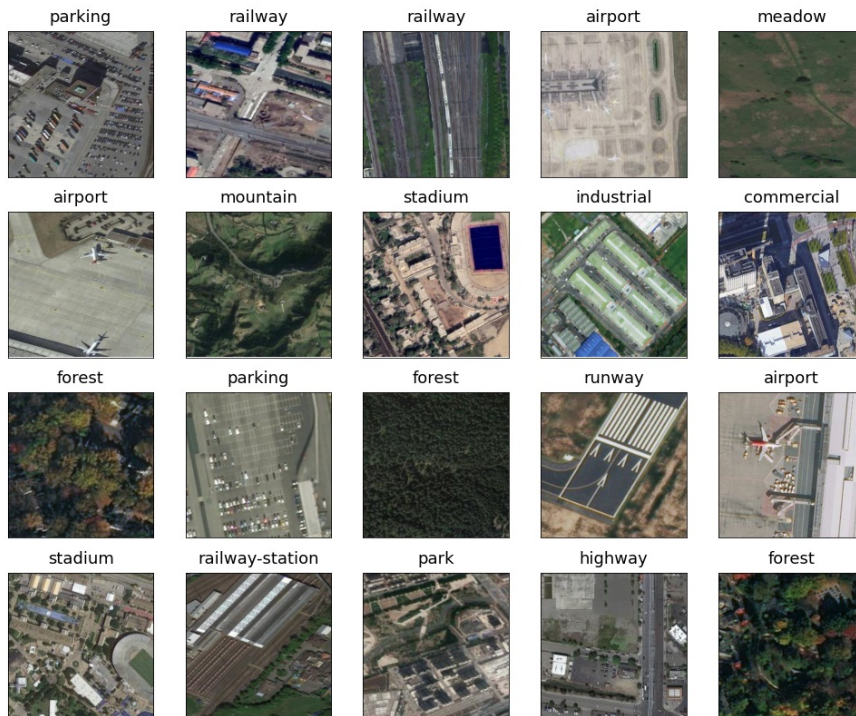


Figure D.31: Example images with labels from the CLRS dataset.

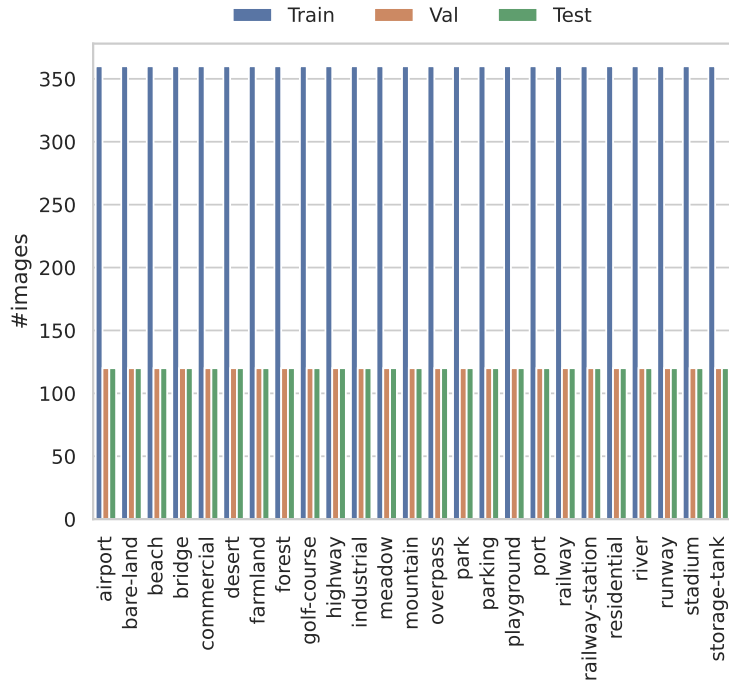


Figure D.32: Class distribution for the CLRS dataset.

Table D.32: Detailed results for pre-trained models on the CLRS dataset.

Model \ Metric	Accuracy	Macro Precision	Weighted Precision	Macro Recall	Weighted Recall	Macro F1 score	Weighted F1 score	Avg. time / epoch (sec.)	Total time (sec.)	Best epoch
AlexNet	84.10	84.19	84.19	84.10	84.10	84.03	84.03	20.48	635	21
VGG16	89.90	89.97	89.97	89.90	89.90	89.90	89.90	20.23	607	20
ResNet50	91.57	91.67	91.67	91.57	91.57	91.58	91.58	18.60	279	15
ResNet152	91.90	91.99	91.99	91.90	91.90	91.91	91.91	31.96	799	15
DenseNet161	92.20	92.29	92.29	92.20	92.20	92.20	92.20	35.46	993	18
EfficientNetB0	90.50	90.61	90.61	90.50	90.50	90.49	90.49	19.73	513	16
ConvNeXt	91.10	91.29	91.29	91.10	91.10	91.12	91.12	23.62	496	11
Vision Transformer	<b>93.20</b>	93.29	93.29	93.20	93.20	93.22	93.22	25.32	785	21
MLP Mixer	90.10	90.21	90.21	90.10	90.10	90.05	90.05	19.75	316	6
Swin Transformer	92.53	92.53	92.53	92.53	92.53	92.51	92.51	68.93	1861	17

Table D.33: Detailed results for models trained from scratch on the CLRS dataset.

Model \ Metric	Accuracy	Macro Precision	Weighted Precision	Macro Recall	Weighted Recall	Macro F1 score	Weighted F1 score	Avg. time / epoch (sec.)	Total time (sec.)	Best epoch
AlexNet	71.40	71.59	71.59	71.40	71.40	71.33	71.33	20.35	2035	92
VGG16	76.07	76.20	76.20	76.07	76.07	76.00	76.00	19.33	1450	60
ResNet50	85.57	85.72	85.72	85.57	85.57	85.57	85.57	19.43	1788	77
ResNet152	82.30	82.47	82.47	82.30	82.30	82.19	82.19	32.05	2373	60
DenseNet161	<b>86.17</b>	86.29	86.29	86.17	86.17	86.18	86.18	35.81	2757	62
EfficientNetB0	82.27	82.55	82.55	82.27	82.27	82.31	82.31	20.71	1512	58
ConvNeXt	69.17	69.02	69.02	69.17	69.17	69.01	69.01	23.09	2309	96
Vision Transformer	65.47	66.41	66.41	65.47	65.47	65.49	65.49	24.96	1173	32
MLP Mixer	61.13	62.18	62.18	61.13	61.13	60.87	60.87	17.98	809	30
Swin Transformer	80.00	80.10	80.10	80.00	80.00	79.91	79.91	69.19	5535	65

Table D.34: Per class results for the pre-trained Vision Transformer model on the CLRS dataset.

Label	Precision	Recall	F1 score
airport	97.48	96.67	97.07
bare-land	92.00	95.83	93.88
beach	99.15	97.50	98.32
bridge	90.91	91.67	91.29
commercial	79.84	85.83	82.73
desert	97.50	97.50	97.50
farmland	93.70	99.17	96.36
forest	100.00	100.00	100.00
golf-course	94.96	94.17	94.56
highway	92.11	87.50	89.74
industrial	88.79	85.83	87.29
meadow	96.72	98.33	97.52
mountain	99.15	97.50	98.32
overpass	89.68	94.17	91.87
park	85.60	89.17	87.35
parking	98.25	93.33	95.73
playground	95.04	95.83	95.44
port	94.74	90.00	92.31
railway	86.29	89.17	87.70
railway-station	88.79	85.83	87.29
residential	90.68	89.17	89.92
river	90.32	93.33	91.80
runway	98.33	98.33	98.33
stadium	95.61	90.83	93.16
storage-tank	96.55	93.33	94.92

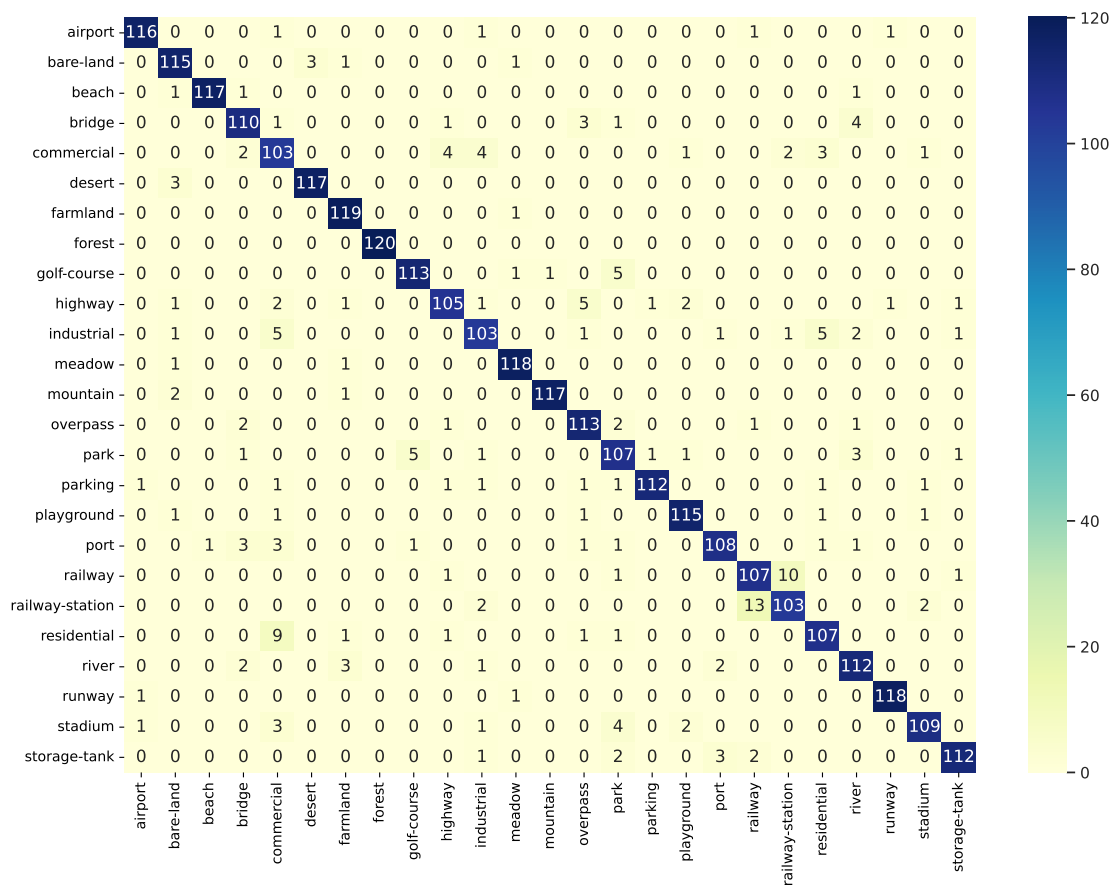


Figure D.33: Confusion matrix for the pre-trained Vision Transformer model on the CLRS dataset.

D.12 RSD46-WHU

RSD46-WHU is a large-scale open dataset for scene classification in remote sensing images. The dataset is manually collected from Google Earth and Tianditu. The ground resolution of most classes is 0.5m, and the others are about 2m. There are 500-3000 images in each class. The RSD46-WHU dataset contains around 117000 images with 46 classes (Figure D.34). The images are not evenly distributed between classes and each class contains between 428 to 3000 images. The dataset comes with predefined train and test splits. For creating the validation split we used 20% of the images from the train split. The class distribution of the different splits is presented on Figure D.35.

Detailed results for all pre-trained models are shown on Table D.35 and for all the models learned from scratch are presented on Table D.36. The best performing model is the pre-trained DenseNet161 model. The results on a class level are shown on Table D.37 along with a confusion matrix on Figure D.36.



Figure D.34: Example images with labels from the RSD46-WHU dataset.

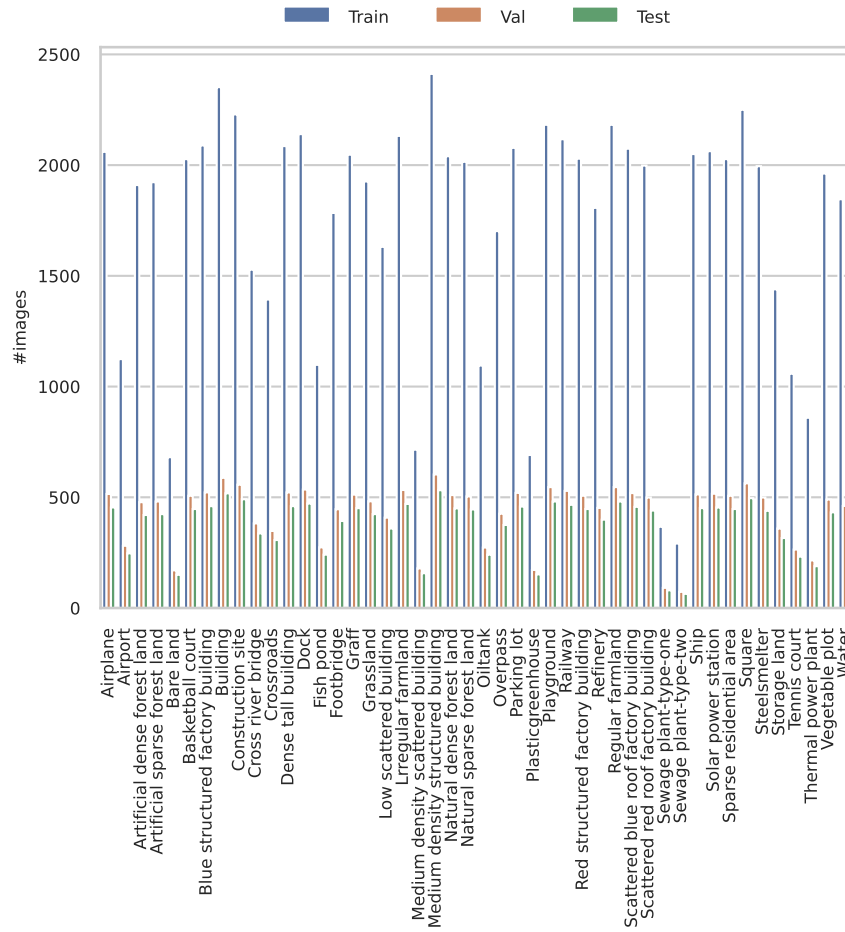


Figure D.35: Class distribution for the RSD46-WHU dataset.

Table D.35: Detailed results for pre-trained models on the RSD46-WHU dataset.

Model \ Metric	Accuracy	Macro Precision	Weighted Precision	Macro Recall	Weighted Recall	Macro F1 score	Weighted F1 score	Avg. time / epoch (sec.)	Total time (sec.)	Best epoch
AlexNet	90.65	90.43	90.61	90.35	90.65	90.36	90.61	58.03	2031	25
VGG16	92.42	92.30	92.38	92.25	92.42	92.22	92.37	158.32	4433	18
ResNet50	94.16	94.07	94.15	94.18	94.16	94.11	94.14	123.27	3205	16
ResNet152	94.40	94.33	94.40	94.41	94.40	94.36	94.39	269.45	7814	19
DenseNet161	<b>94.51</b>	94.36	94.49	94.41	94.51	94.36	94.48	297.70	6847	13
EfficientNetB0	93.39	93.20	93.38	93.39	93.39	93.26	93.35	111.55	2231	10
ConvNeXt	93.63	93.61	93.67	93.47	93.63	93.48	93.60	196.20	3924	10
Vision Transformer	94.24	94.38	94.23	94.08	94.24	94.16	94.20	210.37	3997	9
MLP Mixer	93.67	93.77	93.69	93.47	93.67	93.55	93.65	148.25	3558	14
Swin Transformer	93.54	93.48	93.62	93.62	93.54	93.50	93.52	599.42	11389	9

Table D.36: Detailed results for models trained from scratch on the RSD46-WHU dataset.

Model \ Metric	Accuracy	Macro Precision	Weighted Precision	Macro Recall	Weighted Recall	Macro F1 score	Weighted F1 score	Avg. time / epoch (sec.)	Total time (sec.)	Best epoch
AlexNet	86.03	85.83	86.03	85.67	86.03	85.71	85.99	58.84	3707	48
VGG16	88.62	88.37	88.56	88.37	88.62	88.32	88.55	162.89	8796	39
ResNet50	90.55	90.40	90.53	90.26	90.55	90.30	90.52	127.53	8672	53
ResNet152	89.94	89.84	89.99	89.77	89.94	89.78	89.95	272.70	19907	58
DenseNet161	<b>92.21</b>	92.11	92.23	92.03	92.21	92.06	92.21	301.16	15318	36
EfficientNetB0	90.61	90.57	90.61	90.25	90.61	90.37	90.58	113.93	6446	40
ConvNeXt	88.69	88.66	88.67	88.33	88.69	88.46	88.66	194.93	11891	46
Vision Transformer	86.47	86.22	86.45	85.94	86.47	86.02	86.42	211.93	9325	29
MLP Mixer	81.25	81.56	81.59	80.11	81.25	80.51	81.19	148.42	4149	12
Swin Transformer	91.81	91.50	91.79	91.48	91.81	91.47	91.79	588.25	41766	56

Table D.37: Per class results for the pre-trained DenseNet161 model on the RSD46-WHU dataset.

Label	Precision	Recall	F1 score
Airplane	99.56	99.78	99.67
Airport	98.39	99.19	98.79
Artificial dense forest land	87.11	86.90	87.01
Artificial sparse forest land	87.06	82.55	84.75
Bare land	94.12	96.00	95.05
Basketball court	90.37	92.39	91.37
Blue structured factory building	96.57	97.83	97.19
Building	82.44	83.40	82.92
Construction site	82.11	79.43	80.75
Cross river bridge	99.70	99.70	99.70
Crossroads	97.74	98.70	98.22
Dense tall building	94.35	94.35	94.35
Dock	98.94	98.73	98.83
Fish pond	97.52	97.93	97.72
Footbridge	99.49	99.24	99.36
Graff	98.37	93.79	96.03
Grassland	95.07	95.52	95.29
Low scattered building	96.15	97.49	96.82
Lrregular farmland	97.68	98.51	98.09
Medium density scattered building	76.98	68.15	72.30
Medium density structured building	89.58	92.11	90.82
Natural dense forest land	95.40	96.89	96.14
Natural sparse forest land	93.16	97.98	95.51
Oiltank	90.66	96.68	93.57
Overpass	99.19	98.13	98.66
Parking lot	96.49	96.07	96.28
Plasticgreenhouse	100.00	99.34	99.67
Playground	96.85	95.84	96.34
Railway	99.14	99.14	99.14
Red structured factory building	97.78	98.66	98.22
Refinery	92.84	87.72	90.21
Regular farmland	95.20	94.80	95.00
Scattered blue roof factory building	94.44	96.72	95.57
Scattered red roof factory building	93.28	97.73	95.45
Sewage plant-type-one	95.06	96.25	95.65
Sewage plant-type-two	88.73	98.44	93.33
Ship	99.56	99.33	99.45
Solar power station	99.78	99.78	99.78
Sparse residential area	91.42	88.14	89.75
Square	94.52	97.38	95.93
Steelsmelter	90.48	90.89	90.68
Storage land	99.03	96.52	97.76
Tennis court	95.93	91.38	93.60
Thermal power plant	88.95	85.19	87.03
Vegetable plot	94.12	92.59	93.35
Water	99.02	99.51	99.26

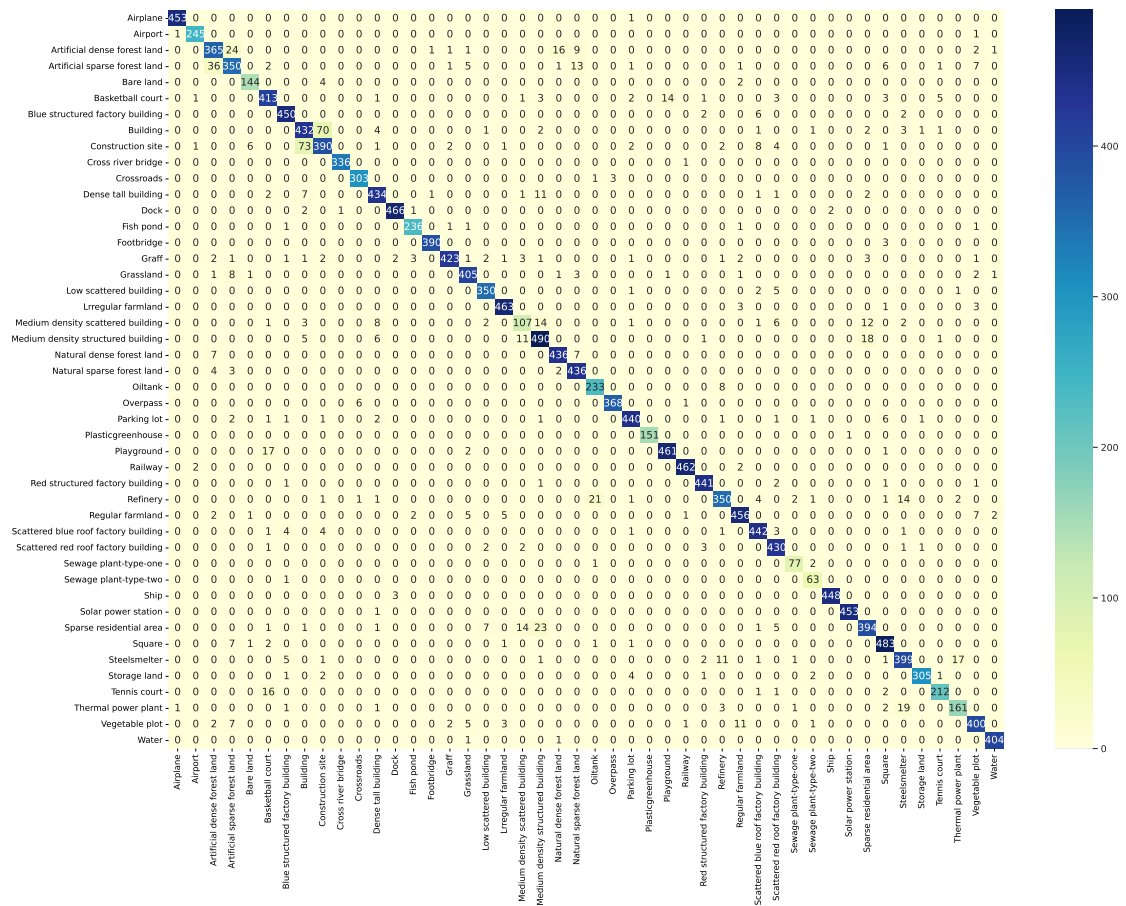


Figure D.36: Confusion matrix for the pre-trained DenseNet161 model on the RSD46-WHU dataset.

### D.13 Brazilian Coffee Scenes

The Brazilian Coffee Scenes dataset [52] consists of only two classes: coffee and non-coffee class. Each class has 1438 images with 64x64 pixels cropped from SPOT satellite images over four counties in the state of Minas Gerais, Brazil: Arceburgo, Guarania, Guaxupe, and Monte Santo (Figure D.37). The images in the dataset are in green, red and near-infrared spectral bands, since these are most useful and representative for distinguishing vegetation areas. The dataset is manually annotated by agricultural researchers. Images which contain coffee pixels in at least 85% of the image were assigned to the coffee class. Image with less than 10% of coffee pixels are assigned to the non-coffee class. The number of classes and the degree to which the data is tailored, should make this less challenging dataset. The class distribution is presented on Figure D.38.

Detailed results for all pre-trained models are shown on Table D.38 and for all the models learned from scratch are presented on Table D.39. The best performing model is the pre-trained Swin Transformer model. The results on a class level are show on Table D.40 along with a confusion matrix on Figure D.39.

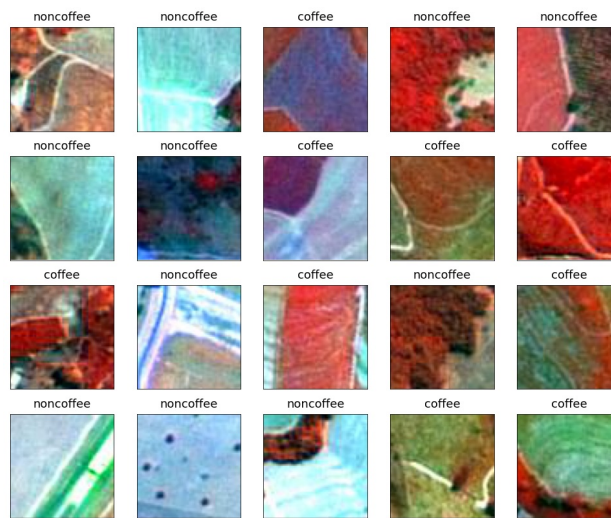


Figure D.37: Example images with labels from the Brazilian Coffee Scenes dataset.

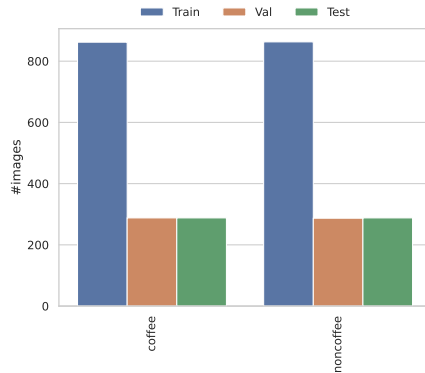


Figure D.38: Class distribution for the Brazilian Coffee Scenes dataset.

Table D.38: Detailed results for pre-trained models on the Brazilian Coffee Scenes dataset.

Model \ Metric	Accuracy	Macro Precision	Weighted Precision	Macro Recall	Weighted Recall	Macro F1 score	Weighted F1 score	Avg. time / epoch (sec.)	Total time (sec.)	Best epoch
AlexNet	89.58	89.59	89.59	89.58	89.58	89.58	89.58	1.48	43	19
VGG16	90.97	91.00	91.00	90.97	90.97	90.97	90.97	4.17	121	19
ResNet50	92.01	92.06	92.06	92.01	92.01	92.01	92.01	3.45	76	12
ResNet152	92.36	92.37	92.37	92.36	92.36	92.36	92.36	6.61	119	8
DenseNet161	92.71	92.81	92.81	92.71	92.71	92.71	92.70	7.33	176	14
EfficientNetB0	91.32	91.32	91.32	91.32	91.32	91.32	91.32	3.17	133	32
ConvNeXt	91.49	91.58	91.58	91.49	91.49	91.49	91.49	5.08	132	16
Vision Transformer	92.01	92.03	92.03	92.01	92.01	92.01	92.01	5.07	76	5
MLP Mixer	93.06	93.07	93.07	93.06	93.06	93.05	93.05	3.94	67	7
Swin Transformer	<b>93.40</b>	93.40	93.40	93.40	93.40	93.40	93.40	13.88	222	6

Table D.39: Detailed results for models trained from scratch on the Brazilian Coffee Scenes dataset.

Model \ Metric	Accuracy	Macro Precision	Weighted Precision	Macro Recall	Weighted Recall	Macro F1 score	Weighted F1 score	Avg. time / epoch (sec.)	Total time (sec.)	Best epoch
AlexNet	89.41	89.62	89.62	89.41	89.41	89.40	89.40	1.53	115	60
VGG16	89.41	89.45	89.45	89.41	89.41	89.41	89.41	5.95	440	59
ResNet50	89.24	89.39	89.39	89.24	89.24	89.23	89.23	4.55	296	50
ResNet152	88.54	88.56	88.56	88.54	88.54	88.54	88.54	7.95	469	44
DenseNet161	<b>90.80</b>	90.80	90.80	90.80	90.80	90.80	90.80	7.31	373	36
EfficientNetB0	85.42	85.71	85.71	85.42	85.42	85.39	85.39	3.26	326	98
ConvNeXt	84.38	84.39	84.39	84.38	84.38	84.37	84.37	5.09	509	95
Vision Transformer	87.85	87.89	87.89	87.85	87.85	87.84	87.84	5.55	322	43
MLP Mixer	86.28	86.29	86.29	86.28	86.28	86.28	86.28	4.47	201	30
Swin Transformer	89.24	89.33	89.33	89.24	89.24	89.23	89.23	13.59	1169	71

Table D.40: Per class results for Swin Transformer on the Brazilian Coffee Scenes dataset.

Label	Precision	Recall	F1 score
coffee	93.10	93.75	93.43
noncoffee	93.71	93.06	93.38

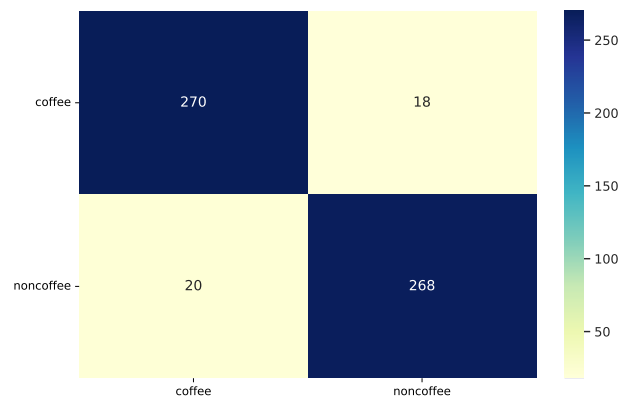


Figure D.39: Confusion matrix for Swin Transformer on the Brazilian Coffee Scenes dataset.

D.14 Optimal 31

The Optimal 31 dataset [51] is for remote sensing image scene classification. The dataset contains 31 classes, each class contains 60 images with a size of 256×256 pixels. Totaling 1860 aerial RGB images (Figure D.40). These classes include: airplane, airport, basketball court, baseball field, bridge, beach, bushes, crossroads, church, round farmland, business district, desert, harbor, dense houses, factory, forest, freeway, golf field, island, lake, meadow, medium houses, mountain, mobile house area, overpass, playground, parking lot, roundabout, runway, railway, and square farmland. It is considered challenging due to small number of images dispersed across many classes. We have generated train, test and validation splits for our study and their class distribution is presented on Figure D.41.

Detailed results for all pre-trained models are shown on Table D.41 and for all the models learned from scratch are presented on Table D.42. The best performing model is the pre-trained Vision Transformer model. The results on a class level are show on Table D.43 along with a confusion matrix on Figure D.42.

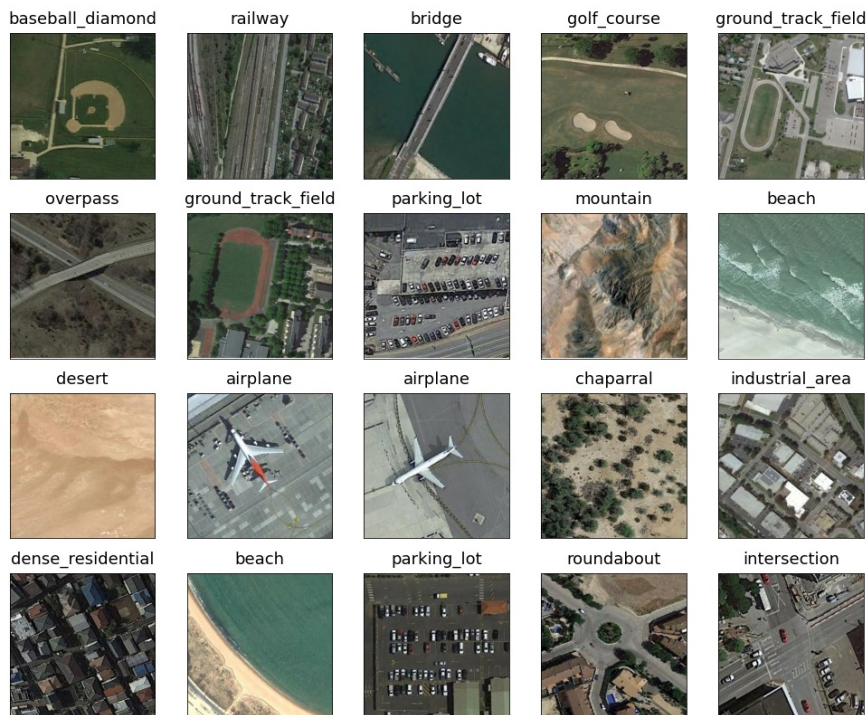


Figure D.40: Example images with labels from the Optimal 31 dataset.

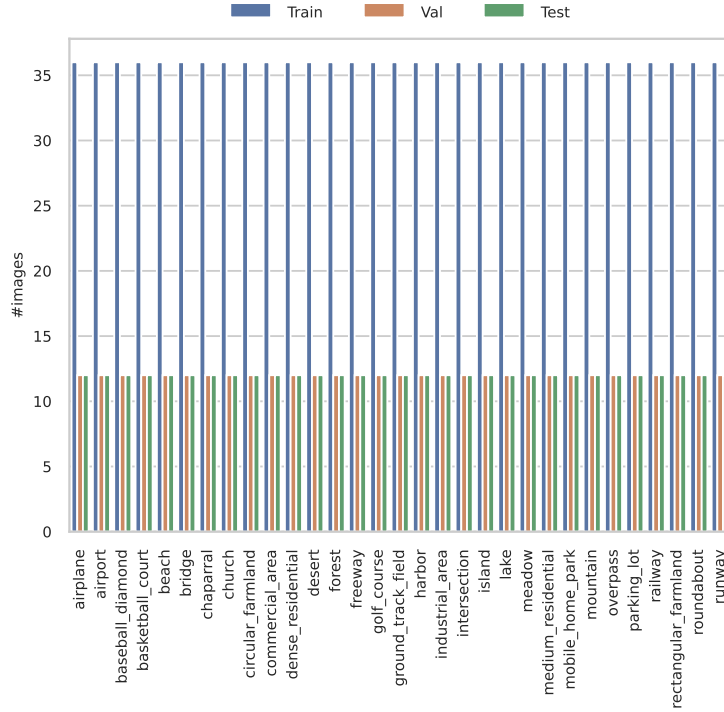


Figure D.41: Class distribution for the Optimal 31 dataset.

Table D.41: Detailed results for pre-trained models on the Optimal 31 dataset.

Model \ Metric	Accuracy	Macro Precision	Weighted Precision	Macro Recall	Weighted Recall	Macro F1 score	Weighted F1 score	Avg. time / epoch (sec.)	Total time (sec.)	Best epoch
AlexNet	80.91	81.90	81.90	80.91	80.91	80.74	80.74	1.10	45	31
VGG16	88.71	89.58	89.58	88.71	88.71	88.79	88.79	2.97	95	22
ResNet50	92.20	92.85	92.85	92.20	92.20	92.25	92.25	2.58	129	40
ResNet152	92.47	92.99	92.99	92.47	92.47	92.47	92.47	4.62	217	37
DenseNet161	94.35	94.92	94.92	94.35	94.35	94.43	94.43	5.02	306	51
EfficientNetB0	91.67	92.04	92.04	91.67	91.67	91.60	91.60	2.25	187	73
ConvNeXt	93.01	93.33	93.33	93.01	93.01	92.99	92.99	3.50	203	48
Vision Transformer	<b>94.62</b>	94.85	94.85	94.62	94.62	94.56	94.56	3.71	126	24
MLP Mixer	92.74	93.17	93.17	92.74	92.74	92.74	92.74	2.82	141	40
Swin Transformer	92.47	92.92	92.92	92.47	92.47	92.51	92.51	9.19	340	27

Table D.42: Detailed results for models trained from scratch on the Optimal 31 dataset.

Model \ Metric	Accuracy	Macro Precision	Weighted Precision	Macro Recall	Weighted Recall	Macro F1 score	Weighted F1 score	Avg. time / epoch (sec.)	Total time (sec.)	Best epoch
AlexNet	55.11	55.61	55.61	55.11	55.11	54.24	54.24	1.23	101	67
VGG16	56.72	58.89	58.89	56.72	56.72	56.58	56.58	4.81	409	70
ResNet50	67.20	69.56	69.56	67.20	67.20	67.17	67.17	2.60	161	47
ResNet152	62.90	64.95	64.95	62.90	62.90	62.78	62.78	5.92	314	38
DenseNet161	<b>71.24</b>	72.01	72.01	71.24	71.24	70.65	70.65	5.16	330	49
EfficientNetB0	68.55	70.59	70.59	68.55	68.55	68.70	68.70	2.36	156	51
ConvNeXt	58.87	60.69	60.69	58.87	58.87	58.92	58.92	3.59	330	77
Vision Transformer	62.63	63.89	63.89	62.63	62.63	62.32	62.32	3.79	235	47
MLP Mixer	59.14	60.36	60.36	59.14	59.14	58.47	58.47	3.26	326	98
Swin Transformer	66.13	67.47	67.47	66.13	66.13	65.62	65.62	9.51	951	89

Table D.43: Per class results for the pre-trained Vision Transformer model on the Optimal 31 dataset.

Label	Precision	Recall	F1 score
airplane	100.00	100.00	100.00
airport	100.00	100.00	100.00
baseball_diamond	92.31	100.00	96.00
basketball_court	100.00	100.00	100.00
beach	100.00	100.00	100.00
bridge	100.00	91.67	95.65
chaparral	100.00	100.00	100.00
church	100.00	91.67	95.65
circular_farmland	92.31	100.00	96.00
commercial_area	85.71	100.00	92.31
dense_residential	84.62	91.67	88.00
desert	100.00	91.67	95.65
forest	91.67	91.67	91.67
freeway	100.00	91.67	95.65
golf_course	91.67	91.67	91.67
ground_track_field	92.31	100.00	96.00
harbor	85.71	100.00	92.31
industrial_area	84.62	91.67	88.00
intersection	100.00	100.00	100.00
island	100.00	100.00	100.00
lake	91.67	91.67	91.67
meadow	83.33	83.33	83.33
medium_residential	88.89	66.67	76.19
mobile_home_park	90.91	83.33	86.96
mountain	100.00	100.00	100.00
overpass	92.31	100.00	96.00
parking_lot	100.00	100.00	100.00
railway	92.31	100.00	96.00
rectangular_farmland	100.00	83.33	90.91
roundabout	100.00	100.00	100.00
runway	100.00	91.67	95.65

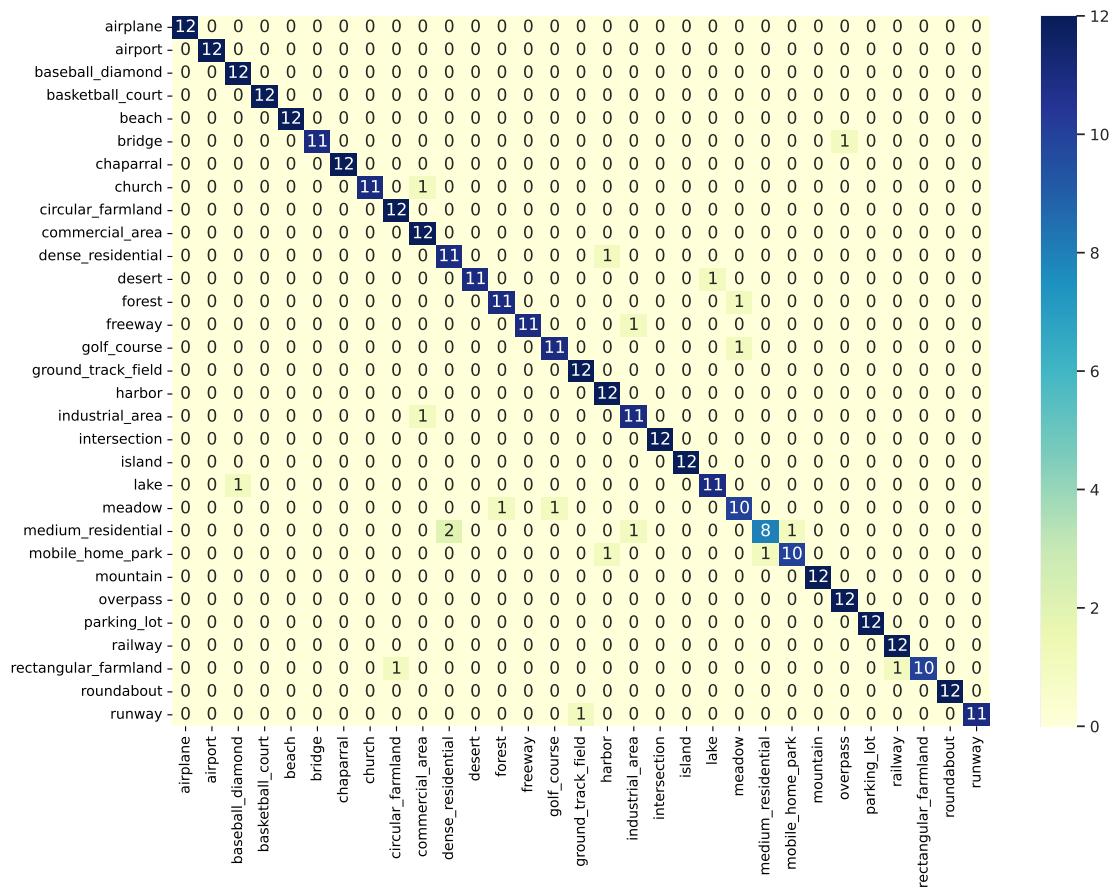


Figure D.42: Confusion matrix for the pre-trained Vision Transformer model on the Optimal 31 dataset.

### D.15 So2Sat

This dataset [53] consists of co-registered synthetic aperture radar and multispectral optical image patches acquired by the Sentinel-1 and Sentinel-2 remote sensing satellites, and the corresponding local climate zones (LCZ) label. So2Sat has a total of 400673 images of size 32x32 pixels organized into 17 classes. Sample images are shown on Figure D.40.

The dataset is distributed over 42 cities across different continents and cultural regions of the world. The classes include: compact high rise, compact middle rise, compact low rise, open high rise, open middle rise, open low rise, lightweight low rise, large low rise, sparsely built, heavy industry, dense trees, scattered trees, bush scrub, low plants, bare rock or paved, bare soil or sand, and water.

The creators of So2Sat have provided different versions for train, test and validation splits for the dataset. The class distribution of the splits is depicted on Figure D.44. We are using Version 2<sup>5</sup> with only Sentinel 2 data. Version 2 provides a training set covering 42 cities around the world, a validation set covering western half of 10 other cities covering 10 cultural zones and a test set containing the eastern half of the 10 other cities.

Detailed results for all pre-trained models are shown on Table D.44 and for all the models learned from scratch are presented on Table D.45. The best performing model is the pre-trained Vision Transformer model. The results on a class level are show on Table D.46 along with a confusion matrix on Figure D.45.

---

<sup>5</sup>available at So2Sat-LCZ42 repo <https://github.com/zhu-xlab/So2Sat-LCZ42>.



Figure D.43: Example images with labels from the So2Sat dataset.

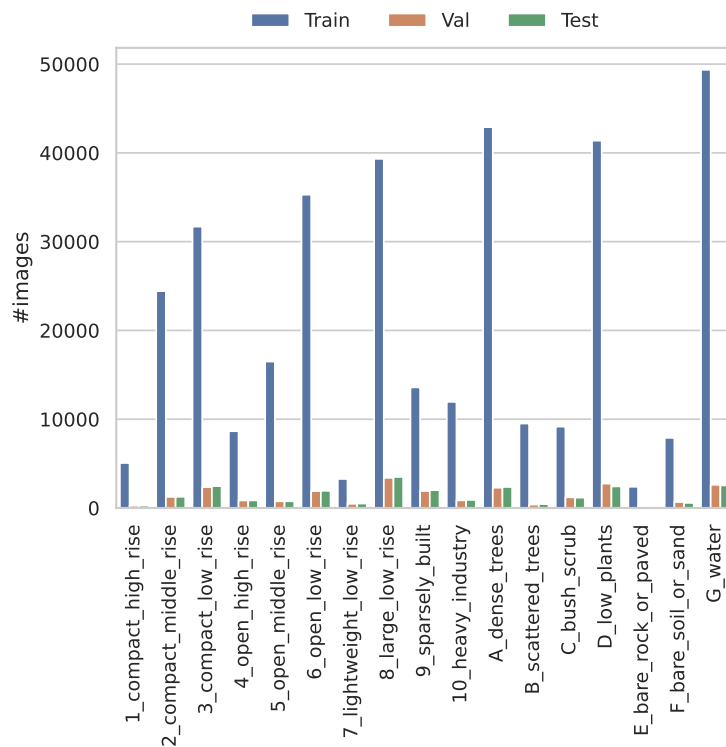


Figure D.44: Class distribution for the So2Sat dataset.

Table D.44: Detailed results for pre-trained models on the So2Sat dataset.

Model \ Metric	Accuracy	Macro Precision	Weighted Precision	Macro Recall	Weighted Recall	Macro F1 score	Weighted F1 score	Avg. time / epoch (sec.)	Total time (sec.)	Best epoch
AlexNet	59.20	46.01	59.31	42.70	59.20	41.57	57.59	158.09	1790	1
VGG16	65.38	57.30	64.34	50.00	65.38	49.64	63.00	716.09	7877	1
ResNet50	61.90	51.01	60.88	48.45	61.90	48.35	60.41	565.55	6221	1
ResNet152	65.17	56.66	64.48	53.42	65.17	52.93	63.75	1,200.64	13207	1
DenseNet161	65.76	55.47	64.58	48.59	65.76	48.67	63.81	1,324.09	14784	1
EfficientNetB0	65.80	56.30	65.64	53.37	65.80	53.65	64.77	510.45	5615	1
ConvNeXt	66.17	59.11	66.87	54.87	66.17	54.71	65.56	853.91	9393	1
Vision Transformer	<b>68.55</b>	62.95	69.64	57.17	68.55	57.26	67.48	925.09	10176	1
MLP Mixer	67.07	63.74	68.25	51.34	67.07	51.94	65.66	643.91	7278	1
Swin Transformer	65.95	59.11	66.82	53.20	65.95	52.89	64.60	2,636.45	29001	1

Table D.45: Detailed results for models trained from scratch on the So2Sat dataset.

Model \ Metric	Accuracy	Macro Precision	Weighted Precision	Macro Recall	Weighted Recall	Macro F1 score	Weighted F1 score	Avg. time / epoch (sec.)	Total time (sec.)	Best epoch
AlexNet	56.51	41.86	54.97	40.70	56.51	39.72	54.65	174.74	3320	4
VGG16	62.27	51.36	61.08	45.40	62.27	45.54	59.78	723.72	13027	3
ResNet50	59.59	46.54	59.35	43.94	59.59	43.37	58.18	558.79	10617	4
ResNet152	61.48	49.43	62.30	48.71	61.48	46.98	60.22	1,198.37	22769	4
DenseNet161	55.43	48.87	60.98	42.53	55.43	40.76	54.11	1,325.67	23862	3
EfficientNetB0	<b>65.17</b>	53.75	64.00	50.34	65.17	50.36	63.88	499.21	11981	9
ConvNeXt	60.15	50.97	61.52	48.03	60.15	47.17	59.73	851.06	15319	3
Vision Transformer	55.33	43.56	55.31	37.42	55.33	37.01	52.20	926.50	14824	1
MLP Mixer	53.58	42.31	53.80	36.73	53.58	36.61	51.19	651.31	10421	1
Swin Transformer	57.13	47.93	56.48	36.29	57.13	35.29	52.28	2,631.44	42103	1

Table D.46: Per class results for the pre-trained ViT model on the So2Sat dataset.

Label	Precision	Recall	F1 score
Compact high_rise	62.37	21.80	32.31
Compact middle_rise	70.74	61.49	65.79
Compact low_rise	68.52	75.33	71.77
Open high_rise	76.54	59.39	66.89
Open middle_rise	56.12	59.50	57.76
Open low_rise	47.29	64.36	54.52
Lightweight low_rise	57.14	39.76	46.89
Large low_rise	87.11	84.87	85.98
Sparsely built	67.30	45.80	54.51
Heavy industry	39.39	69.49	50.28
Dense trees	97.11	73.86	83.91
Scattered trees	26.16	55.89	35.64
Bush or scrub	15.22	1.80	3.22
Low plants	60.68	90.55	72.66
Bare rock or paved	79.38	37.56	50.99
Bare soil or sand	62.05	32.87	42.97
Water	97.10	97.60	97.35

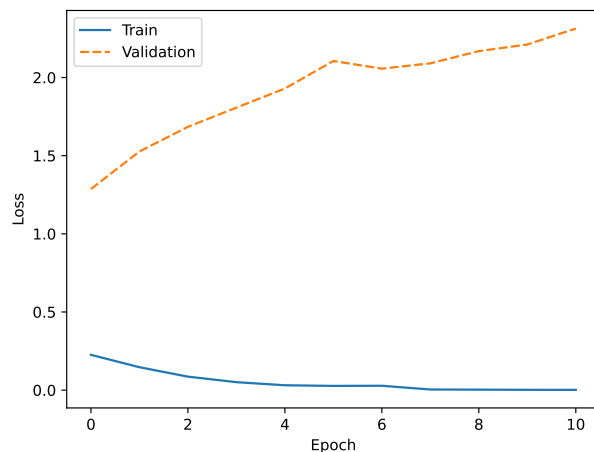


Figure D.46: Train and validation learning curves showing an over-fit of a ViT model on the So2Sat dataset.

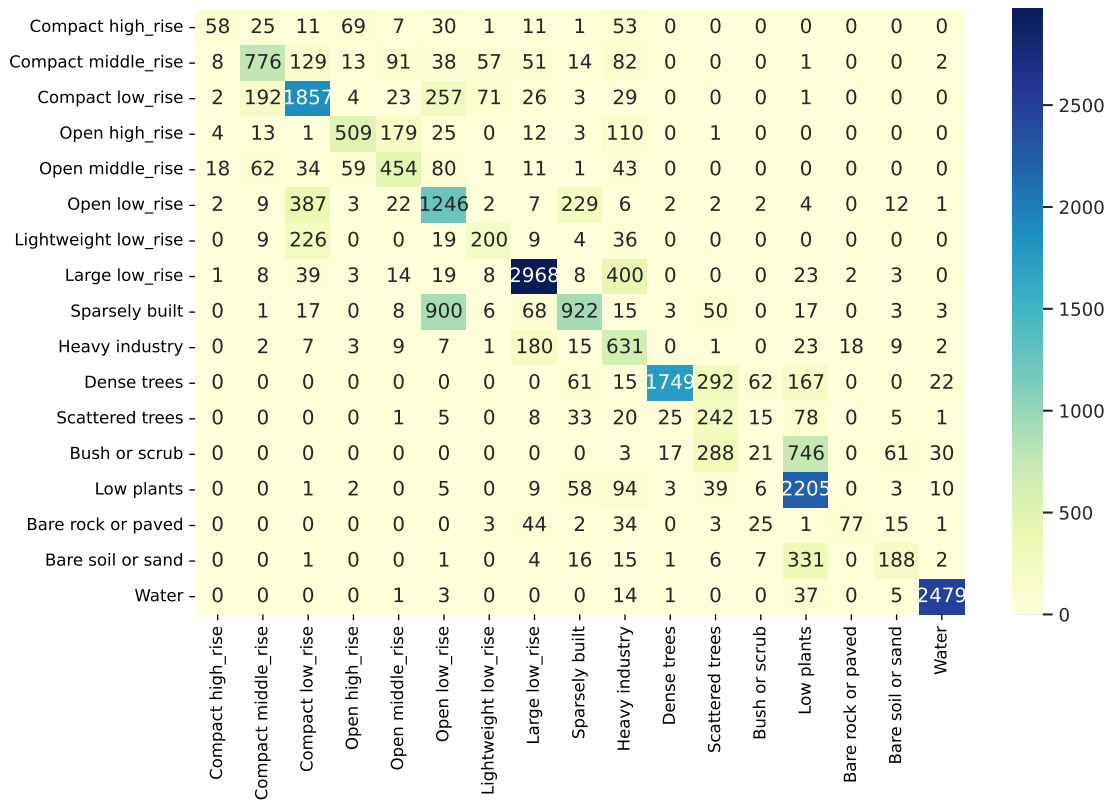


Figure D.45: Confusion matrix for the pre-trained Vision Transformer model on the So2Sat dataset.

D.16 UC Merced multi-label

The UC Merced dataset was extended in [54] for multi-label classification. The dataset still has the same number of 2100 images of 256x256 pixels size (Figure D.47). The difference is in the number of classes (labels) and the number of annotations (classes) an image belongs to. Each image in the dataset has been manually labeled with one or more (maximum seven) labels based on visual inspection in order to create the ground truth data (the multilabels are available at <http://bigearth.eu/datasets>). The total number of distinct class labels in the dataset is 17. The labels are: airplane, bare-soil, buildings, cars, chaparral, court, dock, field, grass, mobile-home, pavement, sand, sea, ship, tanks, trees, water. The average number of labels per image is 3.3. This dataset has no predefined train-test splits by the authors. For our study, we made appropriate splits and their distribution is presented on Figure D.48.

Detailed results for all pre-trained models are shown on Table D.47 and for all the models learned from scratch are presented on Table D.48. The best performing model is the pre-trained Swin Transformer model. The results on a class level are show on Table D.49 along with a confusion matrix on Figure D.49.



Figure D.47: Example images with labels from the UC Merced multi-label dataset.

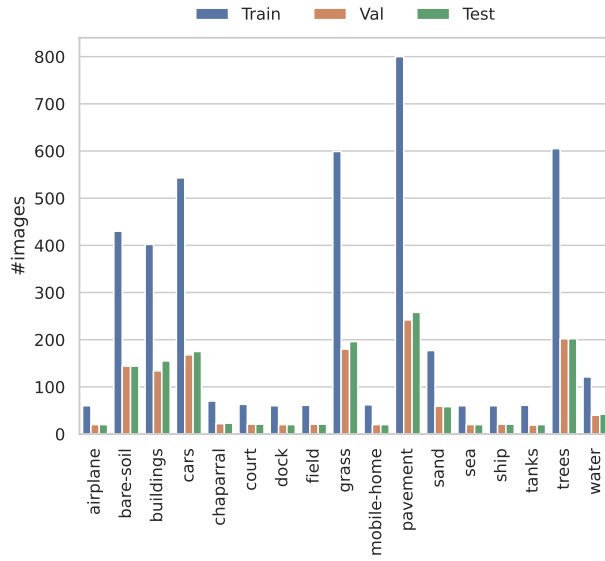


Figure D.48: Label distribution for the UC Merced multi-label dataset.

Table D.47: Detailed results for pre-trained models on the UC Merced multi-label dataset.

	mAP	Micro Precision	Macro Precision	Weighted Precision	Micro Recall	Macro Recall	Weighted Recall	Micro F1 score	Macro F1 score	Weighted F1 score	Avg. time / epoch (sec.)	Total time (sec.)	Best epoch
AlexNet	92.64	82.78	88.47	83.14	86.23	86.07	86.23	84.47	86.91	84.52	1.31	71	44
VGG16	92.85	86.43	91.38	86.61	86.37	87.84	86.37	86.40	89.33	86.39	3.30	132	30
ResNet50	95.66	86.19	92.37	86.53	87.71	88.84	87.71	86.94	90.23	86.95	2.76	124	35
ResNet152	96.01	88.10	93.19	88.33	86.23	89.45	86.23	87.15	91.07	87.13	5.04	227	35
DenseNet161	96.06	88.82	93.99	88.90	87.01	89.69	87.01	87.91	91.51	87.76	5.64	468	73
EfficientNetB0	95.38	87.98	93.22	88.23	87.36	89.19	87.36	87.67	90.92	87.65	2.54	254	98
ConvNeXt	96.43	88.80	94.30	88.91	87.92	89.92	87.92	88.36	91.84	88.32	3.92	259	56
Vision Transformer	96.70	88.87	94.16	89.09	89.62	90.55	89.62	89.24	92.14	89.16	4.13	132	22
MLP Mixer	96.34	88.62	94.38	88.75	87.99	88.16	87.99	88.31	90.77	88.21	3.25	182	46
Swin Transformer	<b>96.83</b>	89.01	93.75	89.08	89.19	91.50	89.19	89.10	92.46	89.06	10.22	552	44

Table D.48: Detailed results for models trained from scratch on the UC Merced multi-label dataset.

	mAP	Micro Precision	Macro Precision	Weighted Precision	Micro Recall	Macro Recall	Weighted Recall	Micro F1 score	Macro F1 score	Weighted F1 score	Avg. time / epoch (sec.)	Total time (sec.)	Best epoch
AlexNet	75.52	72.54	67.64	70.50	73.87	63.95	73.87	73.20	64.95	71.73	1.03	103	91
VGG16	76.80	74.33	72.59	73.65	78.53	70.75	78.53	76.37	71.14	75.77	3.24	324	99
ResNet50	79.87	76.72	77.52	76.42	78.67	71.21	78.67	77.68	72.73	76.99	2.76	276	99
ResNet152	73.66	76.89	69.85	74.78	73.80	65.05	73.80	75.32	66.81	73.92	5.06	506	86
DenseNet161	85.41	81.30	84.62	81.61	79.52	76.19	79.52	80.40	79.63	80.26	5.60	487	72
EfficientNetB0	79.87	78.45	74.10	76.91	75.85	72.13	75.85	77.13	72.89	76.25	2.23	252	99
ConvNeXt	72.27	72.40	69.27	71.19	74.65	62.31	74.65	73.50	63.50	71.89	3.81	381	100
Vision Transformer	<b>87.14</b>	81.02	85.66	81.10	79.31	75.95	79.31	80.16	79.29	79.69	4.12	412	95
MLP Mixer	75.68	75.29	73.64	74.60	73.38	64.54	73.38	74.32	67.44	73.43	3.11	311	99
Swin Transformer	81.07	76.88	75.54	76.02	79.38	72.02	79.38	78.11	72.50	77.27	10.12	1012	99

Table D.49: Per label results for the pre-trained Swin Transformer model on the UC Merced multi-label dataset.

Label	Precision	Recall	F1 score
airplane	95.24	100.00	97.56
bare-soil	83.45	80.56	81.98
buildings	88.31	87.74	88.03
cars	85.89	80.00	82.84
chaparral	100.00	100.00	100.00
court	100.00	76.19	86.49
dock	100.00	100.00	100.00
field	100.00	95.24	97.56
grass	86.21	89.29	87.72
mobile-home	94.44	85.00	89.47
pavement	88.24	93.02	90.57
sand	83.08	93.10	87.80
sea	100.00	100.00	100.00
ship	100.00	95.24	97.56
tanks	100.00	90.00	94.74
trees	91.22	92.57	91.89
water	97.62	97.62	97.62

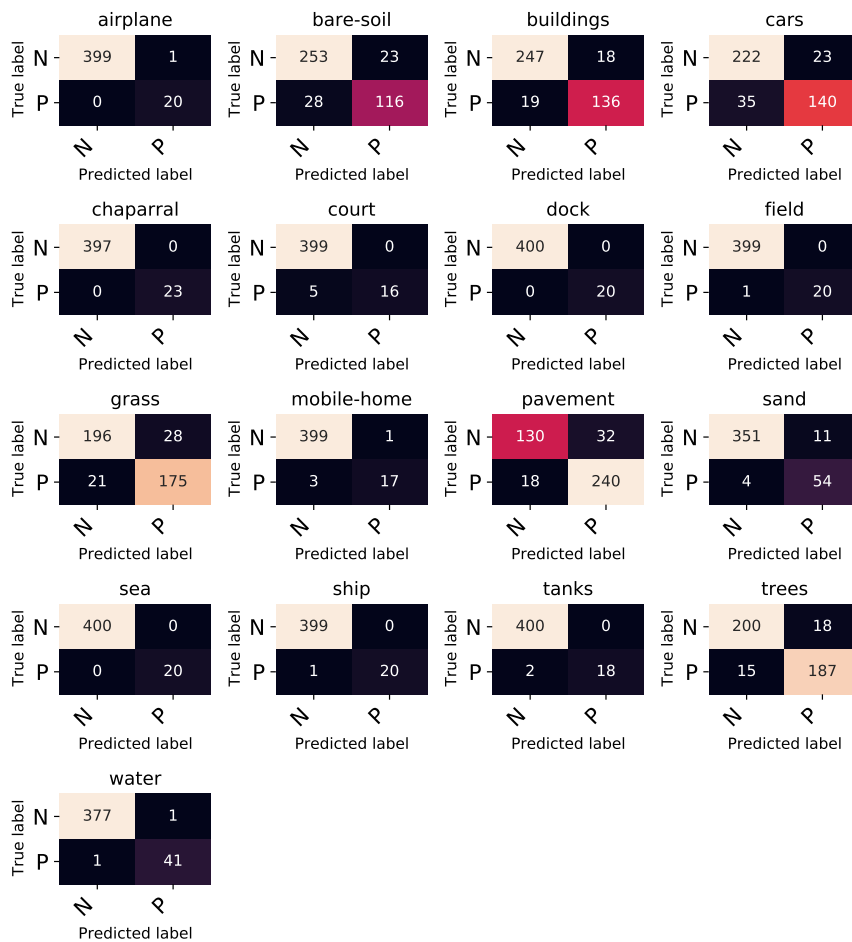


Figure D.49: Confusion matrix for the pre-trained Swin Transformer model on the UC Merced multi-label dataset.

#### D.17 *BigEarthNet*

BigEarthNet is a new large-scale multi-label Sentinel-2 benchmark archive [59] [36]. The BigEarthNet consists of 590326 Sentinel-2 image patches, each of which is a section of: 120x120 pixels for 10m bands; 60x60 pixels for 20m bands; and 20x20 pixels for 60m bands. Each image patch is annotated by multiple land-cover classes (i.e., multi-labels) that are provided from the CORINE Land Cover database. It was constructed by selecting 125 Sentinel-2 tiles acquired between June 2017 and May 2018. Covering different countries and seasonal period. More precisely, the number of images acquired in autumn, winter, spring and summer seasons are 154943, 117156, 189276 and 128951 respectively. The image patches are geographically distributed across 10 countries (Austria, Belgium, Finland, Ireland, Kosovo, Lithuania, Luxembourg, Portugal, Serbia, Switzerland) of Europe. The images are stored in tiff format and accompanied with additional metadata in JSON format.

The authors provide a predefined set of train-validation-test splits. Additionally, they proposed 2 versions of the labels in the dataset.

The first version of the dataset contains 43 labels with an 3.0 labels per image (Figure D.51). The labels in this version are: Continuous urban fabric, Discontinuous urban fabric, Industrial or commercial units, Road and rail networks and associated land, Port areas, Airports, Mineral extraction sites, Dump sites, Construction sites, Green urban areas, Sport and leisure facilities, Non-irrigated arable land, Permanently irrigated land, Rice fields, Vineyards, Fruit trees and berry plantations, Olive groves, Pastures, Annual crops associated with permanent crops, Complex cultivation patterns, Land principally occupied by agriculture, with significant areas of natural vegetation, Agro-forestry areas, Broad-leaved forest, Coniferous forest, Mixed forest, Natural grassland, Moors and heathland, Sclerophyllous vegetation, Transitional woodland/shrub, Beaches, dunes, sands, Bare rock, Sparsely vegetated areas, Burnt areas, Inland marshes, Peatbogs, Salt marshes, Salines, Intertidal flats, Water courses, Water bodies, Coastal lagoons, Estuaries, Sea and ocean. The largest class (label), Mixed forest, appeared in 217119 image, whereas the label with fewest appearances, Burnt areas, appeared in 328 images. This high imbalance should make the dataset more challenging.

Detailed results for all pre-trained models are shown on Table D.50 and for all the models learned from scratch are presented on Table D.51. The best performing model is the pre-trained

Swin Transformer model. The results on a class level are show on Table D.52 along with a confusion matrix on Figure D.52.

The second version of the dataset contains 19 labels with 2.9 labels per image on average (Figure D.53). The labels contained here are: Urban fabric, Industrial or commercial units, Arable land, Permanent crops, Pastures, Complex cultivation patterns, Land principally occupied by agriculture, with significant areas of natural vegetation, Agro-forestry areas, Broad-leaved forest, Coniferous forest, Mixed forest, Natural grassland and sparsely vegetated areas, Moors, heathland and sclerophyllous vegetation, Transitional woodland, shrub, Beaches, dunes, sands, Inland wetlands, Coastal wetlands, Inland waters, Marine waters. The label Mixed forest is most commonly found and is present in 176546 images, whereas Beaches, dunes, sands appears in 1536 images and is the least frequently used label. Sample images are shown on Figure D.50.

Detailed results for all pre-trained models are shown on Table D.53 and for all the models learned from scratch are presented on Table D.54. The best performing model is the pre-trained Swin Transformer model. The results on a class level are show on Table D.55 along with a confusion matrix on Figure D.54.

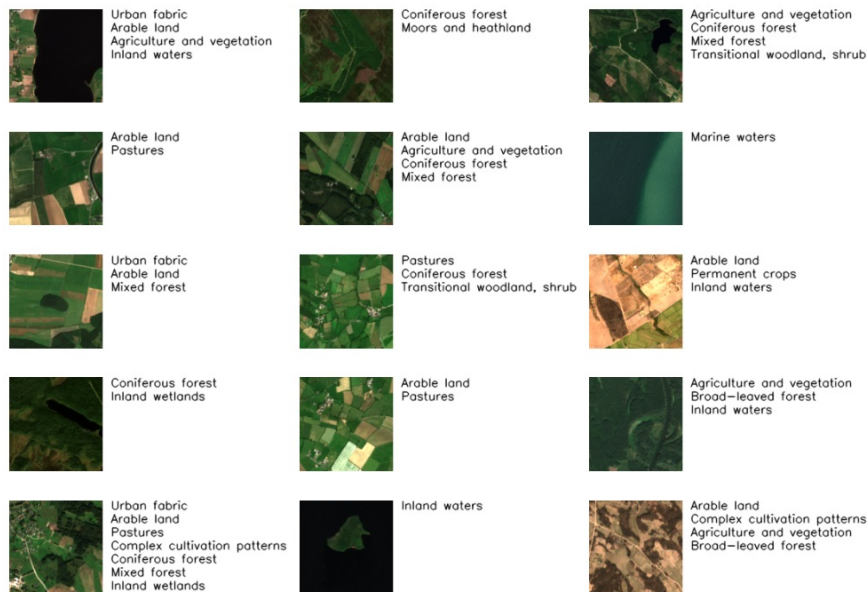


Figure D.50: Example images with labels from the BigEarthNet dataset.

D.17.1 BigEarthNet 43

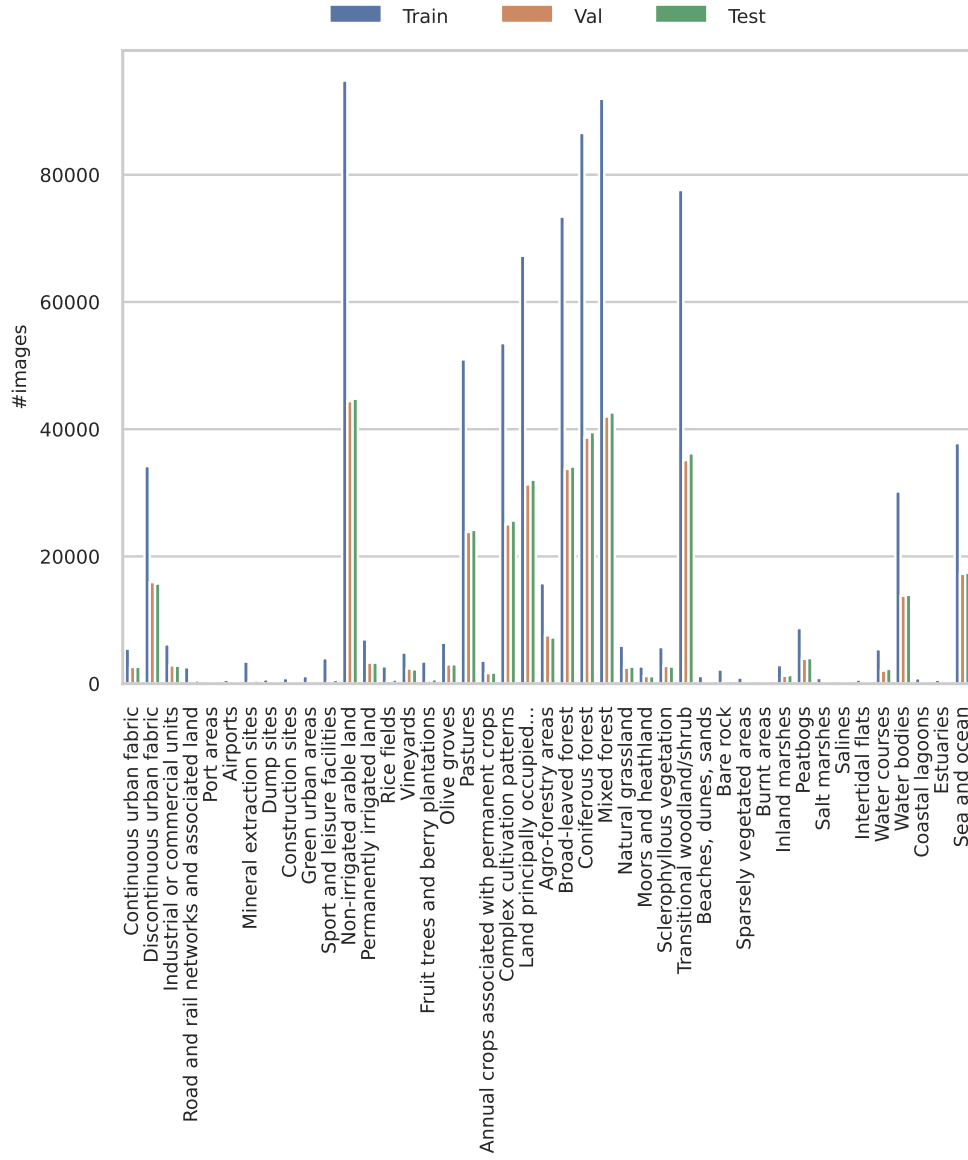


Figure D.51: Label distribution for the BigEarthNet 43 dataset.

Table D.50: Detailed results for pre-trained models on the BigEarthNet 43 dataset.

	mAP	Micro Precision	Macro Precision	Weighted Precision	Micro Recall	Macro Recall	Weighted Recall	Micro F1 score	Macro F1 score	Weighted F1 score	Avg. time / epoch (sec.)	Total time (sec.)	Best epoch
AlexNet	58.55	80.15	61.88	79.67	72.14	51.99	72.14	75.93	55.62	75.48	89.85	7188	70
VGG16	61.21	80.71	64.71	80.29	72.74	53.97	72.74	76.52	57.74	76.08	542.30	12473	13
ResNet50	66.26	81.99	67.47	81.64	74.14	58.15	74.14	77.87	61.87	77.54	414.18	9112	12
ResNet152	64.07	82.17	70.42	81.73	72.08	52.11	72.08	76.80	58.27	76.17	881.69	14107	6
DenseNet161	64.23	81.87	68.31	81.39	72.63	53.58	72.63	76.97	58.80	76.48	969.67	14545	5
EfficientNetB0	64.59	82.14	70.17	81.75	73.37	53.93	73.37	77.51	59.71	77.08	365.40	7308	10
ConvNeXt	66.17	81.67	69.24	81.31	73.93	56.11	73.93	77.61	61.12	77.23	642.81	10285	6
Vision Transformer	59.00	79.77	65.42	79.39	71.39	48.98	71.39	75.35	54.65	74.81	702.00	14742	11
MLP Mixer	59.65	81.18	67.47	80.55	71.30	48.85	71.30	75.92	54.95	75.28	492.84	12321	15
Swin Transformer	<b>67.73</b>	82.43	72.36	82.12	74.18	58.08	74.18	78.09	62.78	77.75	2,016.00	34272	7

Table D.51: Detailed results for models trained from scratch on the BigEarthNet 43 dataset.

	mAP	Micro Precision	Macro Precision	Weighted Precision	Micro Recall	Macro Recall	Weighted Recall	Micro F1 score	Macro F1 score	Weighted F1 score	Avg. time / epoch (sec.)	Total time (sec.)	Best epoch
AlexNet	56.08	79.15	58.19	78.68	71.41	50.79	71.41	75.08	53.54	74.65	84.18	5051	45
VGG16	58.97	80.56	64.94	80.13	71.99	48.02	71.99	76.03	53.38	75.49	544.28	15784	14
ResNet50	64.34	82.07	67.06	81.65	73.47	55.64	73.47	77.53	60.14	77.12	409.87	18854	31
ResNet152	62.74	80.72	66.55	80.30	72.96	53.88	72.96	76.64	58.59	76.12	878.00	32486	22
DenseNet161	63.39	82.20	66.27	81.74	71.83	53.84	71.83	76.67	58.40	76.00	982.63	29479	15
EfficientNetB0	62.17	81.25	66.61	80.90	73.01	52.02	73.01	76.91	56.94	76.48	364.13	11288	16
ConvNeXt	60.47	80.71	67.02	80.19	72.40	51.09	72.40	76.33	56.51	75.81	645.51	26466	26
Vision Transformer	57.41	79.12	63.50	78.74	71.20	47.96	71.20	74.95	52.94	74.31	709.86	20586	14
MLP Mixer	58.77	80.82	65.97	80.10	71.12	48.10	71.12	75.66	53.38	74.90	500.77	15524	16
Swin Transformer	<b>67.49</b>	81.91	68.28	81.62	75.50	59.70	75.50	78.58	63.02	78.29	2,031.64	113772	41

Table D.52: Per label results for the pre-trained Swin Transformer model on the BigEarthNet 43 dataset.

Label	Precision	Recall	F1 score
Continuous urban fabric	85.67	79.44	82.44
Discontinuous urban fabric	83.49	70.72	76.57
Industrial or commercial units	77.21	41.13	53.67
Road and rail networks and associated land	47.17	50.59	48.82
Port areas	63.33	47.50	54.29
Airports	93.18	29.93	45.30
Mineral extraction sites	47.00	47.49	47.24
Dump sites	42.22	22.89	29.69
Construction sites	51.85	35.22	41.95
Green urban areas	51.18	37.24	43.11
Sport and leisure facilities	52.11	40.89	45.83
Non-irrigated arable land	88.42	82.99	85.62
Permanently irrigated land	82.30	53.94	65.17
Rice fields	71.38	58.99	64.59
Vineyards	70.33	53.73	60.92
Fruit trees and berry plantations	54.12	49.57	51.75
Olive groves	72.01	54.77	62.22
Pastures	79.66	75.73	77.65
Annual crops associated with permanent crops	60.34	40.11	48.19
Complex cultivation patterns	76.87	66.05	71.05
Land principally occupied by agriculture, with significant areas of natural vegetation	75.21	61.09	67.42
Agro-forestry areas	86.27	74.22	79.79
Broad-leaved forest	83.35	72.94	77.79
Coniferous forest	88.73	84.79	86.72
Mixed forest	81.94	84.25	83.08
Natural grassland	69.90	48.79	57.46
Moors and heathland	64.58	40.24	49.58
Sclerophyllous vegetation	75.64	71.15	73.33
Transitional woodland/shrub	73.16	64.26	68.42
Beaches, dunes, sands	58.87	61.54	60.18
Bare rock	58.41	75.90	66.01
Sparsely vegetated areas	45.88	53.94	49.58
Burnt areas	100.00	2.78	5.41
Inland marshes	67.74	31.21	42.73
Peatbogs	81.07	62.30	70.45
Salt marshes	60.62	60.62	60.62
Salines	80.00	57.14	66.67
Intertidal flats	70.73	52.10	60.00
Water courses	82.71	71.71	76.82
Water bodies	91.33	77.54	83.87
Coastal lagoons	88.16	81.56	84.73
Estuaries	78.32	70.52	74.21
Sea and ocean	99.20	97.77	98.48



D.17.2 BigEarthNet 19

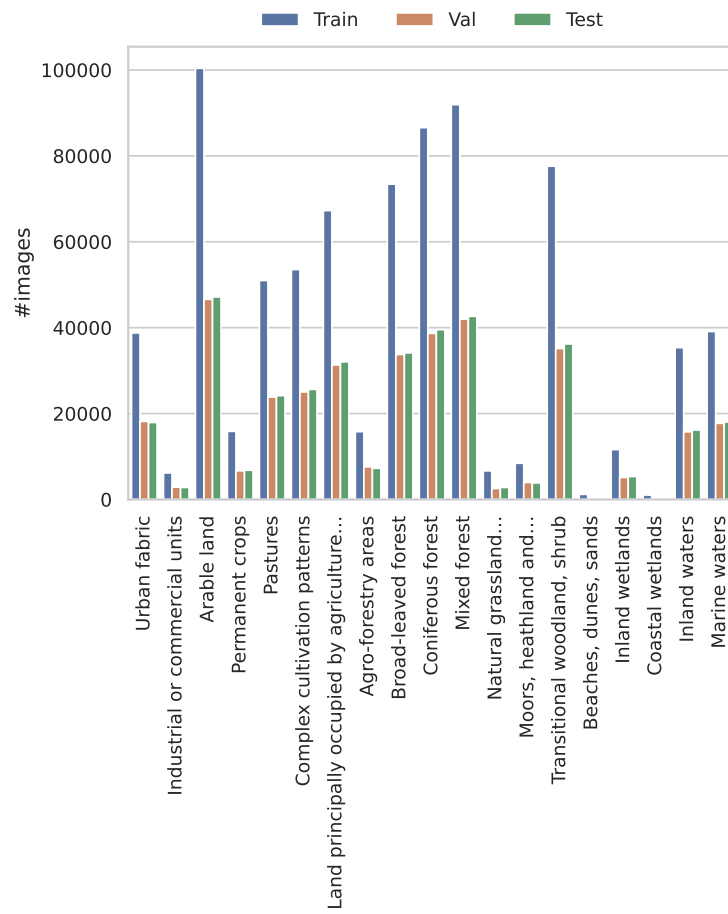


Figure D.53: Label distribution for the BigEarthNet 19 dataset.

Table D.53: Detailed results for pre-trained models on the BigEarthNet 19 dataset.

	mAP	Micro Precision	Macro Precision	Weighted Precision	Micro Recall	Macro Recall	Weighted Recall	Micro F1 score	Macro F1 score	Weighted F1 score	Avg. time / epoch (sec.)	Total time (sec.)	Best epoch
AlexNet	77.15	80.90	75.60	80.58	73.59	66.06	73.59	77.07	70.04	76.77	90.43	5245	48
VGG16	78.42	81.33	77.61	81.02	73.92	66.27	73.92	77.45	70.92	77.11	537.90	10758	10
ResNet50	79.98	82.65	78.57	82.37	73.62	67.74	73.62	77.88	72.12	77.51	413.24	7025	7
ResNet152	79.78	82.58	80.36	82.43	73.95	66.57	73.95	78.03	71.79	77.57	874.56	13993	6
DenseNet161	79.69	81.92	78.55	81.83	74.42	66.99	74.42	77.99	71.61	77.72	976.93	14654	5
EfficientNetB0	80.22	82.87	80.56	82.61	74.36	66.32	74.36	78.38	72.14	78.09	366.35	6228	7
ConvNeXt	80.28	80.95	78.78	80.99	76.72	68.71	76.72	78.78	72.66	78.62	631.67	9475	5
Vision Transformer	77.31	82.31	76.93	81.85	70.99	64.08	70.99	76.23	69.18	75.70	698.50	15367	12
MLP Mixer	77.29	81.41	78.12	80.97	73.20	64.33	73.20	77.09	69.68	76.62	488.68	12217	15
Swin Transformer	<b>81.38</b>	82.19	77.29	82.03	76.51	71.44	76.51	79.25	73.89	79.06	1,990.00	35820	8

Table D.54: Detailed results for models trained from scratch on the BigEarthNet 19 dataset.

	mAP	Micro Precision	Macro Precision	Weighted Precision	Micro Recall	Macro Recall	Weighted Recall	Micro F1 score	Macro F1 score	Weighted F1 score	Avg. time / epoch (sec.)	Total time (sec.)	Best epoch
AlexNet	75.71	80.27	74.63	79.88	72.73	64.83	72.73	76.31	68.89	75.96	86.78	5120	44
VGG16	77.99	80.45	75.61	80.21	74.91	67.63	74.91	77.58	70.90	77.28	542.24	18436	19
ResNet50	78.73	82.94	78.20	82.44	72.61	66.15	72.61	77.44	71.28	76.99	413.89	26489	49
ResNet152	78.52	81.06	75.86	81.02	74.69	68.18	74.69	77.74	71.34	77.55	875.20	43760	35
DenseNet161	79.73	82.24	77.81	82.05	74.77	67.99	74.77	78.33	71.98	78.08	975.34	31211	17
EfficientNetB0	79.21	82.25	78.89	82.02	74.68	66.53	74.68	78.28	71.65	78.01	359.16	11493	17
ConvNeXt	77.91	81.39	78.16	81.18	73.57	64.64	73.57	77.29	70.08	76.95	643.66	24459	23
Vision Transformer	75.87	80.48	75.45	80.14	71.36	63.85	71.36	75.65	68.59	75.23	702.53	21076	15
MLP Mixer	77.01	81.39	77.37	81.12	72.59	64.34	72.59	76.74	69.74	76.42	495.88	15868	17
Swin Transformer	<b>80.59</b>	83.12	80.38	82.76	74.60	66.96	74.60	78.63	72.35	78.22	2,011.29	96542	33

Table D.55: Per label results for the pre-trained Swin Transformer model on the BigEarthNet 19 dataset.

Label	Precision	Recall	F1 score
Urban fabric	82.21	76.09	79.03
Industrial or commercial units	65.47	53.81	59.07
Arable land	88.07	84.53	86.26
Permanent crops	80.24	61.39	69.56
Pastures	82.29	72.91	77.32
Complex cultivation patterns	77.35	66.05	71.25
Land principally occupied by agriculture, with significant areas of natural vegetation	72.72	64.01	68.08
Agro-forestry areas	83.00	80.58	81.77
Broad-leaved forest	82.55	74.08	78.08
Coniferous forest	88.52	85.04	86.74
Mixed forest	80.71	85.67	83.12
Natural grassland and sparsely vegetated areas	72.20	47.05	56.98
Moors, heathland and sclerophyllous vegetation	69.63	69.45	69.54
Transitional woodland, shrub	71.88	66.79	69.24
Beaches, dunes, sands	49.82	63.35	55.78
Inland wetlands	76.50	59.39	66.87
Coastal wetlands	55.81	69.68	61.98
Inland waters	90.53	79.30	84.55
Marine waters	99.10	98.15	98.62



Figure D.54: Confusion matrix for the pre-trained Swin Transformer model on the BigEarthNet 19 dataset.

D.18 MLRSNet

MLRSNet [55] is a multi-label high spatial resolution remote sensing dataset for semantic scene understanding. It is composed of high-resolution optical satellite or aerial RGB images. MLRSNet contains a total of 109161 images (Figure D.55) within 46 scene categories, and each image has at least one of 60 predefined labels. The number of labels associated with each image varies between 1 and 13, but averages at 5.0 labels per image (Figure D.56). The labels annotating the images are: airplane, airport, bare soil, baseball diamond, basketball court, beach, bridge, buildings, cars, cloud, containers, crosswalk, dense residential area, desert, dock, factory, field, football field, forest, freeway, golf course, grass, greenhouse, gully, harbor, intersection, island, lake, mobile home, mountain, overpass, park, parking lot, parkway, pavement, railway, railway station, river, road, roundabout, runway, sand, sea, ships, snow, snowberg, sparse residential area, stadium, swimming pool, tanks, tennis court, terrace, track, trail, transmission tower, trees, water, chaparral, wetland, wind turbine. The dataset does not have predefined train-tests splits.

Detailed results for all pre-trained models are shown on Table D.56 and for all the models learned from scratch are presented on Table D.57. The best performing model is the pre-trained Swin Transformer model. The results on a class level are show on Table D.58 along with a confusion matrix on Figure D.57.

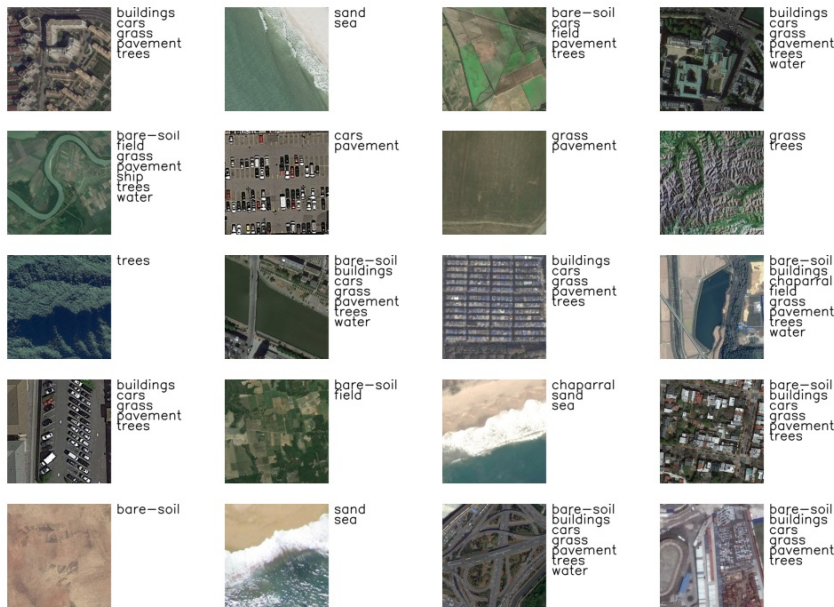


Figure D.55: Example images with labels from the MLRSNet dataset.

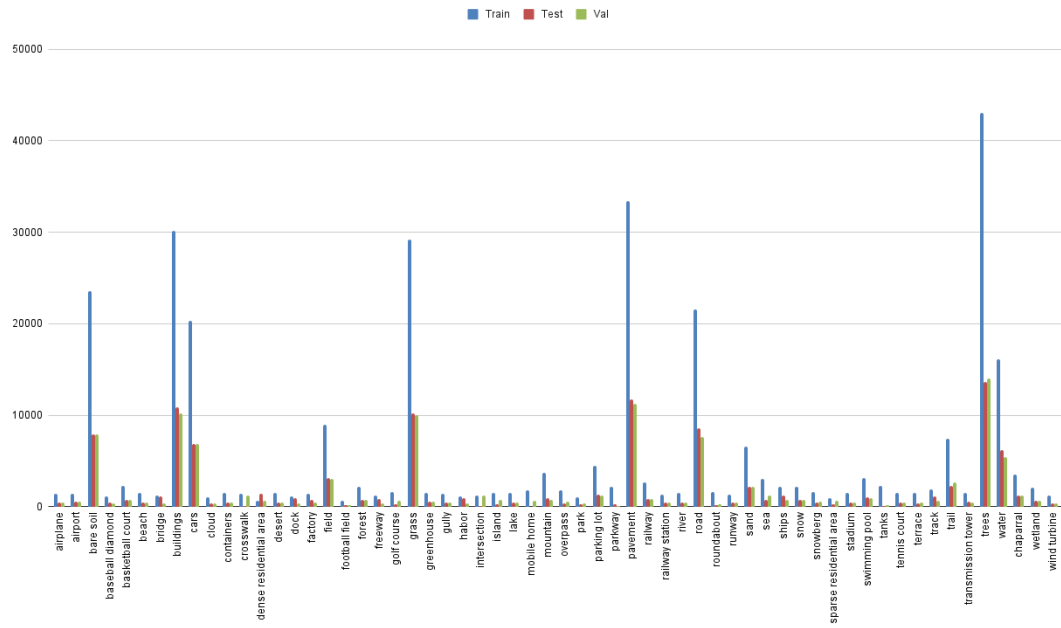


Figure D.56: Label distribution for the MLRSNet dataset.

Table D.56: Detailed results for pre-trained models on the MLRSNet dataset.

	mAP	Micro Precision	Macro Precision	Weighted Precision	Micro Recall	Macro Recall	Weighted Recall	Micro F1 score	Macro F1 score	Weighted F1 score	Avg. time / epoch (sec.)	Total time (sec.)	Best epoch
AlexNet	93.40	87.93	87.37	88.15	88.54	88.95	88.54	88.24	87.73	88.25	34.09	1125	23
VGG16	94.63	89.56	89.05	89.73	89.39	90.06	89.39	89.48	89.18	89.48	132.24	3306	15
ResNet50	96.27	91.33	92.54	91.38	90.72	91.79	90.72	91.03	92.00	91.00	101.67	1726	16
ResNet152	96.43	91.83	92.51	91.84	90.74	92.27	90.74	91.28	92.26	91.25	214.11	5781	17
DenseNet161	96.31	91.61	92.35	91.63	90.85	92.18	90.85	91.23	92.07	91.21	237.35	6171	16
EfficientNetB0	95.39	91.35	91.63	91.37	90.09	90.52	90.09	90.71	90.84	90.67	86.80	2604	20
ConvNeXt	95.81	91.04	90.71	91.12	90.60	91.90	90.60	90.82	91.10	90.81	155.65	3580	13
Vision Transformer	96.41	91.81	91.89	91.84	91.75	93.16	91.75	91.78	92.33	91.77	170.90	3589	11
MLP Mixer	95.05	90.77	91.21	90.83	89.14	89.23	89.14	89.95	89.86	89.88	121.38	1942	6
Swin Transformer	<b>96.62</b>	91.74	91.91	91.83	92.13	93.65	92.13	91.93	92.60	91.95	496.72	12418	15

Table D.57: Detailed results for models trained from scratch on the MLRSNet dataset.

	mAP	Micro Precision	Macro Precision	Weighted Precision	Micro Recall	Macro Recall	Weighted Recall	Micro F1 score	Macro F1 score	Weighted F1 score	Avg. time / epoch (sec.)	Total time (sec.)	Best epoch
AlexNet	90.85	86.53	83.69	86.69	86.58	86.54	86.58	86.56	84.70	86.58	34.92	2549	58
VGG16	91.52	86.63	83.24	87.00	87.98	88.23	87.98	87.30	85.33	87.41	132.22	7272	40
ResNet50	<b>95.26</b>	90.65	90.76	90.68	89.42	90.33	89.42	90.03	90.37	90.00	102.26	6238	46
ResNet152	93.98	89.47	88.92	89.54	88.45	88.55	88.45	88.96	88.51	88.92	214.47	14155	51
DenseNet161	94.74	90.23	89.59	90.23	88.13	88.86	88.13	89.17	88.87	89.08	237.96	11422	33
EfficientNetB0	94.40	89.90	89.09	89.99	89.22	90.19	89.22	89.56	89.40	89.54	89.34	8934	87
ConvNeXt	90.71	87.86	84.80	88.00	85.38	84.73	85.38	86.60	84.36	86.60	159.35	5896	22
Vision Transformer	87.25	85.78	82.28	85.81	84.64	80.90	84.64	85.20	81.06	85.03	170.71	5975	20
MLP Mixer	85.28	84.45	82.59	84.45	82.19	75.60	82.19	83.31	78.11	83.01	123.20	3080	10
Swin Transformer	94.10	89.56	88.56	89.65	89.93	90.17	89.93	89.74	89.11	89.73	482.72	42962	74

Table D.58: Per label results for the pre-trained Swin Transformer model on the MLRSNet dataset.

Label	Precision	Recall	F1 score	Label	Precision	Recall	F1 score
airplane	87.84	92.21	89.97	overpass	93.96	95.99	94.96
airport	87.75	85.71	86.72	park	89.51	93.00	91.22
bare soil	83.04	85.55	84.28	parking lot	70.80	67.36	69.04
baseball diamond	99.59	99.39	99.49	parkway	89.33	91.50	90.40
basketball court	89.43	91.95	90.67	pavement	96.49	96.37	96.43
beach	99.80	99.80	99.80	railway	90.95	95.91	93.36
bridge	95.34	93.80	94.57	railway station	91.44	85.58	88.42
buildings	93.94	91.66	92.78	river	98.01	98.80	98.40
cars	85.20	91.03	88.02	road	92.32	91.71	92.01
cloud	98.63	100.00	99.31	roundabout	95.24	98.52	96.85
containers	99.40	100.00	99.70	runway	99.26	88.50	93.57
crosswalk	77.32	72.12	74.63	sand	98.37	98.68	98.53
dense residential area	99.49	97.55	98.51	sea	98.68	99.73	99.20
desert	97.88	100.00	98.93	ships	89.30	88.80	89.05
dock	99.03	99.24	99.14	snow	96.00	90.88	93.37
factory	91.58	84.47	87.89	snowberg	89.05	98.21	93.40
field	92.62	92.41	92.51	sparse residential area	97.03	97.86	97.45
football field	59.67	84.65	70.00	stadium	92.23	96.35	94.25
forest	85.13	93.97	89.33	swimming pool	89.72	85.67	87.65
freeway	99.18	99.30	99.24	tanks	95.05	98.97	96.97
golf course	98.29	97.46	97.87	tennis court	98.38	97.00	97.68
grass	88.78	88.97	88.87	terrace	92.88	96.31	94.56
greenhouse	99.81	98.65	99.23	track	94.47	94.39	94.43
gully	90.32	94.62	92.42	trail	80.84	83.16	81.99
habor	99.03	99.35	99.19	transmission tower	98.66	99.61	99.14
intersection	70.15	94.00	80.34	trees	92.32	93.72	93.01
island	98.82	99.21	99.02	water	95.30	91.56	93.39
lake	96.51	99.60	98.03	chaparral	96.90	95.26	96.07
mobile home	60.78	100.00	75.61	wetland	90.03	87.26	88.62
mountain	98.00	95.78	96.88	wind turbine	99.76	100.00	99.88



Figure D.57: Confusion matrix for the pre-trained Swin Transformer model on the MLRSNet dataset.

D.19 DFC15

DFC15 [56] is a multi-label dataset created from the semantic segmentation dataset, DFC15 (IEEE GRSS data fusion contest, 2015), which was published and first used in 2015 IEEE GRSS Data Fusion Contest. The dataset is acquired over Zeebrugge with an airborne sensor, which is 300m off the ground. In total, 7 tiles are collected in DFC dataset, and each of them is pixels with a spatial resolution of 5cm. All tiles in DFC15 dataset are labeled in pixel-level, and each pixel is categorized into 8 distinct object classes: impervious, water, clutter, vegetation, building, tree, boat, and car. As a result of this process, the dataset contains 3342 images with a size of 600x600 pixels (Figure D.58). The images are annotated with one or more of the 8 labels in the dataset, with an average of 2.8 labels per image (Figure D.59). The most frequent labels is *impervious* and it appears in 3133 image. The label *tree* is least frequent and it appears in 258 images.

Detailed results for all pre-trained models are shown on Table D.59 and for all the models learned from scratch are presented on Table D.60. The best performing model is the pre-trained Swin Transformer model. The results on a class level are show on Table D.61 along with a confusion matrix on Figure D.60.

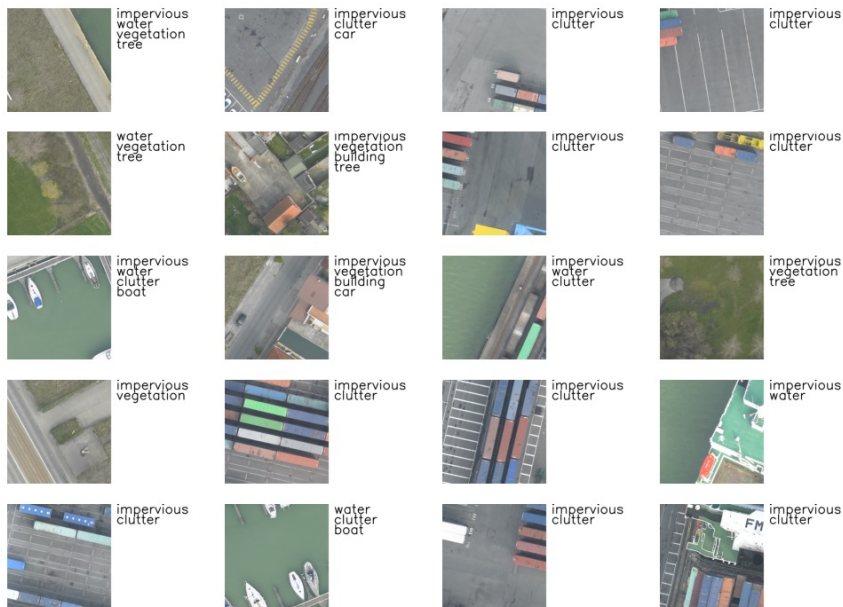


Figure D.58: Example images with labels from the DFC15 dataset.

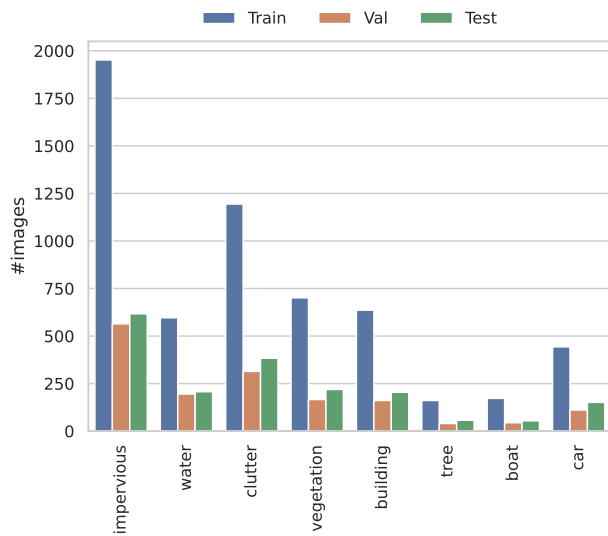


Figure D.59: Label distribution for the DFC15 dataset.

Table D.59: Detailed results for pre-trained models on the DFC15 dataset.

	mAP	Micro Precision	Macro Precision	Weighted Precision	Micro Recall	Macro Recall	Weighted Recall	Micro F1 score	Macro F1 score	Weighted F1 score	Avg. time / epoch (sec.)	Total time (sec.)	Best epoch
AlexNet	94.06	92.33	89.03	92.32	91.01	86.21	91.01	91.67	87.52	91.60	7.74	325	32
VGG16	96.57	94.09	91.75	94.30	92.60	88.57	92.60	93.34	89.79	93.30	8.94	286	22
ResNet50	97.66	95.21	94.19	95.19	93.50	91.54	93.50	94.35	92.81	94.31	8.49	331	29
ResNet152	97.60	95.08	93.78	95.04	93.97	90.88	93.97	94.52	92.25	94.46	9.45	444	37
DenseNet161	97.53	95.07	93.52	95.03	94.71	91.43	94.71	94.89	92.43	94.85	9.54	544	47
EfficientNetB0	96.79	95.54	94.09	95.51	94.08	90.97	94.08	94.81	92.48	94.77	8.33	583	60
ConvNeXt	97.99	94.99	93.84	94.98	94.24	91.39	94.24	94.61	92.55	94.58	8.72	471	44
Vision Transformer	97.62	96.40	94.75	96.33	93.34	89.45	93.34	94.84	91.96	94.77	8.76	219	15
MLP Mixer	97.94	95.23	94.29	95.20	93.92	90.82	93.92	94.57	92.48	94.53	8.18	229	18
Swin Transformer	<b>98.11</b>	95.54	93.90	95.50	93.97	91.18	93.97	94.75	92.49	94.71	17.59	686	29

Table D.60: Detailed results for models trained from scratch on the DFC15 dataset.

	mAP	Micro Precision	Macro Precision	Weighted Precision	Micro Recall	Macro Recall	Weighted Recall	Micro F1 score	Macro F1 score	Weighted F1 score	Avg. time / epoch (sec.)	Total time (sec.)	Best epoch
AlexNet	88.10	90.40	84.01	90.16	85.57	76.29	85.57	87.92	79.75	87.69	7.83	783	99
VGG16	89.87	91.07	86.30	91.03	87.37	79.82	87.37	89.18	82.38	88.98	8.50	799	79
ResNet50	94.67	92.88	89.33	92.84	91.75	87.01	91.75	92.32	88.11	92.26	8.92	464	37
ResNet152	94.19	92.05	89.36	91.91	89.96	83.80	89.96	90.99	86.36	90.82	9.66	647	52
DenseNet161	<b>95.85</b>	94.23	92.10	94.19	92.28	87.62	92.28	93.24	89.65	93.15	9.89	613	47
EfficientNetB0	93.97	93.90	91.67	93.77	91.91	85.64	91.91	92.90	88.40	92.75	8.47	686	66
ConvNeXt	89.56	91.08	87.12	90.85	87.47	79.56	87.47	89.24	82.99	89.03	8.80	880	91
Vision Transformer	94.16	92.45	89.36	92.34	89.96	84.84	89.96	91.19	87.00	91.10	8.85	743	69
MLP Mixer	91.66	90.43	86.00	90.27	88.90	82.91	88.90	89.66	84.40	89.56	8.31	831	100
Swin Transformer	94.35	93.47	91.02	93.43	90.80	84.66	90.80	92.12	87.56	91.97	17.09	1709	95

Table D.61: Per label results for the pre-trained Swin Transformer model on the DFC15 dataset.

Label	Precision	Recall	F1 score
impervious	97.28	98.54	97.91
water	96.52	93.72	95.10
clutter	96.78	94.26	95.50
vegetation	93.64	94.06	93.85
building	94.36	90.20	92.23
tree	90.38	82.46	86.24
boat	90.74	90.74	90.74
car	91.49	85.43	88.36

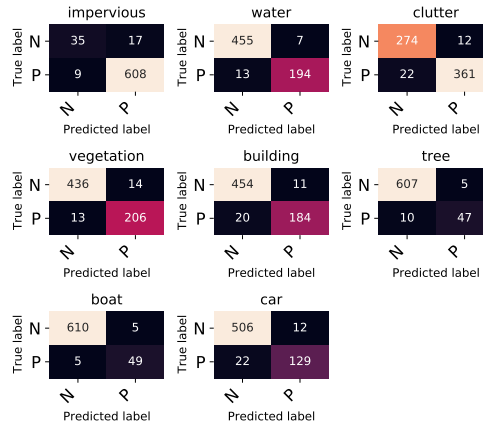


Figure D.60: Confusion matrix for the pre-trained Swin Transformer model on the DFC15 dataset.

#### D.20 Planet UAS

The Planet UAS dataset [58] was created by the company, Planet - designer and builder of the world's largest constellation of Earth-imaging satellites. The aim is to label satellite image chips with atmospheric conditions and various classes of land cover/land use. The dataset is available on Kaggle and is approximately 32 GB worth of data. The data contains 40479 satellite images organized in tiff and jpg files (Figure D.61). The jpg file show the natural light spectrum of the image, whereas the tiff files provide extra information about the infrared features of the satellite image, both with 256x256 pixels resolution. There are a total of 17 different labels with an average of 2.9 labels per image.

The imagery has a ground-sample distance (GSD) of 3.7m and an orthorectified pixel size of 3m. The data comes from Planet's Flock 2 satellites in both sun-synchronous and ISS orbits and was collected between January 1, 2016 and February 1, 2017. All of the scenes come from the Amazon basin which includes Brazil, Peru, Uruguay, Colombia, Venezuela, Guyana, Bolivia, and Ecuador. There are a total of 17 different labels. Out of those, 4 labels correspond to weather: Clear, Cloudy, Partly Cloudy, Haze. The rest of the (13) labels correspond to land: Habitation, Bare Ground, Cultivation, Agriculture, Blow Down, Conventional Mine, Selective Logging, Slash Burn, Artisanal Mine, Blooming, Primary, Water, and None.

The dataset only has the train set publicly available and we use that to generate train, test and validation splits (Figure D.62).

Detailed results for all pre-trained models are shown on Table D.62 and for all the models learned from scratch are presented on Table D.63. The best performing model is the pre-trained Swin Transformer model. The results on a class level are show on Table D.64 along with a confusion matrix on Figure D.63.

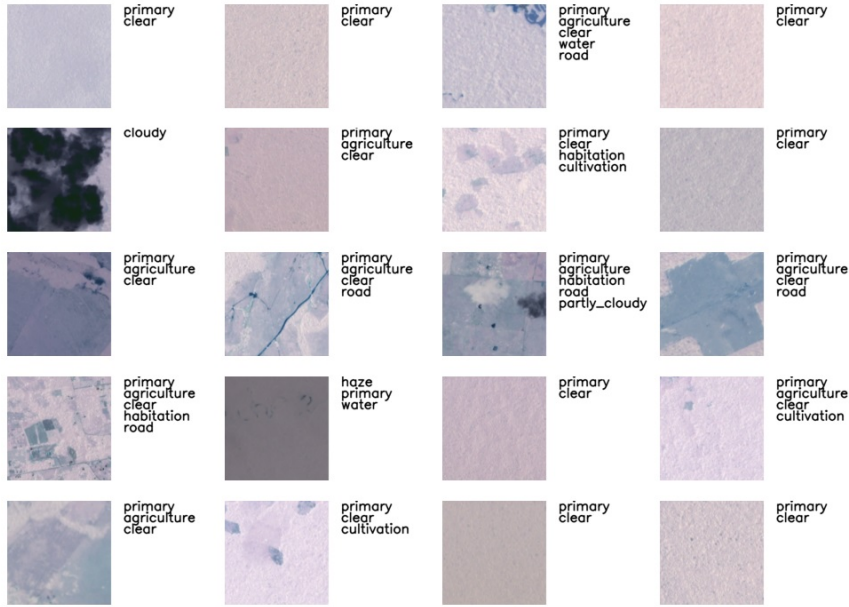


Figure D.61: Example images with labels from the Planet UAS dataset.

Table D.62: Detailed results for pre-trained models on the PlanetUAS dataset.

	mAP	Micro Precision	Macro Precision	Weighted Precision	Micro Recall	Macro Recall	Weighted Recall	Micro F1 score	Macro F1 score	Weighted F1 score	Avg. time / epoch (sec.)	Total time (sec.)	Best epoch
AlexNet	64.05	90.71	66.56	89.39	86.29	54.39	86.29	88.44	57.73	87.49	17.45	576	23
VGG16	65.58	92.09	64.14	90.90	86.88	55.99	86.88	89.41	59.19	88.58	50.38	1058	11
ResNet50	65.53	92.17	67.64	90.91	86.07	54.98	86.07	89.02	58.72	87.91	37.00	740	10
ResNet152	64.82	91.66	66.67	90.52	87.23	56.03	87.23	89.39	59.47	88.60	81.83	1964	14
DenseNet161	66.34	91.75	73.56	90.77	87.42	55.29	87.42	89.53	59.16	88.50	90.40	1808	10
EfficientNetB0	64.16	92.18	69.45	90.98	87.18	52.66	87.18	89.61	56.02	88.62	33.52	771	13
ConvNeXt	66.45	91.52	70.00	90.47	87.95	56.06	87.95	89.70	59.95	88.92	59.63	1431	14
Vision Transformer	66.80	91.31	69.63	90.18	87.79	56.11	87.79	89.52	59.95	88.56	65.71	920	4
MLP Mixer	67.33	92.18	74.70	91.30	86.68	56.56	86.68	89.35	60.79	88.59	45.94	735	6
Swin Transformer	<b>67.84</b>	91.23	67.93	90.33	88.61	58.30	88.61	89.90	60.97	89.27	180.89	3256	8

Table D.63: Detailed results for models trained from scratch on the PlanetUAS dataset.

	mAP	Micro Precision	Macro Precision	Weighted Precision	Micro Recall	Macro Recall	Weighted Recall	Micro F1 score	Macro F1 score	Weighted F1 score	Avg. time / epoch (sec.)	Total time (sec.)	Best epoch
AlexNet	60.28	90.32	67.35	88.88	84.81	51.24	84.81	87.48	54.52	86.25	18.65	1865	87
VGG16	60.68	90.39	60.11	88.74	84.97	50.56	84.97	87.60	53.21	86.44	50.68	2889	42
ResNet50	64.19	92.16	67.02	90.84	86.52	54.31	86.52	89.25	58.47	88.24	37.57	2592	54
ResNet152	64.96	91.57	69.94	90.42	86.97	55.02	86.97	89.21	59.06	88.28	80.86	6792	69
DenseNet161	64.74	91.79	69.52	90.53	87.01	55.20	87.01	89.34	59.12	88.37	90.11	4866	39
EfficientNetB0	63.87	91.70	65.64	90.55	87.03	53.86	87.03	89.30	57.21	88.40	33.47	2711	66
ConvNeXt	61.28	90.92	64.25	89.39	84.29	51.55	84.29	87.48	54.68	86.19	59.35	5935	90
Vision Transformer	59.41	90.35	60.32	88.16	83.12	47.68	83.12	86.58	51.94	84.94	65.52	4128	48
MLP Mixer	58.55	89.67	62.22	87.58	82.21	48.88	82.21	85.78	51.46	84.06	45.93	2572	41
Swin Transformer	<b>65.23</b>	91.53	66.89	90.11	86.34	54.05	86.34	88.86	57.89	87.80	181.83	16365	75

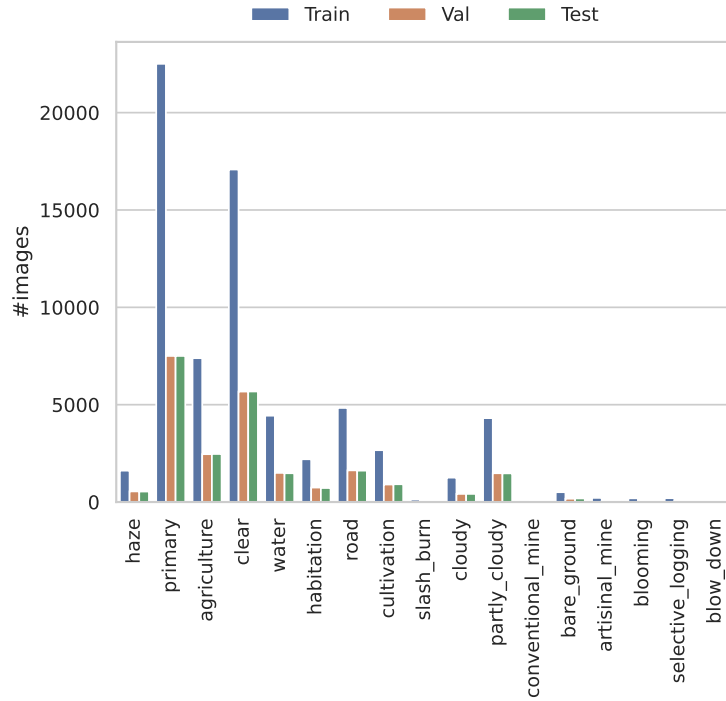


Figure D.62: Label distribution for the PlanetUAS dataset.

Table D.64: Per label results for the pre-trained Swin Transformer model on the PlanetUAS dataset.

Label	Precision	Recall	F1 score
haze	75.05	65.31	69.84
primary	97.86	98.28	98.07
agriculture	83.87	85.74	84.79
clear	96.10	97.25	96.67
water	87.72	73.90	80.22
habitation	77.07	72.36	74.64
road	83.22	85.55	84.37
cultivation	67.48	48.58	56.49
slash_burn	0.00	0.00	0.00
cloudy	87.53	77.27	82.08
partly_cloudy	91.07	92.12	91.60
conventional_mine	58.33	60.87	59.57
bare_ground	58.24	28.65	38.41
artisional_mine	78.79	78.79	78.79
blooming	19.05	6.25	9.41
selective_logging	43.48	15.15	22.47
blow_down	50.00	5.00	9.09

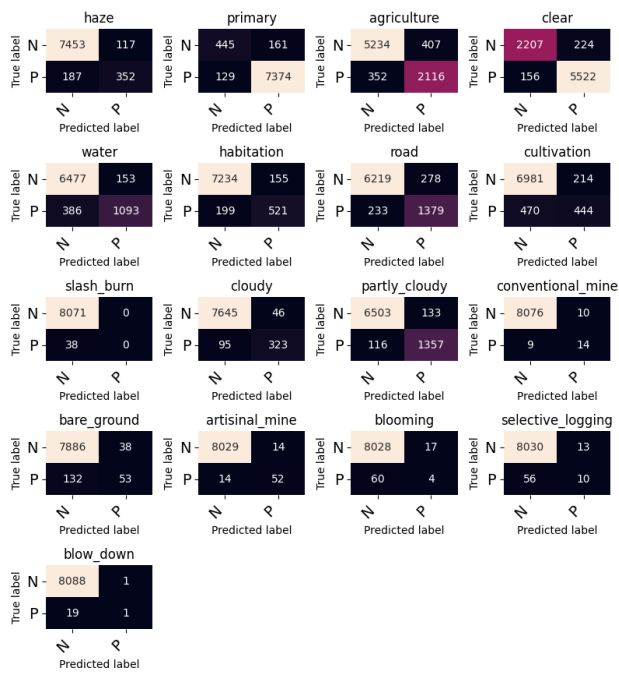


Figure D.63: Confusion matrix for the pre-trained Swin Transformer model on the PlanetUAS dataset.

D.21 AID multi-label

Hua et al. [57] extend the AID dataset for multi-label classification. They manually relabeled some images in the AID dataset. With extensive human visual inspections, 3000 aerial images from 30 scenes in the AID dataset were selected and assigned with multiple object labels. The dataset has 17 labels with 5.2 labels per image on average. The labels are: bare soil, airplane, building, car, charparral, court, dock, field, grass, mobile home, pavement, sand, sea, ship, tank, tree and water. The authors provide a proposed train-test split. Figure D.64 show some example images from the AID multi-label dataset. The distribution of the labels for the train, validation and test splits is shown in Figure D.65 from which we can observe an imbalanced distribution, some of the labels are heavily populated with images/samples, and some of the labels are with only few images/samples (for example the label mobile-home has only one image in the respective train, validation and test splits).

Detailed results for all pre-trained models are shown on Table D.65 and for all the models learned from scratch are presented on Table D.66. The best performing model is the pre-trained ConvNeXt model. The results on a class level are show on Table D.67 along with a confusion matrix on Figure D.66.



Figure D.64: Example images with labels from the AID multilabel dataset.

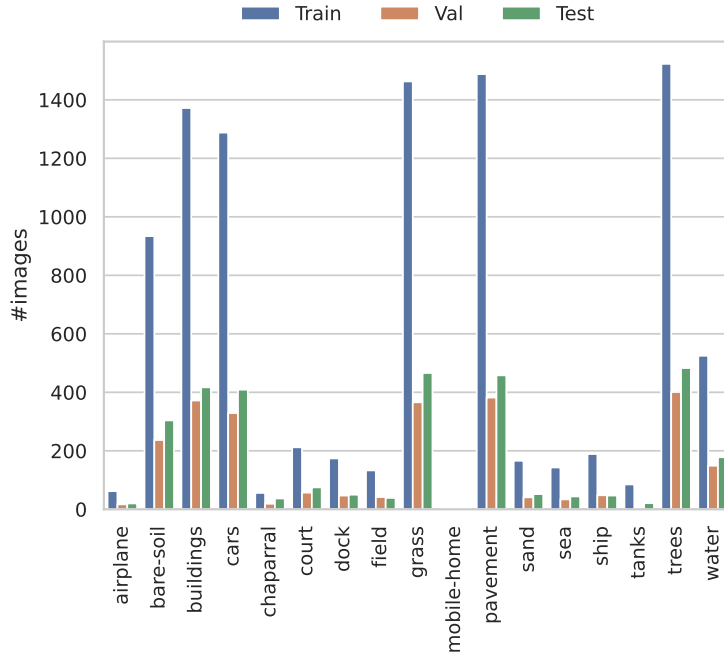


Figure D.65: Label distribution for the AID multilabel dataset.

Table D.65: Detailed results for pre-trained models on AID multi-label

	mAP	Micro Precision	Macro Precision	Weighted Precision	Micro Recall	Macro Recall	Weighted Recall	Micro F1 score	Macro F1 score	Weighted F1 score	Avg. time / epoch (sec.)	Total time (sec.)	Best epoch
AlexNet	75.91	88.34	75.10	87.33	86.04	66.15	86.04	87.18	68.61	86.19	5.55	172	21
VGG16	79.89	90.12	76.29	88.58	87.62	67.13	87.62	88.85	70.03	87.74	6.33	190	20
ResNet50	80.76	91.36	79.13	89.72	87.68	68.37	87.68	89.48	72.34	88.34	5.94	190	22
ResNet152	80.94	91.92	80.10	90.46	86.62	64.52	86.62	89.19	69.53	87.98	7.97	239	20
DenseNet161	81.71	90.77	80.12	89.54	88.84	68.22	88.84	89.80	71.80	88.76	8.71	366	32
EfficientNetB0	78.00	91.38	78.79	89.79	86.81	64.22	86.81	89.04	69.40	87.76	6.15	381	52
ConvNeXt	<b>82.30</b>	92.23	86.10	92.06	88.07	68.96	88.07	90.10	73.01	89.17	6.63	345	42
Vision Transformer	81.54	93.33	81.54	91.76	87.10	67.84	87.10	90.11	73.15	88.96	6.95	146	11
MLP Mixer	80.88	93.09	85.44	92.78	86.88	64.11	86.88	89.87	69.48	88.53	6.35	165	16
Swin Transformer	82.25	91.53	84.73	91.41	89.23	70.89	89.23	90.37	74.04	89.47	15.90	477	20

Table D.66: Detailed results for models trained from scratch on the AID multi-label dataset.

	mAP	Micro Precision	Macro Precision	Weighted Precision	Micro Recall	Macro Recall	Weighted Recall	Micro F1 score	Macro F1 score	Weighted F1 score	Avg. time / epoch (sec.)	Total time (sec.)	Best epoch
AlexNet	68.78	86.93	69.98	85.45	84.33	60.45	84.33	85.61	63.48	84.42	5.82	524	75
VGG16	69.21	87.03	66.46	85.22	84.42	62.06	84.42	85.71	63.75	84.60	6.28	490	63
ResNet50	70.87	89.52	74.76	87.95	84.04	59.51	84.04	86.69	64.46	85.27	5.74	379	51
ResNet152	69.65	87.95	76.32	87.11	84.49	58.55	84.49	86.18	62.72	84.76	8.08	477	44
DenseNet161	71.22	88.57	76.27	87.52	85.23	60.19	85.23	86.87	64.09	85.33	8.47	449	38
EfficientNetB0	<b>72.89</b>	88.51	71.56	86.66	86.42	64.45	86.42	87.45	67.01	86.22	5.94	398	52
ConvNeXt	65.59	87.00	67.56	85.16	83.75	56.43	83.75	85.34	59.44	83.75	6.40	576	75
Vision Transformer	65.58	85.82	63.05	83.61	83.94	56.33	83.94	84.87	58.63	83.37	6.82	627	77
MLP Mixer	64.24	85.72	66.07	83.70	83.46	56.52	83.46	84.58	59.30	83.02	6.41	506	64
Swin Transformer	69.55	87.23	67.48	85.28	85.46	60.09	85.46	86.33	62.57	84.96	15.87	1238	63

Table D.67: Per label results for the pre-trained ConvNeXt model on the AID multi-label dataset.

Label	Precision	Recall	F1 score
airplane	100.00	25.00	40.00
bare-soil	77.30	77.30	77.30
buildings	93.72	96.64	95.16
cars	94.13	94.13	94.13
chaparral	100.00	2.70	5.26
court	80.43	49.33	61.16
dock	82.93	68.00	74.73
field	85.71	61.54	71.64
grass	95.30	95.71	95.50
mobile-home	0.00	0.00	0.00
pavement	97.82	97.82	97.82
sand	97.78	84.62	90.72
sea	100.00	90.91	95.24
ship	82.22	78.72	80.43
tanks	100.00	90.48	95.00
trees	95.42	94.82	95.12
water	80.99	64.61	71.88

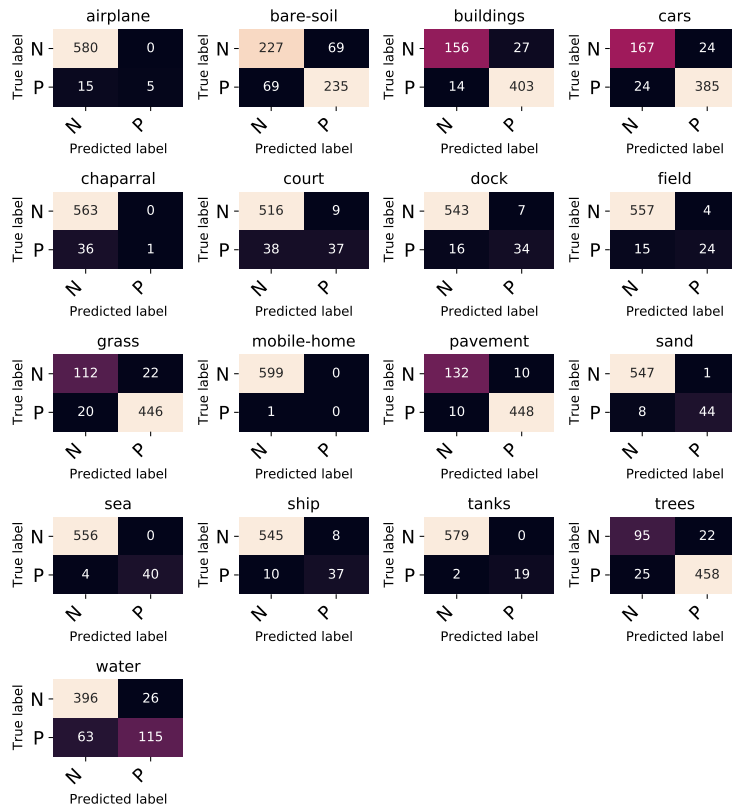


Figure D.66: Confusion matrix for the pre-trained ConvNeXt model on the AID multi-label dataset.